Forschungszentrum Jülich
in der Helmholtz-Gemeinschaft

Microcrystalline Silicon Films and Solar Cells Investigated by Photoluminescence Spectroscopy

Tsvetelina Merdzhanova

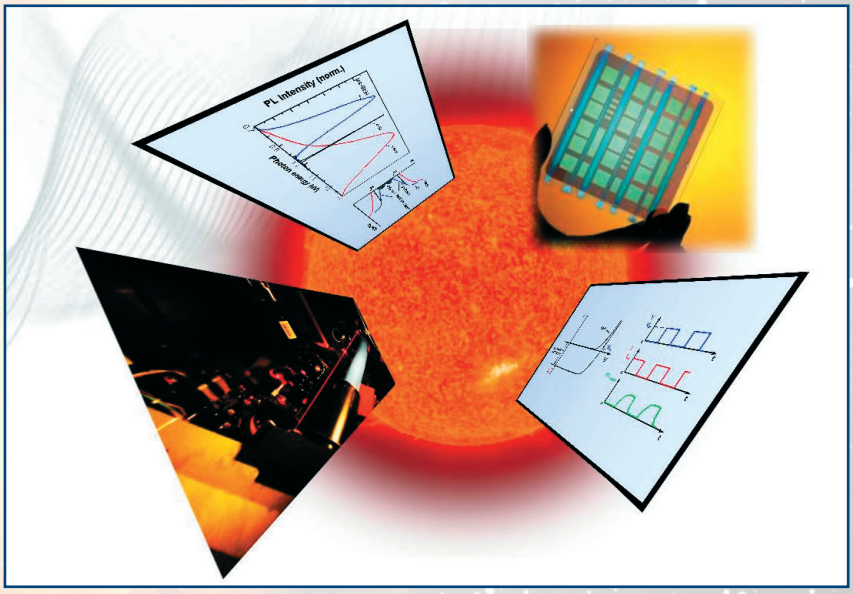

Energietechnik
Energy Technology

Schriften des Forschungszentrums Jülich
Reihe Energietechnik / Energy Technology Band / Volume 41

Forschungszentrum Jülich GmbH
Institut für Photovoltaik

Microcrystalline Silicon Films and Solar Cells Investigated by Photoluminescence Spectroscopy

Tsvetelina Merdzhanova

Schriften des Forschungszentrums Jülich
Reihe Energietechnik / Energy Technology Band / Volume 41

ISSN 1433-5522 ISBN 3-89336-401-3

Bibliographic information published by Die Deutsche Bibliothek.
Die Deutsche Bibliothek lists this publication in the Deutsche Nationalbibliografie; detailed bibliographic data are available in the Internet <http://dnb.ddb.de>.

Publisher and Distributor: Forschungszentrum Jülich GmbH
Zentralbibliothek
52425 Jülich
Phone +49 (0) 24 61 61-53 68 · Fax +49 (0) 24 61 61-61 03
e-mail: zb-publikation@fz-juelich.de
Internet: http://www.fz-juelich.de/zb

Cover Design: Grafische Medien, Forschungszentrum Jülich GmbH

Printer: Grafische Medien, Forschungszentrum Jülich GmbH

Schriften des Forschungszentrums Jülich
Reihe Energietechnik / Energy Technology Band / Volume 41

(Diss., Sofia, Bulgarian Academy of Sciences, 2004)

ISSN 1433-5522
ISBN 3-89336-401-3

Kurzfassung

Eine systematische Untersuchung der Photolumineszenz-Eigenschaften von mikrokristallinen Silizium-Filmen (μc-Si:H) mit strukturellen Zusammensetzungen von hoch-kristallin bis vorwiegend amorph wird hier vorgestellt. Die Proben wurden mit PECVD und HWCVD bei unterschiedlichen Silan-Konzentrationen (*SC*) hergestellt. Mit Hilfe von Photolumineszenz (PL)- in Verbindung mit Raman-Spektroskopie wurde der Zusammenhang zwischen den elektronischen Eigenschaften und der mikroskopischen Struktur des Materials untersucht. Die PL-Spektren von μc-Si:H zeigen eine ziemlich breite (~0,13eV), strukturlose Bande bei ungefähr 1eV ('μc'-Bande). In Materialien mit gemischten Phasen kristalliner und amorpher Regionen wurde eine Bande bei ca. 1,3eV mit einer Halbwertsbreite von ungefähr 0,3eV zusätzlich zu 'μc'-Bande gefunden, welche der amorphen Phase zugeschrieben wird. Ähnlich wie in amorphem Silizium wird auch die 'μc'-Bande der Rekombination von Elektronen und Löchern aus Zuständen in den Bandausläufern zugeschrieben. Eine weitere Bande bei 0,7eV mit einer etwas größeren Halbwertsbreite als die 'μc'-Bande wurde nur in Filmen beobachtet, die bei hoher Substrattemperatur hergestellt wurden und wird hauptsächlich den defektbezogenen Übergängen wie in polykristallinem Silizium zugeordnet. Mit abnehmendem kristalline Volumenanteil verschiebt die 'μc'-Bande aller μc-Si:H-Filme kontinuierlich zu höheren Energien. Die Linienbreite der PL-Spektren ist davon weitgehend unbeeinflusst. Das gilt für alle untersuchten Depositionsmethoden. Die Banden werden unter der Annahme einer abnehmenden Zustandsdichte der Bandausläufer mit abnehmender Silan-Konzentration interpretiert. Der Grund für die Bandausläufer-Zustände und deren Rückgang ist nicht klar, aber Verspannung muss eine entscheidende Rolle spielen und Wasserstoff oder hydrogenisiertes amorphes Silizium ist möglicherweise Auslöser für die Verspannungsreduktion. Unter Anwendung des 'Ladungsträger-Thermalisierungsmodells', das für a-Si:H entwickelt wurde, konnte die Steigung des Leitungsbandausläufers E_o durch die Temperaturabhängigkeit der PL-Ausbeute ($E_o \approx 0{,}035$eV) und durch die Verschiebung der PL-Peakenergie ($E_o \approx 0{,}022$eV) hergeleitet werden. Der Grund für diese Diskrepanz ist noch nicht klar, aber ein einfaches Modell unter der Annahme, dass nur ein Typ von Ladungsträgern in dem Prozess der thermischen Anregung beteiligt ist, ist möglicherweise für μc-Si:H zu einfach.

Unter Anwendung einer neuen Technik, hier spannungsmodulierte PL an Solarzellen genannt, wurden Informationen über die Ladungsträgerverteilung gewonnen. Sie verbindet die Aufspaltung der Quasi-Fermi-Niveaus von Elektronen und Löchern mit der jeweiligen Überschuss-Ladungsträgerverteilung mittels der offenen Klemmspannung V_{oc} und der PL-Energie. Dieser Zusammenhang wurde als Funktion von *SC*, der Temperatur und der optischen Generationsrate g_o untersucht. Ein Anstieg der PL-Energie und V_{oc} wurde für (i) steigendes *SC*, (ii) steigendem g_o und (iii) sinkender Temperatur gefunden. Es wurde vorgeschlagen, dass der Grund für alle Verschiebungen eine Verschiebung der Verteilung der Elektronen und Löcher zu höheren Energien ist. Es wird vorgeschlagen, dass mit steigender *SC* die Dichte der Bandausläuferzustande reduziert wird und die Ladungsträgerverteilung als Ergebnis der steigenden Generationsrate und steigender Lebensdauer mit sinkender Temperatur zu höheren Energien verschiebt. Die Verschiebung der Quasi-Fermi-Niveaus zu höheren Energien ist immer durch eine leichte Verschiebung der Ladungsträgerenergie durch die Zustandsverteilung in den Bandausläufern begleitet. Es wird geschlossen, dass die maximal erreichbaren V_{oc} und PL-Energien durch die Bandausläufer-Zustände bestimmt werden. Bei niedriger Temperatur wurde eine reduzierte Ladungsträger-Extraktion beobachtet, was auf eine reduzierte Drift- oder Diffusionsgeschwindigkeit hinweist.

Multi-Einfangprozesse in den Bandausläuferzuständen werden als Grund hierfür vorgeschlagen.

Ein einfaches Modell wird zur Simulation von PL-Spektren und V_{oc} in µc-Si:H-Solarzellen als Funktion der Temperatur vorgeschlagen, das auf Ladungsträgerverteilungen im Quasi-Gleichgewicht basiert. In dem Modell wurden symmetrische Ladungsträgerverteilungen für Elektronen und Löcher der Valenz- und Leitungsbandzustände angenommen. Die beste Übereinstimmung zwischen den Modellrechnungen und den experimentellen Ergebnissen für zwei Solarzellen mit unterschiedlichen strukturellen Eigenschaften wurde mit $E_o \approx 0{,}03\text{eV}$ für die Steigung beider exponentieller Bandausläufer erreicht, was einigermaßen gut mit $E_o \approx 0{,}035\text{eV}$ aus der Temperaturabhängigkeit der Lumineszenzintensität übereinstimmt.

Abstract

A systematic investigation on photoluminescence (PL) properties of microcrystalline silicon (μc-Si:H) films with structural composition changing from highly crystalline to predominantly amorphous is presented. The samples were prepared by PECVD and HWCVD with different silane concentration in hydrogen (*SC*). By using photoluminescence in combination with Raman spectroscopy the relationship between electronic properties and the microstructure of the material is studied. The PL spectra of μc-Si:H reveal a rather broad (~0.13eV) featureless band at about 1eV ('μc'-Si-band). In mixed phase material of crystalline and amorphous regions, a band at about 1.3eV with halfwidth of about 0.3eV is found in addition to 'μc'-Si-band, which is attributed to the amorphous phase ('a'-Si-band). Similarly to amorphous silicon, the 'μc'-Si-band is assigned to recombination between electrons and holes in band tail states. An additional PL band centred at about 0.7eV with halfwidth slightly broader than the 'μc'-Si-band is observed only for films prepared at high substrate temperature and it is preliminarily assigned to defect-related transitions as in polycrystalline silicon. With decreasing crystalline volume fraction, the 'μc'-Si-band shifts continuously to higher energies for all μc-Si:H films but the linewidth of the PL spectra is almost unaffected. This is valid for all deposition conditions investigated. The results are interpreted, assuming decease of the density of band tail states with decreasing crystalline volume fraction. The reason for the band tails and their reduction is not clear but strain might play a critical role and hydrogen or hydrogenated amorphous silicon might be effective for strain reduction. By applying the 'carrier thermalization model' developed for a-Si:H the slope, E_o, of the conduction band tail states are derived from temperature dependence of the PL intensity quenching ($E_o \approx 0.035$eV) and from the shift of the PL peak energy ($E_o \approx 0.022$eV). The reason for this discrepancy is not clear yet, but the simple model assuming that only one type of carriers are involved in the process of thermal excitation might be too simple for μc-Si:H.

By using a new technique, namely voltage modulated PL on solar cells, information on the carrier distributions is obtained. It relates the splitting of the quasi-Fermi-levels of electrons and holes and the respective excess carrier distributions via open circuit voltage V_{oc} and the PL energy. This relationship is studied as a function of *SC*, temperature and optical generation rate g_o. An increase of the PL energy and V_{oc} is found for (i) increasing *SC*, (ii) increasing g_o and (iii) decreasing temperature. It is suggested that the reason in all cases is the shift of the distribution of electrons and holes to higher energies. We propose that with increasing *SC*, the density of band tail states is reduced and the carrier distributions shift to higher energies as a result of an increasing generation rate and increasing carrier lifetime with decreasing temperature, respectively. The shift of quasi-Fermi levels to higher energies is always accompanied by a weak shift of carrier distributions in the band tails. It is concluded that the maximum achievable V_{oc} and the PL peak energy are determined by the band tail states. At low temperature, a strongly reduced carrier extraction is observed, which indicates reduced a drift or a diffusion length. Multiple trapping processes in the band tail states are suggested as the reason for this.

A simple model is proposed to simulate PL spectra and V_{oc} in μc-Si:H solar cells as a function of temperature, based on carrier distributions in quasi-equilibrium conditions. In the model is assumed symmetric density of states distributions for electrons and holes in the conduction and the valence band tail states. The best agreement between the model calculations and experimental results for two solar cells with different structural properties was obtained by using a $E_o \approx 0.03$eV for the slope of both exponential band tail states, which fits reasonably well with $E_o \approx 0.035$eV from the temperature dependence of the luminescence intensity.

Contents

Chapter 1

1 Introduction

Electricity generation by using solar cells is a clean and reliable alternative to grid-supplied electricity from conventional sources. Coal-fired and nuclear fission power stations are today the most commonly applied methods of energy generation, but solar energy has the advantages of totally non-polluting, almost infinite supply and not much requirements for maintenance. Today most commercially available solar cells are made of very pure monocrystalline[1] and polycrystalline silicon by using of energy consuming wafer production process. Such solar cells can attain efficiencies of up 18% in commercial manufacture and over 20% in the laboratory (Green et al. 2002). However, their photovoltaic (PV) module cost of about 3.3ecu/W_P is still too high to be competitive with classical electricity production.

The goal of worldwide research and development activities is to reduce the cost of photovoltaic systems. Thin film solar cell technology has been attracted much attention, as a cost effective alternative for generally expensive wafer-based crystalline and polycrystalline silicon. Thin film solar cells based on hydrogenated amorphous silicon (a-Si:H) and compound semiconductors as cadmium telluride (CdTe), copper-indium-diselenide ($CuInSe_2$) promises a large area production and low process temperatures, allowing to use a large area of low coast substrate material, e.g. glass, metal or plastic. Because of their high absorption coefficient they can be very thin (a few micrometers for CdTe and less than 1μm for a-Si:H), in contrast to the several hundred micron thickness required for crystalline silicon solar cells.

Amorphous silicon PV modules were the first thin-film modules to be commercially produced and are presently the only thin-film technology that has had an impact on the overall world market, contributing thereby to a reduction of the price per W_P. However, the efficiencies of these modules have not yet reached levels that were predicted in the 1980's. Solar cells based on amorphous silicon has always been associate with low efficiencies and with further efficiencies losses during operation due to the light indicated degradation, e.g. Staebler-Wronski effect (Staebler and Wronski 1977). The origin of the effect is the generation of additional defect states under illumination.

---

[1] The terms 'monocrystalline' and 'crystalline' silicon are not strictly differentiated and most often used as synonyms. In this work the term 'crystalline' silicon will be used throughout the text.

Although, stacked (tandem or triple) solar cells applying material with different band gap have reached stable efficiencies above 13% in the laboratory conditions, i.e. triple-junction amorphous silicon alloys solar cells (a-Si:H/a-Si:Ge:H/a-Si:Ge:H) have been realized (Yang et al. 1997).

Hydrogenated microcrystalline silicon (μc-Si:H) is now an attractive choice as the carrier generation layer in single or tandem thin film solar cells, where its increased optical absorption over amorphous silicon in long-wavelength region of the solar spectrum offers potential improvement in conversion efficiency. It is also more resistant, but not impervious, to light induced degradation. Another technologically relevant application of μc-Si:H is its use in colour sensors as shown by Stiebig et al. (1998). For the first time microcrystalline silicon was produced as a thin film in 1968 by Vepřek and Mareček, who employed a hydrogen plasma chemical transport technique (Vepřek and Mareček 1968). After that Usui and Kikuchi (1979) showed that, like in the case of a-Si:H, the preparation of μc-Si:H is possible by radio frequency plasma enhanced chemical vapor deposition (RF-PECVD) method, providing full compatibility with amorphous silicon thin film technology. However, due to the strong *n*-type character of this undoped μc-Si:H and very low deposition rates typically of a few 0.1Å/s, until very recently the material was only used in its doped form as a contact material in amorphous silicon solar cells. In the late 1980's and in the beginning of 1990's a new preparation technique based on glow discharge frequencies above standard value of 13.56MHz, so-called very high frequency (VHF)-PECVD has booted the development not only of a-Si:H but also of μc-Si:H films (Curtins et al. 1987, Oda and Noda et al. 1988, Prasad et al. 1990, Meier et al. 1994). It was found that an increase of the plasma excitation frequency leads to a simultaneous increase of the deposition rate, the grain size, and the Hall mobility of microcrystalline silicon (Finger et al. 1994). The work of Meier et al. (1996) has shown that the use of μc-Si:H prepared by VHF-PECVD as absorber layer in combination with a-Si:H in tandem cell structure is perspective to achieve high single-junction efficiencies of 7.7%.

In the Institut für Photvoltaik (IPV), in the recent years the dependence of structural, electronic and optical properties of μc-Si:H prepared by VHF-PECVD method has been a subject of considerable research and development activities (Hapke et al. 1996, Luysberg et al. 1997, Finger et al. 1997, Carius et al. 1997, Houben et al. 1998a, Vetterl et al. 2002). They have shown that the μc-Si:H is not homogeneous but has to be considered as a composite material of crystalline grains containing structural defects, grain boundaries, disordered (amorphous) regions and voids. For VHF-PECVD material it was found that not, as one might have expected, material the highest crystalline volume fractions and the largest crystallite size but material prepared close to the transition to amorphous growth yields the highest conversion efficiencies (Vetterl et al. 2000).

Nowadays, the PECVD is the most prominent method for preparing microcrystalline silicon with very high quality and performance in solar cells, as the technique is well established for manufacturing device-grade amorphous silicon thin films. The single junction solar cells efficiencies of 9% and above, improvements in the deposition rates and process up-scaling to large areas have been obtained (Keppner et al. 1999, Vetterl et al. 2000, Yamamoto et al. 2000, Saito et al. 2001, Rech et al. 2002).

More recently, hot wire chemical vapor deposition (HWCVD) has attracted attention, to improve deposition rates, stability and quality of amorphous and microcrystalline silicon. However, the quality of intrinsic microcrystalline silicon was too poor to yield reasonable solar cell efficiencies (Middya et al. 1995, Matsumura 1998, Rath et al. 1998, Klein et al. 2001, Schropp et al. 2002). Significant progress in the material quality prepared by HWCVD has been achieved in the IPV by lowering the substrate temperature to values typically used in PECVD processes (Klein et al. 2002). Microcrystalline silicon thin film solar cells employing this material as absorber layer show record solar cell efficiency of 9.4%, close to the maximum values achieved with PECVD material (Klein et al. 2002). Moreover, very similar electronic and device properties are observed for both materials. An interesting findings for material prepared close to the transition to amorphous growth is the decrease of the dark conductivity in films and an increase of the open circuit voltage V_{oc} in solar cells with decreasing crystalline volume fraction (Vetterl et al. 2002, Klein et al. 2003). These effects are not understood, and in particular the high V_{oc} of more than 590mV obtained for HWCVD, while retaining a high fill factor and current density, is of a current interest (Klein et al. 2003).

Photoluminescence spectroscopy is a powerful technique to investigate the electronic properties of semiconductor materials, providing information on the localized band tail states and defect states within the band gap. The technique is therefore particularly applicable to amorphous semiconductors, such as hydrogenated amorphous and microcrystalline silicon, since these materials exhibit a high density of localized states at the band edges compared to crystalline semiconductors. The band tail states dominate the transport properties, and so an understanding of their nature is of a technological as well as of scientific interest to obtain high quality microcrystalline silicon for solar cell application. Since 1973, when Engemann and Fischer (Engemann and Fischer 1973) reported for the first time the photoluminescence in hydrogenated amorphous silicon, many studies of the emission have been reported. An extensive review of the photoluminescence properties of a-Si:H, including a detailed model of the localized states and their influence on the recombination processes provides the reviews of Street (1981, 1991) and references therein.

Already, in the earlier studies of microcrystalline silicon, photoluminescence experiment indicated similarities of microcrystalline and amorphous silicon, e.g. broad featureless PL band at energies significantly below the band gap of crystalline silicon and a distribution of recombination lifetimes (Bhat et al. 1983). The interpretation was based on transitions involving distributions of defect states in the crystalline environment (Bhat et al. 1983a). More recent work revealed a systematic decrease of the PL energy as a function of the crystalline volume fraction (Carius et al. 1997, Yue et al. 2000). Both authors give evidence for radiative recombination of carriers trapped in band tail states as the caused of the PL band in the μc-Si:H films. A decrease of the PL energy was also observed with increasing substrate temperature and correlated with a decreasing optical gap (defined at high absorption coefficient) and interpreted in terms of quantum size effects (Kaan Kalkan et al. 2000). Clearly, the origin of the 0.9eV emission band in μc-Si:H and the continues decrease of its PL energy with increasing crystalline volume fraction needs to be clarified.

For microcrystalline silicon thin films and solar cells, however, a detailed investigation of the photoluminescence properties of well-characterized samples series upon changes of the preparation conditions (like silane concentration, substrate temperature, etc.) and also measurement temperatures was missing.

The aim of the proposed Ph.D. thesis is to provide a systematic study of the photoluminescence properties of microcrystalline silicon thin films and solar cells grown with different structural composition from highly crystalline to predominantly amorphous. In particular, the influence of the silane concentration (and thus the crystalline volume fraction), and the substrate temperature on the electronic properties and the microstructure will be addressed by a comparison of photoluminescence and Raman spectra for sample series of high quality μc-Si:H films prepared by PECVD and HWCVD.

By using a new technique information on the carrier distributions is obtained by monitoring the splitting of the quasi-Fermi levels of electrons and holes via open circuit voltage V_{oc} and the energy distribution of occupied states via PL energy in μc-Si:H solar cells. It will be shown that the increase of the V_{oc} and the increase of the PL energy with increasing silane concentration are likely caused by a decrease of the density of band tail states, which leads to shift of the carrier distributions to higher energies.

The outline of the present work is as follows:

- In Chapter 2 a short summary of the structural properties of microcrystalline silicon and the consequence for the electronic properties is given. The electronic properties of crystalline and amorphous silicon are described and the electronic structure of μc-Si:H mixed phase material is introduced. Next, the different recombination mechanisms with emphases on the photoluminescence are outlined for the understanding of the results presented and discussed in this work. At the end the carrier distributions in non-equilibrium and the quasi-Fermi level splitting for electrons and holes are introduced.
- A short description of the deposition processes used for the preparation of μc-Si:H thin films and *p-i-n* solar cells is given in Chapter 3. The second part provides an overview of the photoluminescence (PL) experiment used in this work as the main characterization technique to investigate the electronic properties of μc-Si:H. Then the details of the modulation technique applied to study the photoluminescence in solar cells are outlined, followed by a short discussion on the optical generation rate measurements of solar cells. The last part introduced some details of the Raman spectroscopy method, applied to explore the structural properties of μc-Si:H films and solar cells.
- In Chapter 4 the influence of the silane concentration on the photoluminescence properties is addressed by a detailed investigation of sample series of well characterized high quality μc-Si:H films prepared by PECVD and HWCVD. By a comparison of photoluminescence and Raman spectra of these sample series, a correlation between microstructure and photoluminescence energy is found.

Furthermore, the effect of the substrate temperature on the photoluminescence properties is presented in relation to observed additional PL band centred at 0.7eV ('poly'-Si-band). The photoluminescence experiment is also used as a sensitive probe for small amorphous volume fraction at the front surface or at the film/substrate interface. Furthermore, to separate 'μc'-Si-band from 'a'-Si-band in μc-Si:H films with very low crystalline volume fraction, a excitation at 1.59eV is performed. Finally, the temperature dependences of the PL intensity and PL peak energy have been also studied. Information considering the both, the diffusion of carriers and the distributions of states upon temperature in μc-Si:H films were explored.

- Chapter 5 addresses the relationship between PL peak energy and open circuit voltage, V_{oc}, in solar cells, which is studied as a function of silane concentration, temperature and optical generation rate. A modulation technique is applied in order to investigate only those carriers, which are taking part in the photovoltaic process. The focus is on temperature and generation rate dependences of the PL energy, V_{oc} and the short circuit current density, j_{sc}, for μc-Si:H solar cells compared to those of crystalline and amorphous silicon *p-i-n* diodes.
- In Chapter 6, the photoluminescence results of the material and the solar cells are discussed. This includes, an analysis of the shift of the PL band in microcrystalline silicon to higher energies with increasing silane concentration in terms of band tail states. Then, to determine the slope of the conduction band tail states, a 'carrier thermalization model' developed for a-Si:H is applied for μc-Si:H thin films. For comparison of differently prepared series of thin films, the Raman intensity ratio obtained by Raman spectroscopy is used, in addition to the silane concentration. Furthermore, the link between PL energy and V_{oc} in μc-Si:H solar cells via carrier distributions in the band tail states and the splitting of the quasi-Fremi levels for electrons and holes is discussed as a function of silane concentration, temperature and generation rate. At the end, a simple physical model is proposed to simulate the PL spectra and V_{oc} in solar cells as a function of temperature.
- In the last Chapter 7, the most important photoluminescence results are summarized and the conclusions are drawn.

Chapter 2

2 Fundamentals

In this first chapter the basic structural properties of microcrystalline silicon and the consequences for the electronic states are introduced. Microcrystalline silicon has turned out to be not homogeneous and is considered as a composite material of crystalline regions containing structural defects, column boundaries, disordered (amorphous) regions and voids (see Luysberg et al. 1997, Houben et al. 1998a). Therefore, the electronic properties of crystalline, amorphous and polycrystalline silicon are shortly reviewed. Furthermore, different recombination mechanisms, mainly photoluminescence (PL) are outlined for the understanding of the results presented and discussed in this thesis. At the end, the carrier distributions in non-equilibrium and the quasi-Fermi levels are introduced, as this provides the link between photoluminescence spectra and open circuit voltage V_{oc} in μc-Si:H solar cells.

2.1 Structural Properties of Microcrystalline Silicon

The microstructure of the material has a direct influence on the optical and electronic properties of the μc-Si:H thin films. Thus it is the most important property when the deposition conditions, such as silane to hydrogen ratio in the gas phase, plasma excitation frequency, substrate temperature, plasma power, etc. are varied. In the recent years, a number of studies have been published, treating the dependence of structural, electronic and optical properties of μc-Si:H (Hapke et al. 1996, Luysberg et al. 1997, Finger et al. 1997, Carius et al. 1997, Houben et al. 1998a, Vetterl et al. 2002).

A schematic picture of the structural composition of microcrystalline silicon, obtained from material studies with a combination of experimental techniques, like transmission electron microscopy (TEM), Raman scattering and X-ray diffraction (XRD) is shown in Figure 2.1. Under highly crystalline growth conditions, i.e. low silane concentration, films with columnar clusters of smaller grains with coherent crystalline regions are found (left hand side of Figure 2.1). The columns are separated from each other by disordered regions or regions of low density (voids), depending on the deposition conditions and the substrate (Tzolov et al. 1997).

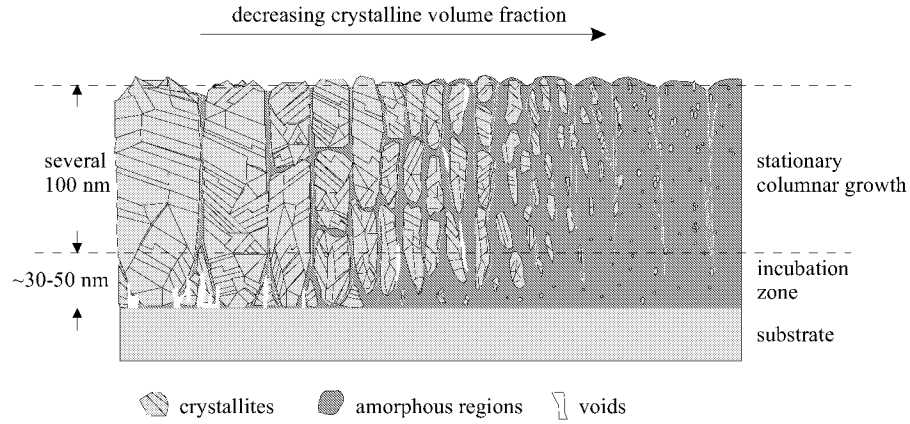

Figure 2.1: Schematic diagram showing the prominent microstructure characteristics of μc-Si:H grown by very high frequency PECVD. From the left to the right, the film composition changes from highly crystalline to predominantly amorphous. The figure is taken from (Finger et al. 2000).

Also very narrow boundaries between adjacent crystalline columns are possible, where the majority of defects and bonded hydrogen is located (see Finger et al. 2000). Here, it is important to note that depending on the experimental method and evaluations considerable differences in what one can refer to, as 'grain' and 'grain size' exist. The coherent regions, which formed the columnar clusters, can be called 'grains'. On the other hand the whole columns are sometimes called 'grains' since the lattice orientation is maintained at least within the columns. The structure of the material inside these columns is not perfectly single crystalline. It exhibits a high density of twin boundaries and stacking faults, between the coherent regions, thus the size of coherent 'grains' (regions with perfect translation symmetry) is considerably smaller (~20nm) than that of the column (Luysberg et al. 1997, Houben et al. 1998a, Finger et al. 2002). Upon increasing silane concentration the high crystalline volume fraction is maintained at first, but drops significantly at the transition to amorphous growth (from the left to the right in Figure 2.1). A further decrease of the crystalline fraction leads to interruptions of the columnar crystalline structure and small coherent 'grains' are embedded in the amorphous matrix. Such material does not represent standard a-Si:H used e.g. for solar cells, instead such as material is referred to as transition material between amorphous and microcrystalline silicon. Another additional structural feature is the incubation zone, which also influences the photoluminescence properties of the material (see Carius et al. 1997).

2.2 Electronic Properties

Since μc-Si:H is inhomogeneous on the scale of tens of nm, the question arises: how the structural defects between the coherent 'grains', disordered (amorphous) regions and voids (between the columnar clusters) affect the electronic states of the material.

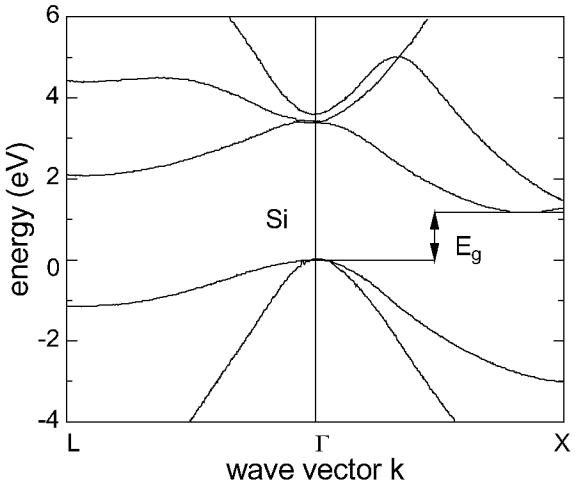

Figure 2.2: Energy band structure of crystalline silicon, where E_g is the energy band gap (after Chelikowsky and Cohen 1976).

Some of these aspects will be outlined below. However, before starting discussion on microcrystalline silicon it is necessary to describe briefly the electronic structure of crystalline and amorphous silicon.

2.2.1 Crystalline Silicon

Crystalline silicon has a diamond lattice structure with four tetrahedrally bonded next neighbours. The covalent bonding between the silicon atoms is a directional bonding with a bond length of 2.35Å and a bond angle of 109°. Both are of importance for the translation symmetry of the lattice (long-range order of the ideal network). Detailed survey on the topic crystalline silicon can be found in the work of (e.g. Sze 1981, Böer 1990).

The band structure of crystalline silicon is shown in Figure 2.2, where the energy bands are described by the energy-momentum relationship E (**k**) derived from solving the Schrödinger equation for a periodic potential of the crystal. This periodic lattice structure is responsible for presence of a well-defined band gap in crystalline silicon. The energy difference between the top of the valence band and the bottom of the conduction band defines the band gap in crystalline silicon, amounts to 1.12 eV at room temperature and normal pressure. Crystalline silicon has an indirect band gap, i.e. the lowest energy minimum of the conduction band is not at the same momentum **k** as the highest maximum of the valence band. The valence band maximum is at the centre of the Brillouin zone while the conduction band minima are at a momentum $\mathbf{k}_0$ which is near to the zone edge. As a result of the indirect band gap, the optical absorption is significantly reduced in the visible spectral region because the absorption of photons involves phonons for momentum conservation (see e.g. Figure 2.4). Here, the shift of the band gap in crystalline silicon with the temperature has to be mentioned.

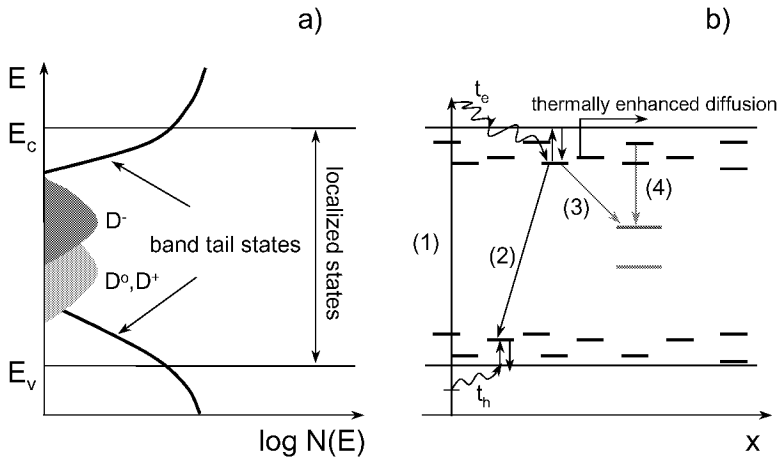

Figure 2.3: (a) Schematic density of states diagram for amorphous silicon as the function of the energy showing the localized band tail states and the different charged defect states (D^-, D^0 and D^+) in the gap. (b) Energy space diagram illustrating excitation (transition 1) and thermalization processes (t_h, t_e) together with the model for the different recombination mechanisms (transitions 2, 3, and 4).

Experimental results show that the band gap in crystalline silicon decreases with increasing temperature, the variation of the band gap with the temperature can be expressed approximately by a universal function: $E_g = E_g(0) - \alpha T^2/(T+\beta)$. The value of the band gap for c-Si at 0K is $E_g(0) = 1.17\,\text{eV}$ and $\alpha = 4.73\times10^{-4}\text{eV/K}$, $\beta = 636\,\text{K}$ are empirical parameter listed by Varshni (1967).

2.2.2 Amorphous Silicon

The main difference between amorphous and crystalline silicon is the structural disorder related to the small deviations in the bond length and bond angle. This bonding disorder creates localized tail states in the gap of amorphous silicon (e.g. Overhof and Thomas 1989). However, the tetrahedral short-range order of a few neighbour atoms is very similar in both materials. The most important consequence of the missing translation symmetry is the lack of conservation of the momentum **k** in the electronic transitions. Thus, for amorphous silicon, the energy-dependent density of states distribution $N(E)$ is introduced in Figure 2.3(a), instead of the energy-momentum band structure. There, the localized band tail states and defect states are illustrated together with the corresponding energy space diagram (Figure 2.3(b)), showing a model for the different recombination processes. The main radiative and non-radiative recombination processes in amorphous silicon are outlined in Section 2.4. The bonding disorder leads to broadening of the density of states distributions to form band tails, instead of sharp band edges of c-Si.

In amorphous silicon, such band tails of localized states extend from the band edges into the gap over an energy range of about 0.2eV (conduction band tail) or 0.3-0.4eV (valence band tail) (Stutzmann et al. 1987). The presence of localized states, which fall off exponentially with energy into the band gap does not allow exact definition of the optical band gap. Instead, several definitions exist, e.g. Tauc gap, mobility gap, E_{04}. All gaps are larger than that of c-Si, e.g. mobility gap is ~1.6-1.8eV. Unsaturated silicon bonds (dangling bonds) cause defect states within the band gap, which can exist in the three differently charged states D^-, D^0 and D^+, are illustrated in Figure 2.3(a). High defect density leads to material with bad semiconductor properties. Saturation by hydrogen reduces the density of dangling bonds and localized band tail states and the electronic properties of the material are improved. This material is then called hydrogenated amorphous silicon (a-Si:H). Since in a-Si:H the conservation of the momentum **k** in the electronic transitions is not longer granted, the material acts as a 'quasi'-direct semiconductor with a much higher absorption probability of photons in the visible spectral region (photon energies above 1.8eV), compared to c-Si (see Figure 2.4). Therefore, film thicknesses of about 1μm for a-Si:H are sufficient to absorbed the light with wavelengths, $\lambda \leq 600\,\text{nm}$. Below 1.8eV, the absorption in a-Si:H is determined by the density of tail states and deep defects, such as dangling bonds, and can be used as a measure for the electronic quality of the material. An extensive review on the properties of a-Si:H is given e.g. in the monograph of Street (1991).

2.2.3 Microcrystalline Silicon

There are a number of modifications of silicon, such as e.g. polycrystalline (poly-Si), microcrystalline (μc-Si:H) and nanocrystalline (nc-Si:H) silicon. They are roughly characterized by the size of the crystalline domains and their composition. The complex heterogeneous structure of these materials has very likely an important influence on their electronic states. Therefore, the proposed section deals with the electronic properties of the different modifications of silicon, studied in relation to their microstructure. Here, microcrystalline silicon or some times called nanocrystalline silicon is considered as a composite material of grains cluster columns with diameters up to tens of μm (μc-Si:H) or tens of nm (nc-Si:H), extending over the whole sample thickness (see e.g. Figure 2.1), column boundaries, amorphous regions and voids. In contrast, polycrystalline silicon (poly-Si) consists of crystalline regions, from several μm to cm in size with different orientation, which are separated from grain boundaries. Various experimental studies in this material indicated the existence of band tail states at grain boundaries, comparable to the energy distributions of band gap states in amorphous silicon (see e.g. Werner and Peisl 1985, Werner and Peisl 1985a). They originate generally from local distortions in bond length and dihedral angle. This kind of disorder at grain boundaries leads to small potential fluctuations on a length scale of the lattice constant resulting in a localization of free carriers (Werner 1989).

In μc-Si:H the disordered regions and voids which separate the grains cluster columns (see Figure 2.1) are believed to contain the majority of defects and hydrogen atoms in μc-Si:H thin films.

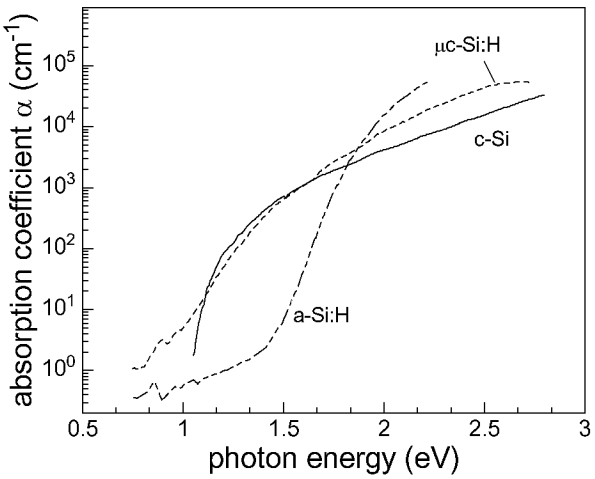

Figure 2.4: Absorption coefficient α of crystalline silicon (c-Si), hydrogenated amorphous silicon (a-Si:H) and microcrystalline silicon (μc-Si:H) measured by photothermal deflection spectroscopy (PDS). The data are taken from Carius et al. (1997).

For the coherent crystalline regions with typical diameters of about 20nm, which are inside the grains we can assume a crystalline silicon band structure. Since they are separated from each other by high density of twin boundaries and stacking faults, no grain boundaries in a classical polycrystalline silicon sense are expected. Instead, a very low dangling bond spin density[2] of less than $10^{16}cm^{-3}$ can be obtained from electron spin resonance (ESR) measurements (Finger et al. 1998). The coherent regions do not create dangling bonds and it is not clear if stacking faults may result in band tail states. The expression 'band tails' has a different meaning than in homogeneous amorphous material. It is expected that the transport and recombination processes might be very different from a homogeneous distribution of these states throughout the material.

2.3 Optical Properties of Microcrystalline Silicon

In the following paragraph the optical absorption coefficient, α, of microcrystalline silicon evaluated from photothermal deflection spectroscopy (PDS) is compared with absorption spectra of crystalline (c-Si) and hydrogenated amorphous silicon (a-Si:H). The optical absorption spectra shown in Figure 2.4 suggest, a higher absorption coefficient for μc-Si:H than for c-Si in the visible spectral region (at photon energies above 1.8eV). Absorption in disordered phase and internal light scattering in μc-Si:H has been proposed as a possible reasons for this effect (Diehl et al. 1998, Beck et al. 1996).

[2] Dangling bond spin densities N_S in μc-Si:H are obtained from a numerical integration of the electron spin resonance (ESR) spectra, i.e. the db-signal at g=2.0043 and g=2.0052. For more details see e.g. Dylla et al. (2002).

Between 1.1eV and 1.8eV, μc-Si:H almost reproduced the absorption coefficient values of c-Si, while the values of α for a-Si:H decreases rapidly towards lower energies. In the sub-band gap absorption region (at energies below 1.1eV), the absorption coefficient of μc-Si:H significantly exceed the one for c-Si and is slightly higher than that for a-Si:H. Two possible reasons for such as enhanced absorption for μc-Si:H are proposed in the literature: (i) the indication of an exponential band tails at grain boundaries like in polycrystalline silicon (see e.g. Section 2.2.3) and (ii) the presence of electronic defect states similar to amorphous silicon (Jackson et al. 1983, Beck et al. 1996).

2.4 Generation and Recombination Processes

A semiconductor at a constant temperature, without optical or electrical excitation, establishes a thermal equilibrium. The electrons and holes are generated by thermal excitation. A recombination process must occur for every generation process in equilibrium for reasons of detailed balance (see e.g. Section 2.5, Eq.2.15). When non-thermal carrier generation is introduced through e.g. excitation by light (optical generation of charge carriers) or by electric field (injected charge carriers through electric field) the equilibrium density distribution is no longer valid. Here, optical generation and different recombination processes at or below the band edge in hydrogenated amorphous silicon are considered. In Figure 2.3(b) the energy space diagram for amorphous silicon illustrating the excitation (transition 1) and thermalization (t_h, t_e) process together with the model for the different recombination mechanisms (transitions 2, 3 and 4) are shown. The electron-hole pair creation can occur directly by exiting an electron from the valence band into the conduction band if the photon energy is larger than the band gap energy (transition 1). After excitation, the carriers thermalize, i.e. they lose their energy by moving rapidly to the band edges and further into shallow traps such as band tail states (transitions t_e and t_h). Three mechanisms of carrier thermalization apply to hydrogenated amorphous silicon (i) rapid thermalization in extended states is completed in less than $< 10^{-12}$s and happens by emission of phonons from carriers scattering from one state to another (ii) thermalization by tunnelling between localized states (hopping down) occurs at low temperature (Street 1981) and (iii) thermalization by multiple trapping mechanism dominates above 200K for the holes and 50K for electrons (Tieje and Rose 1980, Orenstein and Kastner 1981).

Recombination processes occur after the carriers are thermalized and trapped into the band tail states. There are two competing recombination channels, radiative transitions between band tail states (transition 2 in Figure 2.3(b)) and non-radiative transitions from the band edge to defect states (transitions 3 and 4 in Figure 2.3(b)). The former involves the conversion of excitation energy into photons, the latter the conversion of the excitation energy into phonons. The radiative processes can for example be studied in photoluminescence experiments. Furthermore, depending on the temperature, one can distinguish between two different recombination mechanisms, i.e. tunnelling (transitions 2, 3 in Figure 2.3(b)) and direct capture to defects (transition 4 in Figure 2.3(b)). For example, recombination at low temperature occurs by tunnelling of carriers, because there is not enough thermal energy to excite the carriers from band tail states to more mobile states (mobility edge).

Thermal excitation becomes significant at high temperature and enhances the non-radiative recombination via direct capture to defects. In Sections 2.4.1 and 2.4.2 the main radiative- and non-radiative recombination processes in a-Si:H are outlined in respect of their influence on the photoluminescence results, obtained in this work.

2.4.1 Radiative Recombination

In amorphous silicon, the dominant recombination mechanism at low temperature and low defect density is the radiative tunnelling transition between localized tail states of the conduction and valence band, so-called band tail luminescence (transition 2 in Figure 2.3(b)). The transition probability P_r for radiative recombination between localized states depends exponentially on the overlap of electron and hole wavefunctions, i.e. on the distance between recombination partners, and can be expressed as

$$P_r = P_o \exp\left(-\frac{2R}{R_o}\right) \tag{2.1}$$

Here R_o is the localization radius of the less localized wavefunction of the two states involved and P_o the transition probability for complete overlap (Street 1991, p.278). One further distinguishes between geminate and non-geminate recombination. In the geminate pair model proposed by Street (1981) it is assumed that diffusion during thermalization does not separate the photo-exited electrons and holes such that the recombination occurs between trapped geminate pairs. Geminate recombination occurs preferably at low temperature and low density of charge carriers, when thermal energy is insufficient to separate the pairs and the overlap between neighbouring pairs is negligible. In the distant pair model of Dunstan and Boulitrop (1984) it is supposed that the carriers are able to diffuse and are tapped at random in the band tail states. In this case the carriers recombine with the nearest available partner, which is a non-geminate processes. Common to both models is that the recombination occurs by radiative tunnelling and that therefore the distribution of intra-pair separation causes a broad distribution of lifetimes.

Band Tail Luminescence

The band tail luminescence process can generally be considered as comprising three distinct events in sequence. First, an electron-hole pair is excited and if this occurs by the absorption of a photon the luminescence is called photoluminescence, PL. Second, the electron and hole thermalize by emitting a series of phonons, and usually end up at the band edge or in localized states below the band edge. Finally, there is a recombination, either by luminescence or by some non-radiative mechanism. The radiative process is accompanied by the emission of photon. The first photoluminescence observation in a-Si:H was reported by Engemann and Fischer (1973) and an extensive review of the photoluminescence in this material can be found in the work of Street (1981, 1991) and references therein.

Already in the early stages of research on microcrystalline silicon, PL measurements indicate similarities of microcrystalline and amorphous silicon, i.e. a broad featureless PL band and distributions of recombination lifetimes (Bhat et al. 1983). Before starting the discussion of hydrogenated amorphous and microcrystalline silicon, it may be helpful to add briefly information on the luminescence in crystalline silicon, which has a very similar tetrahedral short-range order as in amorphous silicon.

Energy, Lineshape and Linewidth of Photoluminescence Band

The lineshape and linewidth of a photoluminescence spectrum contains a large amount of information about the occupation and energy position of electronic states. Although this information is not easily accessible and often masked in disordered system like μc-Si:H, the analyses of lineshape and linewidth is an important tool to study the localized band tail and defect states in the material. The PL peak energy position is determined simply as the maximum of the curve. The spectral linewidth differs from the linewidth at half maximum (FWHM or ΔE_{pl}) by a numerical factor that depends on the particular lineshape. The emphasis here is to show the important differences of lineshapes and linewidths of crystalline (c-Si) hydrogenated amorphous (a-Si:H) and microcrystalline (μc-Si:H) silicon as a result of their electronic structures.

Figure 2.5 represents typical photoluminescence spectra, taken at low temperature of 10-20K for crystalline, hydrogenated amorphous and microcrystalline silicon. The photoluminescence measurements are usually performed at low temperature to avoid the thermally activated non-radiative transitions. Crystalline silicon exhibits sharp spectral lines due to the well-defined band structure. As a result of the indirect band gap, phonons must compensate the change of electron momentum. This leads to four lines in the PL spectrum of c-Si, corresponding to the emission of four phonons plus donor-acceptor pairs, etc. Four types of radiative transitions are often observed in c-Si: free exciton, bound exciton, free carrier to neutral acceptor (or donor), or donor-acceptor pairs. In Figure 2.5 a photoluminescence spectrum of c-Si dominated by a transverse optical (TO) phonon emission line at D is shown, originating from bound exciton (BE) recombination. The sharp spectral maximum of the corresponding narrow PL band ('c'-Si-band) is found to be at about 1.1eV and is of a major importance for the present work. It was interpreted as indirect transitions of electrons from the minimum at centre of the Brillouin zone to the top of the valence band, involving phonons for momentum conservation (Haynes et al. 1959). A second line is seen at the higher energy (E), which involves transverse acoustical (TA) phonon emission, attributed to free exciton recombination. The small spike at C is due to donor state in crystalline silicon. The two emission lines at the lowest energy are produced by emission of two phonons and marked with A and B. At the energy region below about 1.02eV, the radiative recombination occurs predominantly at deep defect levels such as dislocation rather than band edge recombination (Sauer et al. 1985, Robbins et al. 1985, Duncan et al. 1987).

In hydrogenated amorphous silicon, a broad and featureless band is observed. The peak energy at low temperature (~10K) is usually between 1.25 and 1.4eV and varies over this range depending on the deposition conditions.

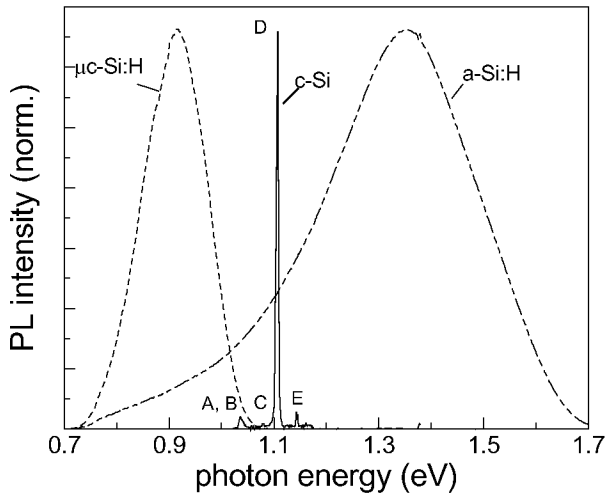

Figure 2.5: Composite photoluminescence spectra of crystalline (c-Si), hydrogenated amorphous (a-Si:H) and microcrystalline (μc-Si:H) silicon. For excitation of PL spectra at 10K for the a-Si:H and μc-Si:H films, a photon of energy $E_x = 2.54$ eV is used. The PL spectrum of crystalline silicon was illuminated with light from a high intensity mercury arc at 18K and was taken from Varshni (1967).

It does not mean that photoluminescence has many different origins but rather that the band gap and the disorder are varying upon the change in the microstructure and hydrogen content. The PL band has a width of about 0.25-0.35eV. There are two possible models proposed in the literature to explain the width of the PL band in a-Si:H, i.e. Stokes shift model (electron-phonon coupling energy distribution) and rigid band model (zero phonon energy distribution). Following Street (1978a), the band tail states have a considerable electron-phonon interaction (of some 200-250meV), leading to a Stokes shift[3] of 0.4-0.5eV. In the Stokes shift model, the width of the PL emission band are due to electron-phonon coupling, and the zero-phonon energies of the radiative states are distributed over a relatively narrow band of energies at about 1.6eV. The evidence for the this model lies in its good fit to the experimental spectra, and also in a comparison between the absorption strength at the emission energies and the intensity of the emission at saturation (detailed balance).

Other authors have explained the PL spectrum without a Stokes shift, by assuming a density of radiative states corresponding to the emission spectrum (see Collins et al. 1980a, Pankove et al. 1980). Further, the calculations of absorption and emission spectra based on the assumption of exponential band tails (taking into account the slope) and the convolution of the one-electron density of state within a rigid band model (no phonon coupling) find reasonable agreement with experimental data (Dunstan and Boulitrop 1981, 1984).

[3] The difference between absorption and emission of photons is called Stokes shift. The electron-phonon coupling (excitonic effects), occurring in photoluminescence are the reason for the Stokes shift.

According to rigid band model, there is no influence of the thermalization on the low-energy part of the spectrum and the spectrum follows the joint density of states. Whereas the high -energy part of the spectrum decreases monotonically to zero in the time when the thermalization to low energy states is complete.

Another much weaker luminescence band is fond at about 0.8-0.9eV. It is observed in hydrogenated amorphous silicon doped with boron or phosphorus, and also in high defect density undoped material at room temperature (Rehm et al. 1976, Engemann and Fischer 1977, Street et al. 1979, Voget-Grote et al. 1980). The band reveals a temperature independent linewidth of about 0.35eV and is seen best at high temperature due to weaker thermal quenching of this band compare to the intrinsic band at 1.25-1.4eV. The 0.9eV luminescence is usually associated with a high defect density material and the transitions of band tail carriers to defects states and subsequent recombination is proposed to explain its origin (Street and Biegelsen 1980). But the mechanism of non-radiative capture at defects remains unclear and in Figure 2.3(b) the corresponding transition is therefore not indicated. Another evidence for the association with defects is that this luminescence for doped and undoped a-Si:H (at 10K) can be exited by the sub-gap excitation energy, unlike the band-tail luminescence (Ulber et al. 1995).

Now, the luminescence lineshape, energy and the width of PL band in μc-Si:H are briefly described. The PL spectrum with almost Gaussian shape exhibits a rather broad featureless band at 0.9-1.05eV (at 10K) with a full width at half maximum (FWHM) of 0.13-0.15eV (see Figure 2.5). An additional emission band at 1.3-1.36eV with a spectral width of 0.3-0.4eV is frequently observed in μc-Si:H, and is attributed to an amorphous phase (Bhat et al. 1983b, Deppina et al. 1983, Carius et al. 1997, Han et al. 2000). The interpretation was based on transitions involving distributions of defect states in a much more ordered environment (Bhat et al. 1983a) or arising from donor-acceptor transitions as deduced from optical detected magnetic resonance (O.D.M.R.) (Depinna et al. 1983). In a later investigation, a shift of the PL energy as a function of the plasma excitation frequency was observed but no shift of the band gap derived from the absorption measurements was found (Carius et al. 1997). Although transitions between tail states were discussed as a possible source for the PL band, the similarities with well-known defect bands (D_1-D_4) in crystalline silicon was taken as the evidence to favour the defect model. Further, the features of the μc -Si-band are explained by the tail-to-tail radiative transition in two types of grain boundaries by Yue et al. (1999). More recent work revealed a systematic decrease of the PL energy as a function of the crystalline volume fraction (Carius et al. 2003, Yue et al. 2000). Both authors give evidence for radiative recombination of carriers trapped in band tail states as the caused of the PL band in the μc-Si:H films. A decrease of the PL energy was also observed with increasing substrate temperature and correlated with a decreasing optical gap (defined at high absorption coefficient) and interpreted in terms of quantum size effects (Kaan Kalkan et al. 2000). Clearly, the origin of the 0.9eV emission band in μc-Si:H and the systematic decrease of its PL energy with increasing crystalline volume fraction needs to be clarified. Therefore, this thesis will focus on the systematic study of the photoluminescence properties of μc-Si:H thin films and solar cells with well characterised structural and electrical properties.

Thermal Quenching of Photoluminescence

As previously discussed, the tunnelling transitions of electrons and holes trapped at their respective band tail states occur as a dominant radiative recombination mechanism at low temperatures for hydrogenated amorphous silicon. Experimental observations revealed that the photoluminescence intensity exhibits the highest values and remains constant with increasing temperature up to about 50K. A further increase of the temperature causes a competing non-radiative recombination that quenches the photoluminescence intensity. The photoluminescence intensity as a function of temperature, $I(T)$, can be expressed by the following form (Collins et al. 1980)

$$I(T) = I_o \frac{P_r}{P_r + P_{nr}} \tag{2.2}$$

where I_o is the temperature independent PL intensity at low temperature, P_r is the temperature independent probability for radiative recombination and P_{nr} is the competing probability for non-radiative recombination. The non-radiative quenching of the luminescence intensity at high temperature occurs due to thermally enhanced diffusion of carriers from the band tail states to more mobile states (mobility edge). That enhances their probability for a non -radiative recombination via capture to defects (transition 4 in Figure 2.3(b)). Several authors have plotted $[I_o / I(T) - 1]$ vs. $1/T$ to see if the non-radiative probability (or P_{nr} / P_r) is thermally activated as one may expected for non-radiative processes involving electron-hole pair dissociation (Austin et al. 1979, Tsang and Street 1979, Paesler and Paul 1980). These published data appear to fit a double activated behaviour with low temperature activation energy of about 0.05eV for a range 60K < T < 125K and high activation energy of about 0.02eV for T > 150K, i.e. no single activation energy could be defined in a-Si:H.

Another approach assumes thermally activated release of carriers from exponential band tail states $\exp(-E/kT_o)$, i.e. 'carrier thermalization model' proposed from Street (1981) to explain the thermal quenching of the luminescence intensity and the redshift of the PL energy with increasing temperature for a-Si:H. The temperature dependence of the PL intensity is empirically found in a-Si:H and follow the relation (Collins and Paul 1981)

$$I(T) = I_o \left(1 + A \exp\left(\frac{T}{T_o} \right) \right)^{-1} \tag{2.3}$$

with a characteristic temperature T_o derived from the slope of the curves in a plot $[I_o / I(T) - 1]$ vs. temperature. In the model it is assumed that for a single average value of the radiative lifetime τ_r, there is an energy E_d given by:

$$E_d(T) = kT \ln(v_o \tau_r) \tag{2.4}$$

where $E_d(T)$ is the temperature dependent demarcation energy at which the probability for non-radiative thermal excitation equals the probability for radiative recombination, $\nu \approx 10^{12}\text{s}^{-1}$ is the attempt to escape frequency for excitation out of the trapping site and k is the Boltzmann constant. E_d is defined as the energy distance to the band edge or mobility edge. In the model is also assumed that only electrons are the particles that diffuse away, whereas the holes are deeply trapped and therefore immobile. All electrons trapped into states deeper than E_d will have a high probability of radiative recombination, while those trapped in shallower states will be thermally exited to the mobility edge, and will either find other traps or diffuse away to a non-radiative centre. Based on this model, the luminescence intensity is given by the fraction of carriers deeper than E_d by the following expression:

$$\frac{I(T)}{I_o} = \exp\left(-\frac{E_d}{E_o}\right) = \exp\left(-\frac{kT\ln(\nu_o \tau_r)}{E_o}\right) \tag{2.5}$$

The Eq.2.5 is of the form of Eq.2.3 (for $I(T)/I_o << 1$), by this

$$T_o = E_o / k\ln(\nu_o \tau_r) \tag{2.6}$$

For device quality intrinsic a-Si:H, $T_o \approx 23\text{K}$ is observed. By using an average radiative lifetime of $\tau_r \approx 10^{-3}\text{s}$, one obtains $E_o \approx 0.04\text{eV}$, which is of the correct magnitude for the slope of the band tails.

Further, information on the distribution of states in a-Si:H can be gained from the temperature dependence of the luminescence peak energy and the spectral width of the luminescence spectra. The experimental observations show that the PL peak shifts to lower energies and the width of the spectrum increases with temperature (Austin et al. 1979, Tsang and Street 1979). As a consequence of the preceding discussion, the luminescence energy E_{pl} should have the same temperature dependence as the E_d given by the following relation:

$$\frac{dE_{pl}}{dT} \cong -\frac{dE_d}{dT} \tag{2.7}$$

where the negative gradient of E_d is due to a negative change of the photoluminescence with respect of the energy scale chosen. A positive energy scale was chosen (see Figure 2.3(b)) and therefore the temperature dependent demarcation level of the electrons moves towards deeper states as given by Eq.2.4. Consequently, the shift of the PL peak energy can be explained by the thermal excitation of carriers from the deeper states, resulting in a lower energy of luminescence. According to the model, the values of characteristic temperature T_o and $(-dE_d/dT)$ are connected by the slope of the band tails E_o involved:

$$\frac{dE_d}{dT} = -\frac{E_o}{T_o} \tag{2.8}$$

In Section 6.1.2, 'carrier thermalization model' created for a-Si:H will be applied for μc-Si:H thin films to obtain the slope of conduction band tail.

2.4.2 Non-Radiative Recombination

Non-radiative recombination is usually an undesired effect, since it involves the conversion of excitation energy into phonons. Thus the entropy of the system increases. There are four types of non-radiative mechanisms that are of importance for most of non-radiative recombination processes in semiconductors. These are multi-phonon transitions via deep defects (transitions 3 and 4 in Figure 2.3(b)), thermal quenching, Auger and surface recombination (not indicated transition in Figure 2.3(b)). The last two are relatively weak effects and can be avoided by using low intensity and weakly absorbed illumination. Consequently, only two non-radiative mechanisms were found to affect our photoluminescence results. For example, thermal quenching occurs at high temperature due to thermally enhanced diffusion of carriers (probably electrons) to more mobile states (see Figure 2.3(b)), allowing them to undergo further non-radiative recombination. In fact, thermal quenching is not a separate non-radiative process, since the carriers do not lose any energy and the actual non-radiative process of direct capture at defect occurs later (transition 4 in Figure 2.3(b)). This non-radiative recombination is found to have a strong influence on the PL properties such as quenching of PL intensity and redshift of the peak energy position with rise of the temperature and therefore has been already discussed (see e.g. Section 2.4.1). The emphasis here is therefore on non-radiative recombination which takes place via so-called recombination centres, i.e. deep defect levels that can effectively capture excess carries. In that case, the energy difference between ground and excited states is too large to be taken up by a single phonon and thus involves the emission of multiple phonons. In this case, the recombination probability is strongly dependent on the transition energy of the recombination.

Non-Radiative Recombination via Defects

When speaking of non-radiative recombination at defects one has to distinguish between two different non-radiative mechanisms, which occur by tunnelling (transition 3 in Figure 2.3(b)) or by direct capture of electrons or holes (transition 4 in Figure 2.3(b)), respectively. The former is the dominant recombination path at low temperature for material containing a high density of defects. The non-radiative mechanism of carriers directly captured at defects tends to dominate at temperatures above about 100K. For simplicity, the following discussion will be restricted to amorphous semiconductors, in particular hydrogenated amorphous silicon, since the deep defect luminescence in crystalline silicon is much less understood and is not of importance for the photoluminescence results in this work.

The low temperature mechanism is discussed at first. At low temperature, electrons are captured rapidly in the high density of band tail states and the recombination kinetics is determined by tunnelling. Tunnelling can be either a radiative or a non-radiative process. An example of the former is recombination of an electron and a hole trapped in band tail state (see e.g. Section 2.4.1), and the latter occurs by the capture of an electron into a defect.

Since electrons are expected to have the larger localization radius R_o (less localized wavefunction), their probability for direct capture at defect should be greater than that for holes, and so it was assumed that the electron capture is the dominant process. The probability for tunnelling is given by Eq.2.1 in either case of a radiative or a non-radiative transition. The only difference between both possible tunnelling processes lies in the value of the transition probability for completely overlapping wavefunctions P_o in Eq.2.1. The non-radiative tunnelling is effective over a greater distance than is the radiative tunnelling because the P_o is five orders of magnitude larger. And the non-radiative tunnelling transitions is a dominant mechanism when the defects are closer than ~100Å to an electron hole pair, whereas those defects farther away will be not effective. This is also consistent with the experimental finding for undoped a-Si:H, i.e. a rapid decrease of the luminescence intensity observed at a defect density above $10^{17}cm^{-3}$ (Street et al. 1978). The authors deduced the localization radius of the wavefunction of the conduction band tail states as ~10Å from their analysis of PL quenching by dangling bonds.

Finally, a brief discussion of a non-radiative recombination mechanism via direct capture of an electron at a defect is given for complete picture of non-radiative processes. This process has been partially discussed as a final non-radiative recombination path of carriers thermally exited to more mobile states. With increasing temperature, the probability for direct capture at defect states in material with high defect density increases due to high mobility of the electrons. The probability of direct capture of carriers by defects defines the capture cross -section σ_c, such that the free carrier lifetime is proportional to the velocity of the carriers v_c and the defect density N_d, i.e. $(\tau_F^{-1} = \sigma_c v_c N_d)$. A detailed survey on the topic non -radiative recombination processes in amorphous silicon can be found in the work of Street (1991).

Auger and Surface Recombination

A few words should be said about Auger and surface recombination mechanisms, despite their negligible influence on the recombination and on the photoluminescence in μc-Si:H under experimental conditions studied here. When the recombination of an electron-hole pair involves a third particle (electron or hole) exited high into the band, where it can thermalize to the band edge by the emission of phonons. The process is then called Auger recombination. At sufficiently high excitation intensity the free carrier Auger process is predominant e.g. in c -Si.

In case of excitons bound to neutral donors or acceptors in crystalline semiconductors, three particles can be localized at the same site. In intrinsic semiconductors the probability for an Auger recombination (Auger recombination rate) P_a is given by the expression

$$P_a \propto n^2 p + p^2 n \propto n^3 \tag{2.9}$$

Here n and p are the densities of electrons and holes for which the detailed balance equation $n = p$ is valid.

In crystalline semiconductors the Auger recombination can occur at a carrier density of $n > 10^{18}\,\mathrm{cm}^{-3}$, whereas for amorphous materials, it starts already at 10 times lower carrier densities because of the lost momentum conservation requirement (Kuzmany 1989, Stachowitz et al. 1998). The Auger rate may therefore be higher then in the equivalent crystal. However, there have been no detailed theoretical calculations of the rate for any amorphous semiconductor. Evidence for the Auger process in a-Si:H thin films is contained in the low temperature luminescence data of Street (1981) and Ambros (1991).

2.5 Carrier Densities in Non-equilibrium - quasi-Fermi Levels

In this work, a simple numerical model is used in Section 6.2.1 to simulate photoluminescence spectra and open circuit voltage V_{oc} in μc-Si:H solar cells as a function of temperature. The model is based on carrier distributions in quasi-equilibrium conditions, described by single electron statistics so-called Fermi-Dirac statistics, i.e. no interactions between carriers. Here, the basic physics behind this model will be introduced, starting with the case of an intrinsic semiconductor in thermal equilibrium. The thermal equilibrium considers the exchange of entropy between the electrons in conduction band and the lattice, leading to a uniform temperature T of the electrons and the lattice. The same equilibrium exists for the holes in the valence band. The density distributions of electrons or holes in the conduction or valence band can be obtained from the product of the density of states $N(E)$ and the Fermi-Dirac distribution function $f(E,T)$:

$$n(E,T)dE = N(E)f(E,T)dE \tag{2.10}$$

The density distribution for holes, i.e. of missing electrons, is:

$$p(E,T)dE = N(E)(1-f(E,T))dE \tag{2.11}$$

The Fermi-Dirac statistical distribution function gives the probability of occupation of an allowed electron state for any given energy, E, and T:

$$f(E,T) = \frac{1}{\exp\left(\frac{E-E_F}{kT}\right)+1} \tag{2.12}$$

where k is the Bolzmann constant and E_F is the Fermi energy or level[4]. Then, the number of electrons and holes per unit volume in the conduction and valence band at given temperature can be found by performing the integration of Eq.2.10 and Eq.2.11:

[4] In semiconductor physics, the chemical potential μ is referred to as 'Fermi level', i.e. the energy level in solids at which the Fermi-Dirac distribution function is equal to 0.5, i.e. $f(E_F) = 1/2$ for $E = E_F$.

$$n(T) = \int_{E_c=0}^{\infty} N(E) f(E,T) dE \tag{2.13}$$

$$p(T) = \int_{-\infty}^{E_V} N(E)(1 - f(E,T)) dE \tag{2.14}$$

In equilibrium, the intrinsic carrier density n_i is defined through the product of thermally generated electron, n_0, and hole, p_0, density distributions. Therefore, a relation between, n_i, effective density of states at the upper edge of the valence band N_V and at the lower edge of the conduction band N_C, as well as the temperature dependent band gap $E_g(T)$ of the semiconductor is given by the detailed balance equation:

$$n_i^2(T) = np = n_0 p_0 = N_C N_V \exp\left(-\frac{E_g(T)}{kT}\right) \tag{2.15}$$

In steady state, deviations from thermal equilibrium can occur because of non-thermal, additional excitation e.g. by light (optical generation of charge carriers, *G*) or an electric field (injected charge carriers through electric field, *V*). Thus in non-equilibrium ($V \neq 0V, G \neq 0$), the electron *n* and hole *p* densities deviate from thermodynamic equilibrium due to electrical injections or photo-generations of excess electrons Δn and holes Δp, respectively. By making the assumption that $\Delta n >> n_0$ and $\Delta p >> p_0$, the following equations are valid:

$$\Delta n = n - n_0 \cong n \tag{2.16}$$

$$\Delta p = p - p_0 \cong p \tag{2.17}$$

If the increase of the carrier densities above their equilibrium can be described by quasi -equilibrium, this leads to

$$n(T) = N_C \frac{1}{\exp\frac{E_C - E_{Fn}}{kT} + 1} \tag{2.18}$$

and

$$p(T) = N_V \frac{1}{\exp\frac{E_{Fp} - E_V}{kT} + 1} \tag{2.19}$$

where E_{Fn} and E_{Fp} stands for the quasi-Fermi levels for electrons and holes, respectively.

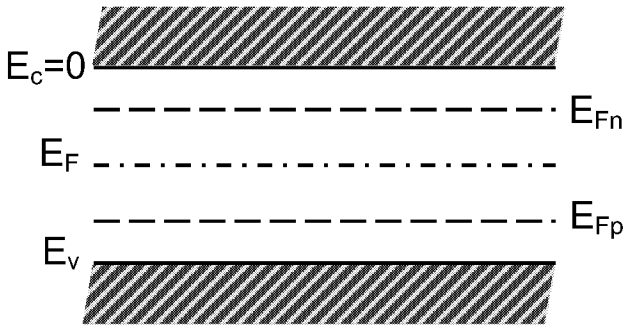

Figure 2.6: Energy diagram showing a band model with external excitation resulting in a splitting of the Fermi level into two quasi-Fermi levels E_{Fn} and E_{Fp}. Note that, only for a symmetric density of states and neglected defect density, the dark Fermi level lies in the middle of the band gap.

Further, the product of the excess carrier density distributions, *np*, determines the energy difference between the quasi-Fermi levels, which is identical to the applied voltage *V*, according to:

$$np \propto \exp\left(\frac{E_{Fn} - E_{Fp}}{kT}\right) \tag{2.20}$$

Hence, the generation of excess carriers lead to splitting of the Fermi level into two quasi-Fermi levels for electrons and holes, respectively, as shown in Figure 2.6. Moreover, the difference of the quasi-Fermi levels is non-zero in any illuminated material as well, with no need for a current collecting structure. The splitting of the quasi-Fermi levels can be related to the open circuit voltage V_{oc} in solar cells (the voltage which is built up at open external circuit in the cell) (e.g. see Würfel 1982).

In this thesis, the occupation of the band tail sates by excess carriers, described by the quasi-Fermi levels and radiative recombination of these carriers are investigated. The relationship between open circuit voltage V_{oc} and PL peak energy position in μc-Si:H solar cells is shown in Sections 5.3, 5.4.2 and 5.5.1 as a function of silane concentration, temperature and generation rate and discussed in Section 6.2.

2.5.1 The 2-Diode Model

The 2-diode model is introduced in case of *p-n* diodes, considering the recombination processes in the space charge region, caused by the presence of defect states within the gap. The theory of the ideal c-Si *p-n* junction is extensively treated in numbers of textbooks (e.g. Ashcroft and Mermin 1976, Sze 1981, Neville 1995, Böer 1995).

The 2-diode model presented here, in analogy to the 2-diode model for *p-n* junction, is needed to describe the influence of the injected charge carriers to the total current density[5] $j(V)$ in the *p-i-n* diode.

$$j(V) = j_{01}\left[\exp\left(\frac{eV}{kT}\right)-1\right] + j_{02}\left[\exp\left(\frac{eV}{2kT}\right)-1\right] + j_{ph}(V) \tag{2.21}$$

In this expression $j_{ph}(V)$ is the voltage dependent current density originating from the electron-hole pair generation by photon absorption in the intrinsic layer. Since in *p-i-n* diodes an applied voltage affect the electric field strength inside the *i*-layer and therefore the charge carrier extraction. In case of *p-n* diodes, due to the material properties and different device structure, the 'superposition principle' is valid and in the illumination case the dark current density and voltage independent photo-generated current density j_{ph} add to the total current[6].

The first term in Eq.2.21 is the so-called 'Shockley equation', Shockley (1949) and describes the current due to generation and recombination of charge carriers for the condition of low carrier injection, i.e. if the excess carrier densities Δn and Δp are small compared to the density of the majority carriers in equilibrium n_0 and p_0 (low level injection LLI). In *p-i-n* diodes this is only the case for the doped layers, because (in ideal case) for highly doped *p*-layer, $\Delta n = \Delta p << p_0$ and for highly doped *n*-layer, $\Delta n = \Delta p << n_0$.

The first term in Eq.2.21 can be neglected, since the PL measurements performed in Chapter 5 do not cover the low-level injection region. We shall consider only the second term in Eq.2.21, which describes the current, originating from recombination in the field-controlled region, i.e. the intrinsic layer in *p-i-n* solar cell. In this so-called high-level injection region (HLI), the quasi-Fermi levels for electrons and holes are defined, if the Eqs.2.16 and 2.17 are fulfilled. Under these conditions, the saturation current density j_0 can be obtained from Eq.2.21, rewritten in terms of Eqs.2.16 and 2.17:

$$np \approx \Delta n \Delta p = \Delta n^2 = n_i^2 \exp\left(\frac{eV}{kT}\right) \tag{2.22}$$

$$\Rightarrow \Delta n \approx n_i \exp\left(\frac{eV}{2kT}\right) \tag{2.23}$$

$$\Rightarrow j_0 \propto n_i \exp\left(\frac{eV}{2kT}\right) \tag{2.24}$$

[5] Since the total current through the diode is proportional to the area, the use of current density *j* is better suited, instead of only current *I*.

[6] The description of the illuminated ideal *p-n* diode I-V characteristic is given by: $j(V) = j_0\left(\exp\frac{eV}{kT}-1\right) + j_{ph}$.

Consequently, the saturation current density j_0 shows linear dependence on the intrinsic charge carrier density n_i. The factor 2 in the exponent of the Eq.2.24, i.e. diode quality factor n, indicates a dominant recombination current in the bulk region of the i-layer. A more general approach allows the two terms in Eq.2.21 to be combined to a single term by introducing the diode quality factor n and the j_0.

$$j(V) = j_0\left[\exp\left(\frac{eV}{nkT}\right) - 1\right] + j_{ph} \tag{2.25}$$

A diode quality factor of $n \approx 2$ is already introduced in Eq.2.24 and indicates a dominant bulk recombination, while $n \approx 1$ indicates a dominant diffusion current and subsequent recombination in the doped layers. Note the different recombination processes.

For our experimental conditions of open external circuit $(j(V) = 0)$, a voltage across the i-layer builds up, which can be identified as open circuit voltage V_{oc}. Since, no current flows via the external circuit, V_{oc} adjusts to a value, which can be described as a compensation of the photo-generated current density j_{ph} by the dark current density $j_{dark}(V_{oc})$. In this case the Eq.2.21 can be rewritten for the ideal case of a voltage independent photo-generated current as:

$$V_{oc} = \frac{nkT}{e}\ln\left(\frac{j_{ph}}{j_0} + 1\right) \tag{2.26}$$

Higher open circuit voltages V_{oc} are obtained, if the saturation current density j_0 of the diode is low, which depends on properties including the band gap, temperature and defect density.

In Eq.2.21, the total current density $j(V)$ at $V = 0$ is defined as short circuit current density j_{sc}. Since there is no contribution from the dark current under these conditions, in the ideal case j_{sc} equals the photo generated current j_{ph}

$$j_{sc} = j(V = 0) = j_{ph}(V = 0) \tag{2.27}$$

If the device shows efficient carrier extraction behaviour at $V = 0$, j_{sc} is mainly determined by the amount of the photo generated charge carriers. The open circuit voltage V_{oc} and j_{sc} together with the fill factor FF are the parameters usually used to describe the solar cells I-V characteristics under illumination. Since the present thesis do not provide I-V characteristics measurements, a detailed discussion on this topic seems to be not appropriate.

Chapter 3

3 Experimental Details

This chapter will start with a short description of the deposition techniques used for the preparation of μc-Si:H films and solar cells, employing the material as absorber layer. A plasma enhanced chemical vapor deposition (PECVD) method and more recently attracted attention hot-wire chemical vapor deposition (HWCVD) process were used to improve deposition rates, the stability and the quality of the microcrystalline material. After that, the cell design of the *p-i-n* configuration used throughout this work is sketched. The second part provides an overview of the photoluminescence (PL) experiment as the main characterization technique used in this work to obtain information on electronic properties of the μc-Si:H films and solar cells. In this section, the advantages of the Fourier transform (FT) method over the grating spectroscopy are reviewed at first, followed by the description of the experimental set-up. Then, an overview of the applied modulation technique used to study photoluminescence in solar cells, together with the corresponding experimental set-up is given. By using this technique, it was made sure that only the recombination of those carriers, which are taking part in the photovoltaic process, is probed. Furthermore, the optical generation rate measurements of solar cells are discussed. The last part, introduces some details of the Raman spectroscopy method used to explore the structural properties of μc-Si:H films and devices.

3.1 Material and Solar Cell Preparation

This section provides a short description of the deposition processes used for the preparation of the μc-Si:H sample series. Following are some brief remarks on the influence of the deposition parameters on the material properties. The experimental details of the investigated sample series are also provided. A brief discussion on the difference between *p-n* and *p-i-n* junction devices is given and the *p-i-n* concept related to μc-Si:H thin film solar cells is reviewed.

3.1.1 Very High Frequency PECVD Process

Various methods for the preparation of amorphous and microcrystalline silicon thin films are currently in use.

Plasma enhanced chemical vapor deposition (PECVD, also: glow discharge deposition) is the most prominent method for deposition of μc-Si:H as this technique is well established for manufacturing device grade amorphous silicon films. In this process hydrogen containing gases like silane (SiH_4) are decomposed in a radio frequency (RF) glow discharge between planar electrodes that serve to couple-in the RF-power of frequency usually 13.56MHz (RF-PECVD). In case of higher excitation frequency (e.g. 95MHz), the preparation technique is referred to as very high frequency PECVD (VHF-PECVD). The schematic outline of the PECVD process between planar electrodes is illustrated in Figure 3.1. Externally applied electrical energy is used to provide the activation energy for gas decomposition in the glow discharge deposition process by the acceleration of electrons. This allows choosing substrate temperature independently from the plasma conditions, which is an important advantage of this technique. When SiH_4 is used as a source gas in the glow discharge process, the electron-impact processes leads to reactive neutral species, e.g. SiH, SiH_2, SiH_3, Si_2H_6, H and ionized species, e.g. SiH^+, SiH_2^+, and so on. The possible electron-impact dissociation reactions, which can be of importance for the growth processes are given by the following equations (Doyle et al. 1990):

$$e^- + SiH_4 \rightarrow SiH_2 + 2H + e^- \tag{3.1}$$

$$e^- + SiH_4 \rightarrow SiH_3 + H + e^- \tag{3.2}$$

Which of the two dissociation products, SiH_2 or SiH_3 contribute to the growth of the solid films onto the substrate is under debate (Vepřek et al. 1989, Gallagher et al. 1989, Perrin 1991). Also the film growth mechanism of amorphous and microcrystalline silicon, in particular the role of hydrogen, is still not clear. Several deposition models exist: partial chemical equilibrium describes the growth of μc-Si:H as a combination of two concurrent processes, deposition of silicon from the gas phase and silicon desorption from the surface due to atomic H (Vepřek 1990); preferential etching describes the microcrystalline growth by the preferred etching of amorphous silicon by hydrogen atoms (Fang et al. 1991, Heintze et al. 1993); the diffusion model refers to H coverage of the surface and the enhanced diffusion of the precursors (Matsuda 1983); chemical annealing model describes the formation μc-Si:H by the relaxation of stressed *Si-Si* bonds in the presence of atomic H (Shirai et al. 1991).

The properties of the resulting films and especially whether its structure is microcrystalline or amorphous depend on the deposition parameters such as silane to hydrogen ratio in the gas phase, plasma excitation frequency, substrate temperature, discharge power density and total gas pressure. One of the most important process parameter to control the structure of the material is silane concentration *SC*, i.e. the ratio of silane gas flow and total gas flow $\left(SC = [SiH_4]/[SiH_4 + H_2]\right)$. In particular, a high concentration of hydrogen in the plasma or high discharge power can establish microcrystalline growth conditions. Moreover, higher excitation frequencies were found not only to improve the deposition rates of RF-PECVD process, but also leads to higher crystalline volume fractions and larger crystallites (Finger et al. 1994).

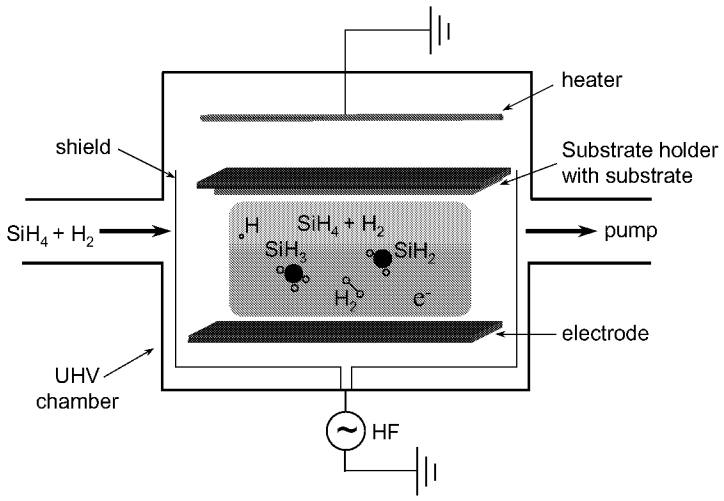

Figure 3.1: Schematic outline of the PECVD process of $SiH_4 + H_2$ decomposition in RF-glow discharge between planar electrodes.

The other deposition parameter, like discharged power density is found to increases the electron temperature of the plasma, resulting in a higher deposition rate. Throughout the present work three undoped μc-Si:H sample series prepared using a very high frequency PECVD process of 95MHz at substrate temperatures T_S of 200°C, 230°C and 325°C, and silane concentrations *SC* between 2% and 17% were studied. The applied discharge power was 8W on a substrate area of 10×10cm^2, and the total process gas pressure was 40Pa. Two deposition systems were used. One sample series was deposited in the multichamber system consisting of six parallel plate reactors ('6K') with optimised design for process temperature of 200°C with silane concentration varied in the range from 2% to 8%. The above outlined series of samples were not only part of extensive photoluminescence measurements (Carius et al. 2003a) but also of electron spin resonance (ESR) and dark conductivity measurements (Baia Neto et al. 2002). For the deposition of the other two sample series, a cluster system with four process chambers and a central transfer lock ('CT') was used, since higher substrate temperatures could be achieved (Gross 2001, Vetterl et al. 2002). The films were deposited on roughened quartz substrates for the photoluminescence measurements to avoid both the interference fringes and to reduce the effect of the internal reflection of the luminescence in the film. Film thickness was about 3-4μm or 0.2-0.5μm for the different series (see Appendix B, Table B.2).

3.1.2 Hot-Wire CVD Process

Hot-wire chemical vapor deposition (HWCVD) is now becoming a mature technique in the field of thin silicon film deposition. In HWCVD, silicon deposition takes place upon catalytic decomposition of the reactant gases (silane and hydrogen in the case of μc-Si:H growth) at the surface of a hot filament heated at temperatures in the range of 1500-2000°C.

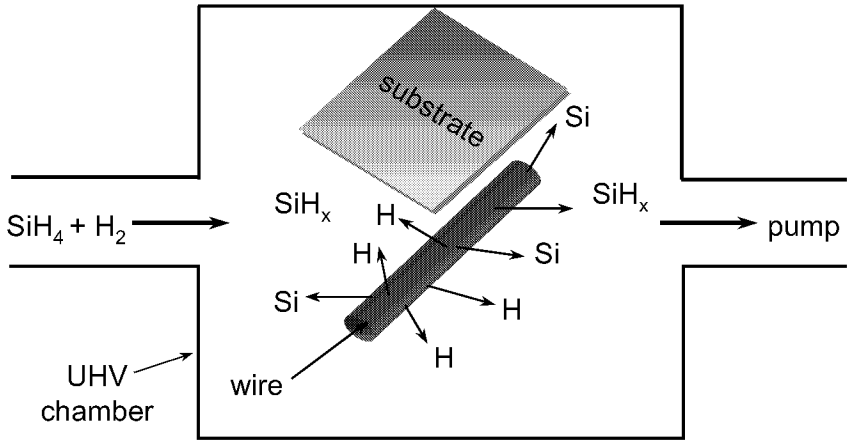

Figure 3.2: Schematic outline of the HWCVD process on the filament. The figure is taken from Klein (1999).

Thus, this technique is also referred to as catalytic CVD (Cat-CVD). HWCVD offers several features that is believed to overcome some limitations of PECVD: lack of electron or ion impact effect during deposition, high deposition rates, unlimited scalability to large areas due to the simplicity of its geometry and low equipment, and upkeep costs. In HWCVD process at first the gas molecules like SiH_4 and H_2 are catalytically dissociated, very likely to *Si* and *H* radicals on hot filament surfaces. Figure 3.2 shows schematic outline of the HWCVD process on the filament. The formation of *Si*- and *H*-atoms are thermally activated processes, since the adsorbed on the filament surface primary radicals are immediately released when the filament temperature T_F is high enough. Then the produced primary species diffused throughout the gas phase. Before reaching the substrate, they can react with other molecules or radicals if the mean free path between collisions is shorter then the filament-substrate distance. That is achieved at high pressures (> 1Pa). The most important gas phase reactions are the reactions of *Si* and *H* radicals with SiH_4 molecules:

$$Si + SiH_4 \rightarrow HSiSiH_3^* \tag{3.3}$$

$$H + SiH_4 \rightarrow SiH_3 + H_2 \tag{3.4}$$

Both reactions are exothermic without energy barrier and the estimation of the reaction rates from Perrin et al. (1996) shows that they are of the same order as the collision rates of *Si* radicals with SiH_4 molecules according to Molenbroek et al. (1996). The product of reaction (3.3) is a $HSiSiH_3^*$ radical with most possible reaction path of isomerisation to disilane H_2SiSiH_2, which likely is a precursor for growing of high quality films.Further insertion of disilane into silane at high pressure leads to formation of higher silanes ($Si_xH_n, x \geq 3$) and porous films with poor electronic properties are grown (Molenbroek et al. 1996).

The product of the reaction (3.4) is the less reactive silane radical SH_3, which cannot react in the gas phase with SiH_4 or H_2 molecules since it can only react by radical-radical reactions, becoming important at high pressures. Therefore H is not likely to cause large variation in film growth but further radical-radical reactions with second SiH_3 radical have high reaction probability to occur. Leading to formation of intermediate product and then trough 'insertation reaction' with SiH_4 to higher silanes Si_2H_6 and Si_3H_8. Finally, surface reactions leads to film growth of microcrystalline silicon. The main parameters here are the kind and the energy of the precursors heating the substrate surface, and the substrate temperature T_S. All existing deposition models (see Section 3.1.1), which try to explain the influence of the hydrogen in the growth of amorphous and microcrystalline PECVD films, can be in principle applied to the HWCVD process (see Klein 2003a).

The material properties of microcrystalline silicon and the deposition rates r_D of HWCVD process are strongly affected by the combination of the deposition parameters used. The main parameters and their major effect in case of silicon deposition from SiH_4 and H_2 are:

- The high filament temperatures T_F and large surface areas of the filaments provide thermally activated dissociation of SiH_4 and H_2 molecules and formation of radicals on the filament therefore high depositions rates were achieved. The filament temperature is found to have a very strong influence on the substrate temperature, i.e. high T_F leads to an increase of T_S (Klein et al. 2001).
- The substrate temperature influences the processes at the growing film surface. The high T_S above 300°C leads to high defect density due to enhanced hydrogen desorption during the deposition process. That results in poor defect passivation, despite the possible positive effects of higher T_S on the grain size and crystalline volume fraction (Finger et al. 2002). Optimised film quality was achieved by lowering the substrate temperature to values typically used in PECVD processes as well as by lowering the deposition pressure, resulting in low deposition rates (Klein et al. 2003).
- The deposition pressure p_D is of importance for the production of radicals on the filaments too. Increasing the pressure leads to formation of more *Si*-radicals and thus to high deposition rate. However at high p_D the reactions in the gas phase have to be considered as the reason for bad material quality.
- The silane concentration has direct impact on the ratio of the growth precursors to hydrogen atoms in the gas phase. Thereby it is an easy tool to control the transition between amorphous and microcrystalline growth.

For the deposition of intrinsic μc-Si:H by HWCVD studied in this work, a tantalum (Ta) wire arrangement was used at a temperature of 1650-1730°C, leading to substrate temperatures of 185-330°C, respectively (see Appendix B, Table B.1). As deposition feed gas, a mixture of silane and hydrogen at different silane concentrations between 2% and 25% were used to obtain material of highly crystalline to amorphous structure and the deposition pressure was maintained at 5Pa. The films had a thickness of 0.3-0.4μm or 1μm for the different series and were prepared on rough quartz substrates for photoluminescence (PL) measurements and on $10\times10cm^2$ in size borosilicate glass for Raman measurements.

The two sample series studied here by PL spectroscopy were part of extensive investigations by Raman spectroscopy, X-ray diffraction, transmission electron microscopy (TEM), infrared spectroscopy, electron spin resonance (ESR), optical absorption and the results are summarised in the work of Klein (2003a). One of the investigated sample series deposited at T_S of 185°C provides an excellent material for solar cell applications. The material exhibits very low spin density, low absorption below the band gap, high hydrogen content and compact structure but the achieved deposition rates are reduced (Klein et al. 2003).

3.1.3 Solar Cell Device Structure

Before starting a discussion on the requirements needed to prepare a μc-Si:H thin films solar cells with appropriate device structure, a few words have to be said about conventional crystalline silicon solar cells and about the concept related to a-Si:H devices. In c-Si based solar cells the electric field is generated by varying the type of impurity doping within the semiconductor (*p-n* homojunction) or by application of semiconductors with different band gaps (heterojunction) and also by formation of Schottky-contact. The space charge region of the *p-n* junction depends on the doping level and is typically less then 0.5μm thick for a wafer based c-Si solar cell. Under illumination charge carriers (usually the main fraction) are generated by photon absorption outside the space charge region. These carriers get by diffusion to the space charge region, where they can be separated by the electric field therein. If the minority carriers, i.e. electrons in the *p*-doped and holes in the *n*-doped regions reach the space charge region, they will contribute to the photo-generated charge current flow (voltage independent). Since the charge carriers diffuse to the *p-n* junction, crystalline silicon solar cells are called 'diffusion solar cells'. In a-Si:H devices, the short diffusion lengths[7] and low mobility-lifetime product for holes, $\mu_p\tau_p$, does not allow the *p-n* cell concept (Sauvain et al. 1990). Therefore, an intrinsic (*i*-) absorber layer between the thin *n*-doped and *p*-doped layers is necessary to expand the electric field across the *i*-layer. Due to expansion of the electric field, generated by the doped layers, a direct separation of the photo-generated charge carriers is achieved by drift in the electric field and the photo-generated charge current is significantly voltage dependent, already for a thickness below 1μm. This type of solar cells is called 'drift solar cells', in contrast to *p-n* junction.

For μc-Si:H thin film solar cells has turned out that the same *p-i-n* (or *n-i-p*) concept as in amorphous silicon is favourable. However, in case of intrinsic μc-Si:H absorber layer, it is still unclear what is the contribution of the diffusion to the transport of the photo-generated charge carries in the device and what is the importance of the electric field for the carrier extraction. In this work, μc-Si:H thin film solar cells in *p-i-n* deposition structure was studied, as shown in Figure 3.3. A *p-i-n* deposition sequence was applied on glass substrates coated with textured aluminium doped zinc oxide (ZnO:Al) for illumination from the *p*-layer. Magnetron sputtered ZnO:Al is used here as transparent conductive oxide (TCO) material.

[7] The diffusion length, *L*, represents the average distance, which photo-generated carriers travel in random walk during their lifetime before recombining, i.e. $L = \sqrt{D\tau}$, where D is diffusion coefficient and τ is the lifetime.

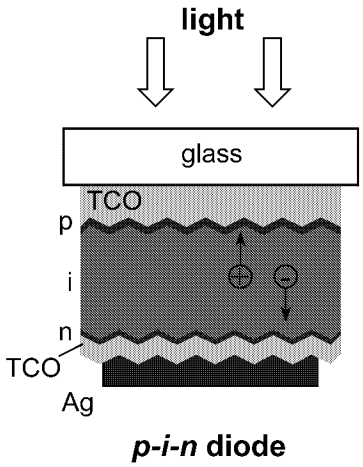

Figure 3.3: Schematic drawing of *p-i-n* structure of μc-Si:H solar cells. The device is illuminated from the *p*-side.

A high transparency in the wavelength range from 300nm to 1100nm and high conductivity to avoid ohmic losses are the requirement for the TCO. Due to low absorption coefficient of μc-Si:H efficient light trapping[8] is also required, achieved by 'texturing' the material surface using a wet-chemical etching in diluted hydrochloric acid (HCl) (Kluth et al. 1997).

The preparation of *p*-doped μc-Si:H layer for *p-i-n* device is a difficult task since the material has to fulfil many requirements. The *p*-layer should be as thin as possible and exhibit a highly crystalline structure in order to avoid carrier losses due to absorption. On the other hand the *p*-doped layer have to be thick enough (~0.02-0.03μm) to build up an efficient electric field together with the *n*-doped layer. In addition, it was found that the use of trimethylboron ($B(CH_3)_3$) as the doping gas deteriorates the crystalline growth and enhances the absorption (Dasgupta et al. 2000).

The *i*-layer has two main functions, namely to provide maximum absorption of the incident light and also a good electrical transport of the photo-generated charged carriers, which are separated and extracted by the electric field, generated by the doped layers. With increasing the thickness of the absorber layer, the absorption increases but at the same time the collection efficiency decreases due to decreasing electric field (increasing recombination probability). Therefore, typical thickness values are between 1μm and 3μm. In this work the *i*-layer, deposited by HWCVD at T_S=185°C was between 0.85μm and 1μm thick. Another important requirement for effective carrier collection is low defect density of the material, since the defects in the *i*-layer leads to recombination of the charged carriers.

The 20nm thick amorphous silicon *n*-layer deposited by RF-PECVD is used as the second doped layer to build up the electric field.

[8] The incident light is scattered by a rough surface. Then significant fraction of the long wavelength light is trapped within the device due to multiple reflections between back reflector and front contact (ignoring reflections at other interfaces) and thereby more efficiently absorbed in the intrinsic layer.

The back-reflector consisting of a second ZnO film and thermally evaporated silver (Ag) is prepared as the contact pad, defending the area of the solar cell. The second ZnO film is of importance since significantly improvements of the reflectivity, increasing the short circuit current, were achieved. The *p-i-n* solar cells investigated in this work provide very high quality μc-Si:H solar cells with *i*-layers covering the structural composition range from fully crystalline (*SC*=3%) to more then 50% amorphous volume fraction. Within this series the highest solar cell efficiency up to 9.4%, reported for microcrystalline HW cells are observed in addition to the highest V_{oc} reported so far for microcrystalline solar cells (Klein et al. 2002).

3.2 Photoluminescence Characterization

Photoluminescence (PL) spectroscopy is proven to be a powerful tool to investigate the electronic structure of material, providing information on the band gap, defect identification and material quality. In the luminescence experiment, the samples are excited with an optical source, typically a laser with $hv > E_g$, generating electron-hole pairs. Photoluminescence is the radiation emitted by the recombination of photo-excited electrons and holes and as such is a direct measure of the radiative transitions. Information about non-radiative recombination can often be deduced from the luminescence intensity, which is reduced by the competing processes. The most useful feature of the luminescence experiment is the ability to measure the emission spectrum to obtain information about the energy levels of the recombination centres. The photoluminescence spectra of μc-Si:H mixed phase material, measured at low temperature reveal two emission bands: one rather broad featureless emission band at about 0.95eV, characteristic for the microcrystalline phase and a second PL band at 1.35eV, often observed at high silane concentration and attributed to amorphous phase. An additional PL band, centred at 0.7eV is also observed for high defect density material. Therefore the photoluminescence measurements on μc-Si:H thin films and solar cells in Chapters 4 and 5 are performed in the near-infrared regions.

3.2.1 Fourier Transform-Photoluminescence Spectroscopy

Until recently, the grating spectroscopy was the general technique to study photoluminescence (PL) in visible and near-infrared spectral range. It is a known fact that grating spectroscopy is not providing the most effective use of limited power of light radiation having wavelengths greater than 1000nm (or $E < 1.24$eV) (Perkowitz 1993). However, spectroscopic studies using Fourier transform (FT) method make efficient use of the available power of light radiation having energies less then about 1.3eV with the help of a basic process namely the light wave interference. Besides the high wavenumber accuracy, FT-PL spectroscopy offers substantial improvement in the analysis of weak signals over grating spectroscopy. One reason is the Fellgett advantage, which states that the signal-to-noise ratio is higher when all relevant wavelengths are measured at the same time (simultaneously), as in FT-PL spectroscopy, as when one wavelength is measured at a time, as in grating spectroscopy.

The second reason is the Jacquinot or throughput advantage, which means that high resolution can be attained in FT-PL spectroscopy without using narrow slits, whereas in conventional spectroscopy there is always a trade-off between resolution and the light flux from the sample. Further advantages of the method can be found in the literature (Bell 1972). Fourier transform spectroscopy was successfully used in the present doctoral thesis for sensitive measurements of the photoluminescence spectra of μc-Si:H thin films and devices.

3.2.2 Experimental Set-up

For the photoluminescence measurements, the microcrystalline silicon thin films were deposited on roughened quartz substrates to suppress the strong optical interference effect, which modulates the spectrum and to reduce the effect of the internal reflection of the luminescence in the film. The photoluminescence experiments were carried out at temperatures of 10-300K, using a FT-IR spectrometer in conventional or in step-scan mode coupled with a liquid-nitrogen (LN_2)-cooled Ge (or InAs) detector, applying a lock-in technique to enhance sensitivity when necessary.

The layout of experimental set-up for the FT photoluminescence measurements is shown in Figure 3.4. For excitation of the photoluminescence, different laser wavelengths of 488nm (excitation energy, $E_x = 2.54\,eV$) from an ion Ar^+ laser, 632.8nm ($E_x = 1.96\,eV$) from a He-Ne laser and 780nm ($E_x = 1.59\,eV$) from an IR diode laser was used. At 488nm the photoluminescence contributions from the surface of the film are probed, while at 632.8nm and 780nm almost homogeneous excitation across the 1μm thick sample can be achieved. Optical filters are important components, which will affect the overall outcome of the PL experiment. Therefore, cold glass KG5 filter was used to suppress the IR emission of the laser light, before the mirror reflects the laser beam into the spectrometer, whereas neutral density filters are used to reduce the intensity of the laser beam. The samples are mounted in a continuous flow cryostat Oxford CF 1204. For the cooling of the system, liquid helium or nitrogen from separate storage vessel is drawn trough a transfer tube and is fed directly into the sample space, providing a flowing or 'dynamic' exchange gas. Precise temperature control is obtained using a temperature sensor and heater attached to the heat exchanger, in conjunction with an automatic temperature controller ITC-4 from the same company. The emitted luminescence light of the sample is collected with a mirror into the entrance aperture of the FT-IR spectrometer Bruker IFS66v with resolution of $0.25cm^{-1}$. In the spectrometer the luminescence light is split into two beams at the beam splitter, which is a partially transmitting mirror. One half of the radiation intensity goes trough the beam splitter, whereas the other half is reflected. Both beams are reflected back to the beam splitter by two mirrors, one fixed and one moving mirror, where an interference occurs. In the present PL experiment a TiO_2 coated quartz beam splitter was used, covering a spectral range from 1.86eV (667nm) to 0.41eV (3030nm). The principle of the FT-IR in conventional mode is to detect small variations in the light intensity as a mirror in one arm of a Michelson interferometer is moved back and forth by the distance x. The modulated radiation, going out from the interferometer, is finally focused on the detector.

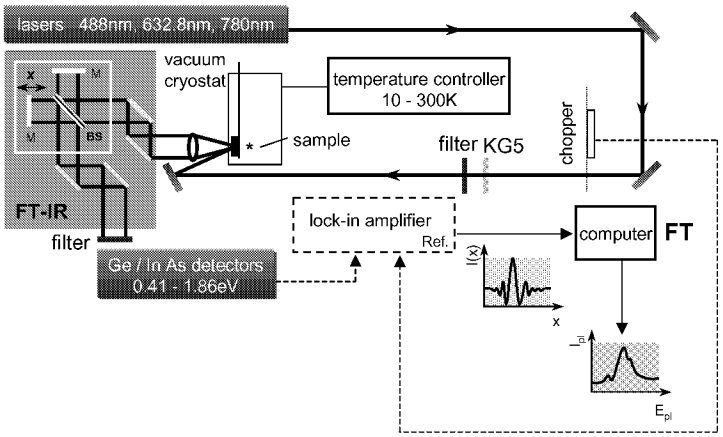

Figure 3.4: The layout of a typical experimental set up for the FT photoluminescence measurements.

The quantity actually measured by the detector is thus the intensity $I(x)$ of a luminescence light of the sample as the function of the moving mirror displacement, the so-called interferogram. The LN_2-cooled (77K) Ge detector built-in amplifier, model EO-817 with high sensitivity and a good signal to noise ratio in the near IR spectral region of 0.7-1.5eV was chosen. The use of edge filters in front of the detector, which are nearly transparent for the near IR and IR spectral region, is necessary to block the internal He-Ne laser used to control the Michelson interferometer as well as to block the wavelength of the exiting laser light. Different edge filters were applied: for the ion Ar^+ laser a RG 695, for the He-Ne laser a RG 715, and for the diode laser emitted in the IR spectral range, a RG 815 and an additional RG 1000. For spectral range extension of the photoluminescence experiment up to 3125nm ($E_x = 0.39\,eV$), an LN_2-cooled InAs detector with lock-in technique was used, to deal with weaker signals and to minimise the effect of the noise. The detector output signal is fed to a lock-in amplifier and synchronized to a chopper in the laser path for enhanced signal-to-noise ratio. An ITHACO 1211 current preamplifier with main amplifications from 10^3 to 10^{11} V/A with a range of nine decades current gain was applied. Before starting the experiment, the dark current of the InAs photodiode was compensated through the output of the current preamplifier. Finally, by the use of computer and special software, the two domains of distance and frequency of the completed interferogram are converted by the mathematical operation called fast Fourier Transformation (FFT) into the PL spectrum.

3.3 Modulation Technique

The photoluminescence on the μc-Si:H solar cells in *p-i-n* deposition sequence, employing the material as absorber layer were exited and measured through the glass substrate. In order to avoid spurious photoluminescence signals from the glass, TCO and *p*-layer and to investigate only those carriers, which are taking part in the photovoltaic process a modulation technique was applied.

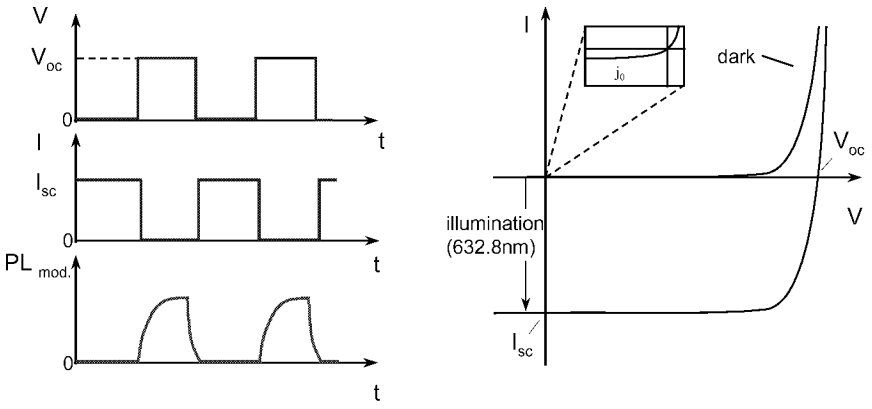

Figure 3.5: Schematic illustration of the modulation technique together with solar cell I-V characteristic in the dark and under illumination.

Figure 3.5 shows the schematic illustration of the applied technique together with solar cell I-V characteristic in the dark and under illumination. By using a pulse generator, an external voltage was applied to the continuously exited solar cells with the excitation light of full intensity. Upon change of the voltage across the cell from 0V to V_{oc}, a change of the PL signal was detected with lock-in technique. The short circuit current I_{sc} was monitored with a digital oscilloscope (Le Croy 9400). The contact area was typically 1mm^2. The maximum PL signal is obtained at V_{oc} where full carrier recombination and no extraction in the *i*-layer are expected. The minimum PL signal is obtained at I_{sc} -full carrier extraction and no recombination in the *i*-layer occurs. By using this technique only carriers relevant for the photovoltaic process are probed.

The solar cell measurements using modulation technique are performed in the similar experimental set up like the FT photoluminescence measurements, shown in Figure 3.6. The experiment was carried out in the same continuous flow helium cryostat using 632.8nm line of a He-Ne laser with a maximum power density of 5.9W/cm^2. The laser spot was adjusted to match the 1mm diameter rear silver contact, determining the contact area of the device. A pulse/function generator HP 8116A was used to modulate the applied voltage and a digital oscilloscope LeCroy 9400 to monitor the current. A modulation frequency of 15Hz was used to assure a full modulation of the current via a load resistor (50Ω). For this measurement the FTIR spectrometer has to be operated in so-called step scan mode. Where, the mirror moves in steps and at each step a data point of the interferogram is taken with lock-in technique. The experiment is repeated at different positions of the interferogram, including a waiting time that allows the lock-in amplifier to settle to a new signal level. By switching between open circuit voltage and short circuit current, the change of the photoluminescence signal (see Figure 3.5) is observed by the Ge detector EO-817L. An additional electronic filter, i.e. Muon filter 829B was used for the Ge detector, as a signal processing unit permits suppression of the signal spikes caused by cosmic and other environment ionizing-radiation, depositing charge in the active volume of the *p-i-n* devices.

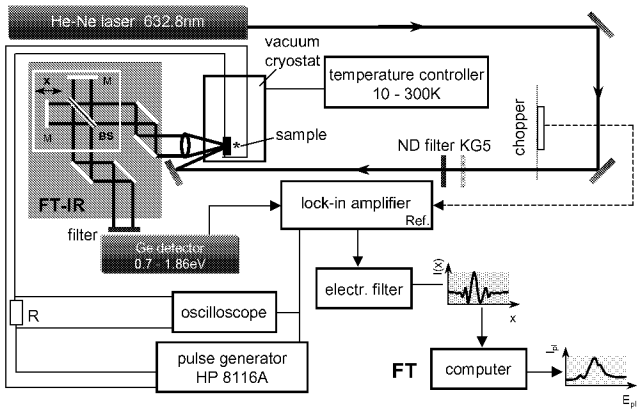

Figure 3.6: The layout of experimental set up for the photoluminescence measurements using modulation technique.

Parallel with the solar cell measurements using modulation technique, for high sensitivity photoluminescence, the excitation light was modulated with modulation frequency of 19Hz by a chopper. A lock-in amplifier technique was applied to measure simultaneously the luminescence signal. The open circuit voltage V_{oc} and short circuit current I_{sc} measurements were performed in the same optical configuration as the photoluminescence by using a Keithley 2400 source meter under DC conditions.

3.4 Optical Generation Rate Measurements

The optical generation rate g_o, denotes the number of optically created electron-hole pairs per second and unit volume. It was calculated by taking into account the photon flux ϕ at the sample and optical absorption coefficient α ($1.4\times10^4 cm^{-1}$ at constant photon energy of 1.96eV, see Figure 2.4). The change of the structural composition of the samples and the temperature dependence of α have been neglected, as errors related to the determination of beam diameter and light scattering effects due to the roughness cannot be quantified sufficiently. In order to calculate the photon flux, one has to determine first, the diameter of the beam and second to measure the laser power by using of standard power meter.

Having in mind that the power of the laser is a product of the number of photons N_{ph} per unit time and the energy of photon E_x, i.e. $P_{laser} = (N_{ph}/t)E_x$. Here, the photon flux of absorbed photons in the sample volume, after the reflection is subtracted, is described by a following expression:

$$\phi = \frac{P_{laser}}{E_x A} = \frac{N_{ph}}{tA} \qquad \left[\frac{1}{cm^2 s}\right], \tag{3.5}$$

where A is the illuminated area of the sample.

A rear silver contact of 1mm diameter determines the contact area and the laser spot was adjusted to match this diameter. The absorption volume can be approximated by $1/\alpha$. Therefore, the optical generation rate can be calculated as a product of the photon flux and optical absorption coefficient taken at the given photon energy by:

$$g_o = \phi\alpha \qquad \left[\frac{1}{cm^3 s}\right] \tag{3.6}$$

Neutral density glass filters have been introduced to vary the photon flux as shown in Figure 3.6 Thus, the intensity of the 632.8nm ($E_x = 1.96\,eV$) laser light with a maximum power density of 5.9W/cm^2 could be reduced over three orders of magnitude.

3.5 Structural Characterization

Characterization of thin film μc-Si:H layers, found to be inhomogeneous of the order of several tens of a nanometer, is a difficult task. The mixed phase structure of μc-Si:H, formed by amorphous and crystalline regions of small crystallites, clustered to a columns or grains (see Section 2.1), makes the task even more complicated. A critical point of the structural investigation is the determination of the crystalline volume fraction, which is an important parameter to correlate the structural and electronic properties. In this section, some details of the Raman spectroscopy as powerful method of semiquantitative determination of the crystalline volume fraction and a very useful technique in predicting trends in the crystallinity in μc-Si:H samples is outlined.

3.5.1 Raman Spectroscopy

Raman spectroscopy is the most commonly used experimental technique to measure the fundamental optical and vibrational properties of solids. Raman scattering in solid state is described as inelastic scattering of a photon under emission (Stokes process) and under absorption (anti-Stokes process) of a phonon. From the Raman spectra information about the structural properties of the material can be obtained. An extensive discussion of the theory of the method is given in the literature (e.g. Long 1977, Cardona 1982). An overview of the application to μc-Si:H can be found in the works of Richter (1983) and Hapke et al. (1995). Due to the long range order of the silicon atoms and hence the appearance of translation symmetry within microscopic regions of μc-Si:H with well defined electronic transitions and selection rules, a clear difference in the Raman spectra of crystalline and amorphous silicon is expected. Figure 3.7 shows typical Raman spectra of crystalline (c-Si), amorphous (a-Si:H) and microcrystalline silicon (μc-Si:H), obtained in the spectral range from 400cm^{-1} to 560cm^{-1} in which the transverse optical (TO) phonon mode in crystalline and amorphous silicon is active. The main feature in the Raman spectrum of crystalline silicon is a band with a full width at half maximum (FWHM) below 15cm^{-1} centred at 520cm^{-1} corresponding to the excitation of the Γ'_{25} phonon.

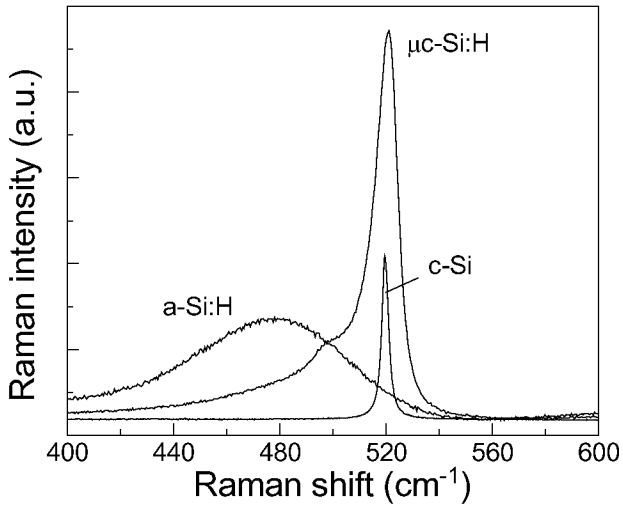

Figure 3.7: Raman spectra of crystalline silicon (c-Si) together with amorphous silicon (a-Si:H) and microcrystalline silicon (μc-Si:H). Note, that the height of the latter two Raman spectra was chosen to have equal intensity.

A broad band with FWHM of about 70cm^{-1}, centred at 480cm^{-1} characterises the Raman spectrum of amorphous silicon, related to the disorder and relaxed momentum selection rules, i.e. all the phonons contribute to the spectrum. Both features are observed in the Raman spectra of microcrystalline silicon with different contributions. An additional contribution from structural defects of the crystalline phase (stacking faults) leads to the hump at 492cm^{-1}. This was previously found in the presence of hexagonal silicon (Kobliska and Solin 1973). Due to finite grain size and stress in μc-Si:H, the peak arising from the crystalline signal contribution is often shifted with respect to the resonance of the Γ'_{25} phonon in c-Si and broadening effects are observed (Richter et al. 1981).

In order to quantify the crystalline volume fraction, the Raman spectrum of a μc-Si:H shown in Figure 3.8 is deconvoluted into three Gaussian lines. The ratio of the integrated Raman intensity of the crystalline phase $I_c = I_{520} + I_{505}$ (fitted by two Gaussian lines at 520cm^{-1} and 505cm^{-1} to take care for the asymmetry) to the total scattering intensity ($I_a + I_c$, where $I_a = I_{480}$ is the amorphous intensity) was taken as a measure of the crystalline volume fraction in Eq.3.7:

$$I_C^{RS} = \frac{I_{520} + I_{505}}{I_{520} + I_{505} + I_{480}} \tag{3.7}$$

where I denote the area of Gaussian lines fitted to the spectra.

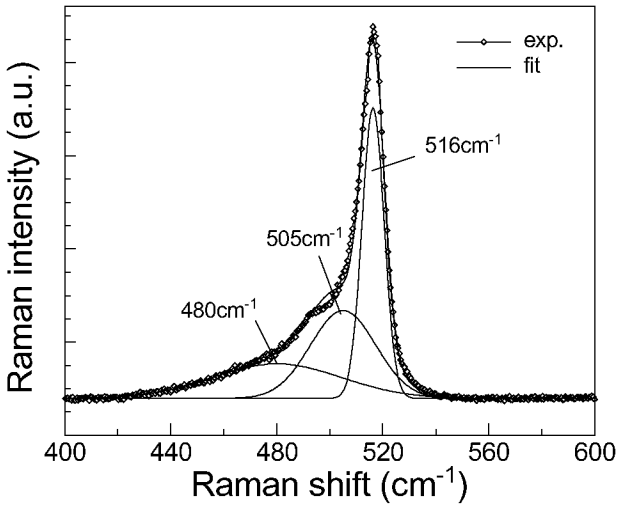

Figure 3.8: Typical Raman spectrum of a μc-Si:H, deposited by PECVD and fitted by three Gaussan peaks centred at 520cm^{-1}, 505cm^{-1} and 480cm^{-1}.

The evaluation of the integrated Raman intensity ratio from Eq.3.7 has to be performed with great caution. In highly crystalline material, assignment of the Raman mode at 480cm^{-1} to amorphous regions leads to strongly overestimation of the contribution of the amorphous phase (Vepřek et al. 1987). One rather can attribute this feature to disordered regions e.g. at the grain boundaries than to extended amorphous phase [9]. On the other side, in predominantly amorphous material, an underestimation of the crystallinity can be seen comparing with results of X-ray diffraction (XRD) measurements (Houben et al. 1998a). Thus the I_C^{RS} only provides a lower limit for the actual crystalline volume fraction, if not corrected for Raman scattering cross section and optical absorption.

To study the distribution of the crystalline volume fraction along the growth direction of the μc-Si:H films and solar cells, Raman scattering measurements were performed using different photon excitation energies[10]. The corresponding information depth of the Raman scattering experiment is half of the absorption depths for probe incident light, absorbed with intensity $I(d) = I_0.e^{-\alpha(\lambda)d}$. The absorption depth is defined as a depth where the intensity of the light decreases to $1/e$ of the incident intensity. The reduced information depth of the Raman experiment is due to of a strong absorption of scattered light at a distance d before it leaves the sample and can be detected.

[9] Since Raman scattering experiment is based on phonon excitation, effects on the spectra by the disorder related to smaller grain size and consequently a higher density of grain boundaries are expected.

[10] The structural thickness dependence of the Raman scattering experiment given by the quantity $e^{-2\alpha d}$ for different excitation light wavelength, using the absorption coefficient α of highly crystalline μc-Si:H film is given in Vetterl (2001), p. 23.

Therefore the Raman signal intensity is proportional to $e^{-(\alpha(\lambda)+\alpha(\lambda+\Delta\lambda))d} \approx e^{-2\alpha(\lambda)d}$, where $\alpha(\lambda+\Delta\lambda)$ is the absorption coefficient of the scattered light with wavelength $\lambda+\Delta\lambda$ ($\Delta\lambda$ is the Stokes shift). In difference to information depth of Raman scattering, the information depth of photoluminescence process is almost equal to the absorption depth, while the absorption coefficient of the PL light is much lower then the absorption coefficient of the incident light. Using photons of energy equal to 2.54eV, contribution from the surface part of the film and *i*-layer of the solar cells are emphasized, while at 1.96eV homogeneous excitation across the 1μm can be assumed. Raman scattering and photoluminescence measurements (see Sections 4.2 and 5.1) performed at various excitation energies are important, because they provide an evidence for significant difference of microcrystalline formation and structural inhomogeneity in the growth direction for most of the samples studied in this work. In particular for material with a significant content of both crystalline and amorphous volume, the nucleation effect near the substrate film interface can play a dominant role. Leading to drastic changes of the crystallinity compared to the bulk growth. The initial amorphous growth in that case may result from suppressed grain growth rather than nucleation, since the high-resolution electron micrographs give an evidence for nucleation of microcrystals (Houben et al. 1998a). In summary, we have to say that despite all discrepancies in the evaluation of the Raman intensities of the different phases, the Raman spectra are very useful in determining trends in the crystallinity of the μc-Si:H samples, demonstrated in Section 6.1.3. However, up to now, they do not allow the quantitative determination of the crystalline volume fraction.

Chapter 4

4 Photoluminescence Results on Undoped μc-Si:H Thin Films

The outline of this chapter is as follows: Firstly, the problem of changes of electronic properties of microcrystalline silicon (μc-Si:H) films upon changes of the hydrogen dilution during film growth is addressed by careful investigation of localized states in this material using photoluminescence spectroscopy. Secondly, the correlation between microstructure and photoluminescence energy is investigated by comparing photoluminescence and Raman spectra of high-quality sample series prepared by PECVD and HWCVD. Then the influence of the deposition parameters like substrate temperature on the photoluminescence properties is presented.

Furthermore, by making use of the good spectral separation of the bands related to amorphous and crystalline volume fractions, photoluminescence measurements are used as a sensitive probe for small amorphous volume fractions in the film or at the film/substrate interface. Moreover, low photon of energy excitation down to 1.59eV was used to suppress the emission band at about 1.35eV characteristic for the amorphous phase to study preferentially the PL properties of the low energy band, identify as 'μc'-Si-band. The study of the temperature dependence measurements of the photoluminescence intensity and peak energy was used to explore information on both, the diffusion of carriers and the distribution of states in microcrystalline silicon.

4.1 Influence of the Silane to Hydrogen Ratio in the Gas Phase on the Photoluminescence Properties

The present section deals with the influence of the process gas mixture of silane to hydrogen, i.e. silane concentration $SC = [SiH_4]/[SiH_4 + H_2]$ on the photoluminescence properties, such as photoluminescence peak position, width and intensity of the luminescence spectra. The influence of SC is studies, since it is one of the key deposition parameter to control the microstructure of μc-Si:H (see Figure 2.1).

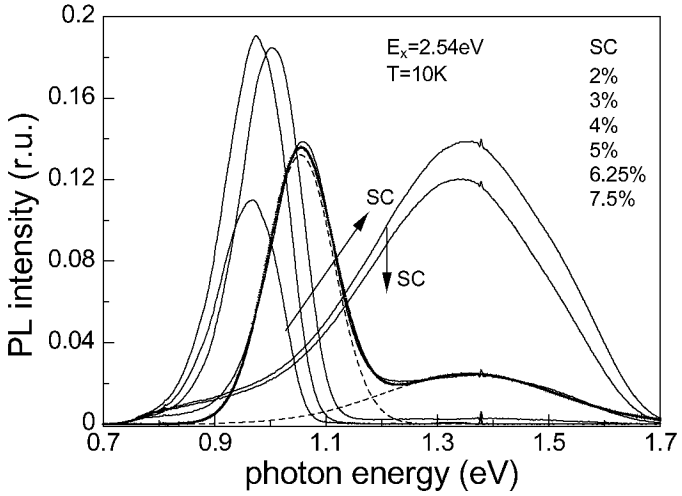

Figure 4.1: Photoluminescence spectra of μc-Si:H thin films prepared by HWCVD at T_S=185°C with the indicated silane concentration values, measured at 10K with a Ge detector. For the sample grown at *SC* of 5%, the solid line is the measured PL data and the dashed lines are the fitted curves.

The photoluminescence was exited with photons of energy E_x = 2.54 eV and performed at 10K to avoid the influence of thermally activated non-radiative transitions. Thereby, a film depth of ~ 0.05-0.15μm for a-Si:H and ~ 0.3μm for fully μc-Si:H was probed. Three well characterised, very high quality sample series of nominally undoped μc-Si:H films prepared with different silane concentrations by hot wire chemical vapor deposition (HWCVD) and plasma enhanced chemical vapor deposition (PECVD) were studied. The HWCVD sample series was deposited at a filament temperature T_F of 1650°C and substrate temperature T_S of 185°C. The thickness of the films was between 0.3μm and 0.4μm (see Section 3.1.2 and Table B.1). Two PECVD series of μc-Si:H thin films were prepared by very high frequency of 95MHz process in two different deposition systems. The PECVD I series was deposited at substrate temperature T_S=200°C with a film thickness of 3-4μm required by ESR measurements (Baia Neto et al. 2002). While PECVD II at T_S=230°C had a thickness of the films 0.2-0.5μm (see Section 3.1.1 and Table B.2).

In Figure 4.1, typical photoluminescence spectra obtained at 10K for μc-Si:H thin films prepared by HWCVD at various silane concentrations from 2% to 7.5% are shown. A linear scale was chosen for the PL intensity to show the almost Gaussian shape of the luminescence spectra, observed for the material with *SC* between 2% and 4%. The corresponding, rather broad featureless emission band with the maximum peak energy at about 0.96eV and a half-width of 0.13eV is attributed to the microcrystalline phase (see Section 2.4.1). At *SC* of 5%, a second emission band at about 1.35eV is visible. This PL band is assigned to recombination in the amorphous phase of low defect density. The halfwidth of this band is about 0.37eV. Two Gaussian functions peaked at 1.05eV and 1.36eV are used to fit the PL spectrum, which obviously exhibits a mixed phase structure of crystalline and amorphous regions.

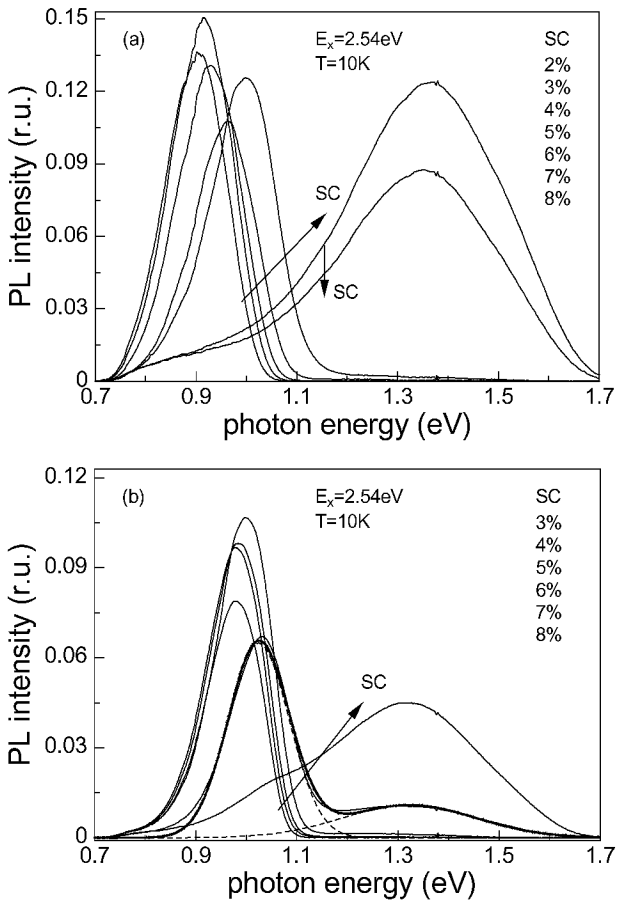

Figure 4.2: Photoluminescence spectra of µc-Si:H thin films prepared by PECVD I at T_S=200°C (a) and PECVD II at 230°C (b) with indicated values of *SC*, performed at 10K with a Ge detector. For sample prepared at *SC* of 7% (Figure 4.2(b)), the solid lines are the measured PL data and the dashed lines are the fitted curves.

Further increasing *SC* up to 7.5%, the PL spectra show typical amorphous characteristics, i.e. the high-energy PL band dominates the spectrum. The quantum efficiency of the photoluminescence is very similar for all films, and is slightly lower than that for high-quality amorphous silicon but much higher then that of single crystalline silicon. The efficiency of the material with *SC* of 2% is lower by a factor of two, which might indicate higher defect density. Figure 4.1 demonstrates two important effects: (i) the PL band at about 0.96eV ('µc'-Si-band), shifts continuously to higher energies (up to 1.05eV) with increasing *SC* and (ii) the broader PL band at 1.35eV, characteristic for the amorphous phase, is visible only at high SC from 5% to 7.5%. A slight shift of this band to lower energies was observed with increasing silane concentration.

The photoluminescence spectra of the two PECVD series of μc-Si:H thin films with different *SC* (2-8%) for PECVD I and *SC* (3-8%) for PECVD II are shown in Figure 4.2, for comparison. The luminescence spectra of the two PECVD series exhibit very similar features like the HWCVD series, i.e. shift of the 'μc'-Si-band towards higher energies by a total of about 0.1eV for PECVD I and by a total of about 0.05eV for PECVD II with increasing *SC*, and a contribution of the PL from amorphous phase for the highest *SC* (7% and 8% samples) for PECVD I and PECVD II, respectively. Also the PL efficiency and the width do not show significant differences from those of the HW series.

4.1.1 Photoluminescence Peak Energy and Width of Luminescence Spectra

In this paragraph the results of the PL peak energy position and the width of the μc-Si:H emission band are summarized with respect to silane concentration. In Figure 4.3 this two features of the 'μc'-band for different silane concentration between 2% and 7% of the investigated HWCVD and PECVD series of μc-Si:H thin films prepared at T_S=185°C and T_S=200, 230°C (PECVD I, II) are compared. In all cases, the shift of the 'μc'-Si-band towards higher energies with increasing *SC* is observed.

HWCVD and PECVD I series show a similar behaviour, i.e. the PL peak energy increases continuously to high energy with increasing *SC*. For thin films (~0.3-0.4μm) prepared by HWCVD, an increasing *SC* from 2% to 5% causes a strong, continuous shift of the PL band from 0.96eV up to particular high energies of 1.05eV. The shift of the PL band is more obvious at the highest *SC* when the emission band related to the amorphous phase appears in the luminescence spectrum of sample with *SC*=5% (see Figure 4.1). However, for significantly thicker (~3-4μm) films deposited by PECVD I, the following differences are observed: (i) the continuous shift of the PL peak energy starts at the lowest energies of 0.9eV and rises up to about 1.0eV (ii) at *SC* of 6% the PL spectrum revealed a negligible contribution from the amorphous growth interface layer (see Figure 4.2(a)). In contrast to PECVD I series, the thin films (~0.2-0.5μm) from PECVD II series show a slight shift of the PL peak energy for *SC* between 3% and 6%, and the only change was observed at a high *SC* of 7%, i.e. strong shift due to the contribution of the amorphous phase (see Figure 4.2(b)).

Furthermore, the width of the 'μc'-band remains without significant changes for a variation of silane concentration for all investigated thin films. The luminescence spectra of the HWCVD and PECVD II series of μc-Si:H thin films prepared at different *SC* show quite similar bandwidth FWHM between 0.13eV and 0.14eV. The FWHM of about 0.15eV was observed for PECVD I, i.e. the broadest 'μc'-band compared to other two sample series.

In summary, the shift of the 'μc'-Si-band to higher energies with almost constant width is observed upon increasing *SC* for all series investigated. A slight variation of the halfwidht and photoluminescence energy between the different sample series has been observed. Figure 4.3 show a correlation between the PL peak energy and the FWHM of the PL band of μc-Si:H films prepared by HWCVD and PECVD, i.e. an increase of the PL peak energy with decreasing of the halfwidth of the PL spectra.

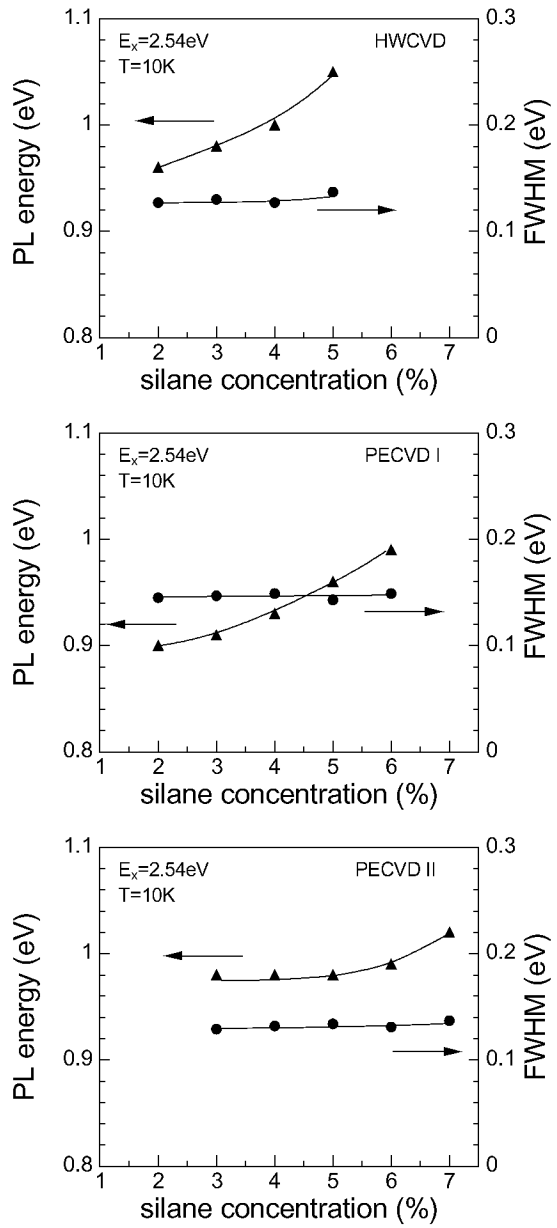

Figure 4.3: Dependence of the photoluminescence energy (▲) and the width (●) of the luminescence spectra on the silane concentration at indicated temperature of 10K for the same sample series as in Figures 4.1 and 4.2. Note the same energy scale for PL peak energy and the width of the 'µc'-band.

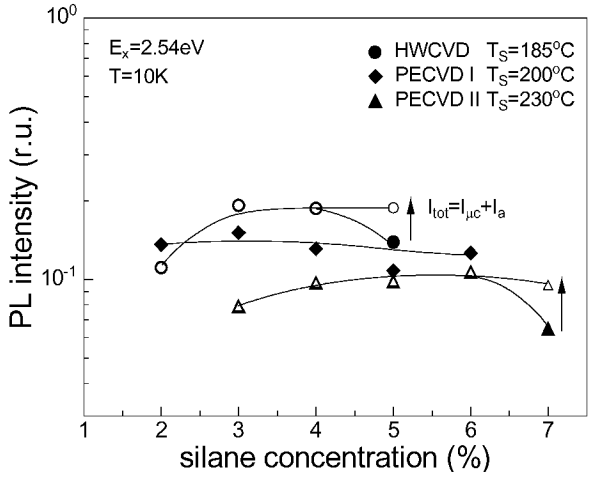

Figure 4.4: Photoluminescence intensity of the 'μc'-Si-band (filled symbols) together with total PL intensity (open symbols) as a function of the silane concentration for three sample series as in Figures 4.1-4.2(a, b) (lines are guides to the eyes). The PL measurements are performed at 10K.

The PL spectra of HWCVD series reveal the highest values of the PL peak energy and the narrower width, in contrast to the lowest PL energy and the broader width of the PL band observed for PECVD I series (T_S=200°C).

4.1.2 Photoluminescence Intensity

The dependence of the luminescence intensity on the silane concentration for the investigated three sample series is shown in Figure 4.4. The filled symbols refer to the luminescence intensity of the 'μc'-band and the open one to the total luminescence intensity, i.e. the intensity obtained from the integrated intensities of the microcrystalline and amorphous emission bands, relevant only for materials with *SC* of 5% and 7% from the HWCVD and PECVD II series, respectively. A weak dependence of the PL intensity on the silane concentration for all investigated thin films was found, independent from the deposition method. The observed value for the luminescence intensity in high-quality μc-Si:H material is slightly lower (in the percentage range) than that for a-Si:H sample with low defect density, used as a reference. For HWCVD material a factor of two higher intensities are obtained compared to PECVD II, whereas PECVD I is between the two. For the HWCVD and PECVD II series, the lowest value of the PL intensity was observed at the lowest silane concentration. Increasing *SC* up to the appearance of the 'a'-Si-band results in improvement of the PL intensity of the material. Further increase of *SC* leads to slightly reduced luminescence intensities of the 'μc'-band (filled circles and triangles) and almost constant behaviour for the total PL intensity (open circles and triangles). For *SC* up to 4% (HWCVD) and 6% (PECVDII), respectively, the luminescence spectra reveal only the μc-Si:H emission band.

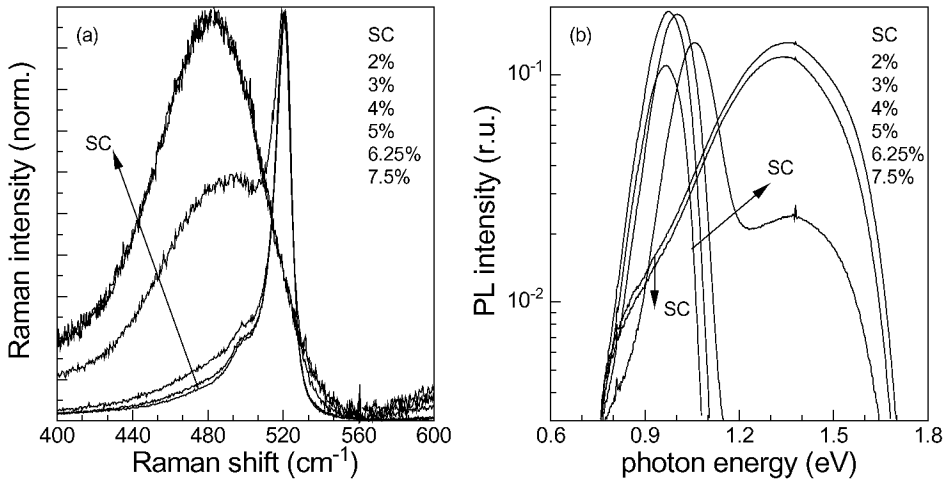

Figure 4.5: Raman (a) and photoluminescence (b) spectra for the same HWCVD sample series as in Figure 4.1. Note the logarithmic intensity scale and the measurements temperature of 10K for Figure 4.5(b).

For the samples prepared at *SC* of 5% and 7%, the band characteristic for amorphous phase contribute significantly to the PL spectra (see Figure 4.1 and Figure 4.2(b)). A slight deviation from this trend was observed for the PECVD I sample series, i.e. the highest value for the luminescence intensity is obtained at low *SC* of 2% and 3%.

4.2 Raman and Photoluminescence Properties of Undoped µc-Si:H Thin Films

Combination of Raman with photoluminescence spectroscopy provides a link between the microstructure and electronic properties of thin films. As the microstructure of the samples turns out to be the most important parameter when the silane concentration is varied, the Raman spectra will be shown together with photoluminescence spectra for the same three sample series. This allows a better comparison of the different samples because the relation between *SC* and the microstructure depends on many process parameters. Figure 4.5(a) shows Raman spectra of µc-Si:H thin films prepared by HWCVD at T_S=185°C for 2% < *SC* < 7.5%. A laser wavelength of 488nm (E_x = 2.54eV) was used for excitation of the Raman spectra, as well as for the PL spectra. Therefore, a similar sample volume is probed by the two experiments, except of a small variation due to the temperature dependence of absorption coefficient α. The Raman spectra are normalized to the height of the narrow peak at 520cm^{-1}, which originates from the crystalline phase. An additional contribution from structural defects of the crystalline phase (stacking faults) leads to the hump at about 492cm^{-1}. The broad band located at about 480cm^{-1} is attributed to the amorphous phase. With increasing silane concentration the relative contribution of the broad band at about 480cm^{-1} increases.

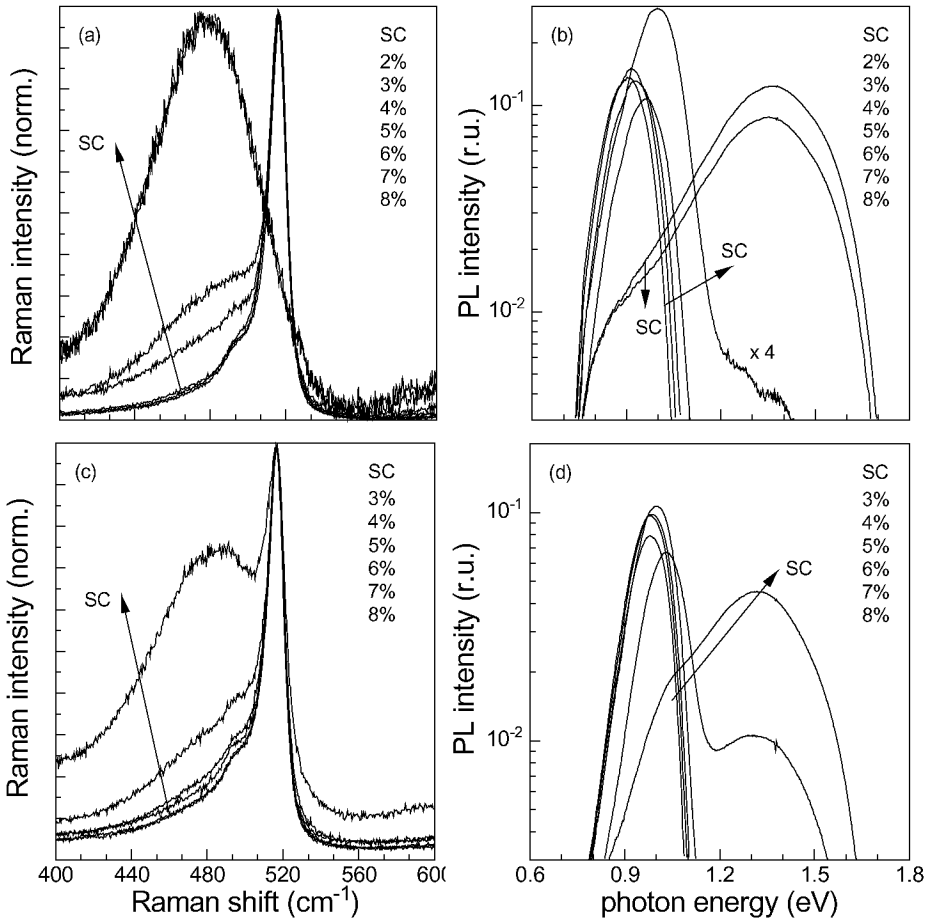

Figure 4.6: Raman (a, c) and photoluminescence (b, d) spectra for the same PECVD sample series as in Figure 4.2(a, b). Note the logarithmic intensity scale and the measurement temperature of 10K for Figure 4.6(b, d).

In particular, at low *SC* values of 2% and 3%, only a small contribution of the amorphous phase is observed. It increases significantly for the sample prepared with *SC* of 4% and dominates the Raman scattering intensity for the sample with *SC* of 5%. The following suggests that this sample is close to the transition to predominantly amorphous growth of the films. At the highest *SC* values of 6.25% and 7.5%, no contribution from the crystalline phase can be identified, i.e. the films are grown beyond the transition from µc-Si:H to a-Si:H. Note, that these two spectra are quite similar and overlap in Figure 4.5(a).

Further information can be obtained from the photoluminescence spectra shown in Figure 4.5(b) on a logarithmic intensity scale vs. photon energy. There are a number of important features to be pointed out: as was already demonstrated (see Figure 4.1), the entire 'µc'-band shifts towards higher energies with increasing *SC*, i.e. the low- as well as the high-energy part of the PL band are shifted continuously to high energy.

The low energy part of the photoluminescence spectra shows an exponential increase. The slope of the PL spectra changes from steeper to less steep at *SC* of 5% when in the Raman spectra an amorphous phase becomes obvious. For this material, an additional PL band at about 1.35eV, characteristic for an amorphous phase appears in the PL spectrum. In contrast to that, the small contributions from the amorphous phase observed at low *SC* from 2% to 4% by Raman experiment (see Figure 4.5(a)), do not lead to a contribution in the luminescence spectra, i.e. no PL peak originating from the amorphous phase is found. At the highest *SC*, when the contribution from crystalline phase disappears in the Raman, the corresponding PL spectra exhibit features typical for the amorphous silicon.

The Raman spectra of the two PECVD series of samples deposited at T_S=200°C (PECVD I) and T_S=230°C (PECVD II) with different *SC* (2-8%) are illustrated in Figure 4.6(a, c) for comparison. The spectra look very similar to those in Figure 4.5(a). A continuous increase in the amorphous contributions is found for *SC* of 5% and 6% (see Figure 4.6(a)), and 7% (see Figure 4.6(c)). It dominates the Raman spectra for *SC* values of 7% and 8% in Figure 4.6(a). While at a *SC* of 8%, the Raman spectrum exhibits only small contribution of the narrow peak at 520cm^{-1} (see Figure 4.6(c)). Compared to HWCVD material deposited at *SC* of 5%, the Raman spectra of samples with *SC* of 6% (PECVD I) and 7% (PECVD II) exhibit lower contribution of the amorphous phase.

The PL spectra of the two PECVD series (see Figure 4.6(b, d)) also exhibit similar features as the HWCVD series, i.e. a shift of the 'μc'-band to higher energies and a contribution of the PL from the amorphous phase for *SC*=7% (see Figure 4.6(d)), when in the corresponding Raman spectra from Figure 4.6(c), an amorphous phase becomes obvious. However, for PECVD material, only the high-energy shoulder of the PL spectra contributes to the shift of the 'μc'-band to higher energies, which is very often observed for this material. Here, has to be pointed out that the PL spectra extended to energies below 0.8eV are beyond the spectral response of the Ge detector. Furthermore, compared to PECVD II material prepared at *SC* of 7% (see Figure 4.6(d)), the PL spectrum of sample with *SC*=6% (see Figure 4.6(b)) shows lower amorphous signal at 1.35eV. In spite of slightly higher contribution of the amorphous phase for this sample (*SC*=6%) shown in Figure 4.6(a).

In summary, the Raman spectra and luminescence spectra of undoped μc-Si:H films grown by HWCVD and PECVD at low substrate temperature do not reveal significant differences. All show an increase in energy of the 'μc'-band with increasing silane concentration and a contribution of the photoluminescence from the amorphous phase, when the amorphous phase in the Raman spectra shows significant contribution.

4.3 Effect of the High Substrate Temperature on the Photoluminescence Properties

The substrate temperature is considered to be a preparation parameter influencing the defect density in microcrystalline silicon. To study the effect of the high substrate temperature on the photoluminescence properties, we performed a detailed investigations on three well-characterised series of nominally undoped μc-Si:H thin films.

Two of them were prepared by HWCVD technique with various silane concentration and are referred to as HWCVD I at T_S=310°C and filament temperature T_F=1730°C and HWCVD II at T_S=330°C and T_F=1710°C. The third sample series was deposited by very high frequency (VHF) PECVD process at T_S=325°C. The PL experiment was carried out at the same experimental conditions like those in Section 4.1. The photoluminescence (at 10K) was also exited with light exceeding the optical gap energy ($E_x = 2.54$eV). Additionally, an InAs detector was used to measure PL spectra in an extended spectral range down up to 0.41eV, in order to get more exact PL features in the low energy region than by the Ge detector.

Figure 4.7(a) shows photoluminescence spectra of HWCVD I series of samples with a *SC* between 10% and 25%. All PL spectra are shifted vertically for clarity. The solid lines correspond to experimental data and the dashed lines are fitting curves with Gaussian lineshape. The luminescence spectra of the films deposited at lower *SC* (10-15%) reveal two broad emission bands. The PL band ('μc'-band) in the range 0.97 to 1.01eV with the halfwidth of about 0.14eV that was already observed for μc-SiH prepared at low T_S and attributed to the microcrystalline phase (see Section 4.1). A slightly broader PL band centred at 0.7eV with a full width at half maximum (FWHM) of about 0.16eV was in addition found. This PL band has not been detected in martial prepared at low T_S (see Figures 4.5(b) and 4.6(b, d)). We note that this PL band is very similar to the one previously observed in polycrystalline silicon (poly-Si) and denoted as 'defect' PL band (Ostapenko et al. 1995, Koshka et al. 1996). Therefore, we use here the notation 'poly'-Si-band.

Now, we will concentrate on the influence of *SC* on the properties of the infrared band at 0.7eV ('poly'-Si-band), which is preliminary assigned to defect-related transition similar to that in poly-Si films. The following can be considered as the distinctive features upon increasing *SC* from 10% to 17.5%: (i) the PL band maintains the spectral maximum at about 0.7eV and the FWHM also holds a constant value of 0.16eV (ii) the PL intensity is slightly higher then the intensity of the 'μc'-band and it increases continuously by a factor of two, until the contribution of the 'a'-Si-band at about 1.25eV appears at *SC*=17.5%. This 'a'-Si-band was already identified for μc-Si:H thin films prepared at low substrate temperature but with slightly different features, i.e. the broader emission band at about 1.35eV. A multiple structure at energies of ~0.7eV, ~1.01eV and ~1.25eV with dominating PL intensity at 0.7eV was observed for material with *SC* of 17.5%. The luminescence spectra of μc-Si:H films deposited with the highest *SC* (18.5% and 25%) suggests a further increase of the signal at high photon energy range and no contribution from the signal at 0.7eV. The 'μc'-Si-band reveals similar properties with increasing *SC* like that already demonstrated in Sections 4.1.1 and 4.1.2. Firstly, the PL maximum energy shifts to higher energy, which is evident for change of the *SC* from 10% to 18.5% and secondly, the PL intensity shows a similar increase like that observed for the 'poly'-Si-band, followed by substantial decrease, i.e. almost the same ratio between the two bands is kept until the contribution of the 'a'-Si-band becomes significant at *SC*=18.5% (see inset in Figure 4.7(a)).

Figure 4.7(b) displays the PL spectra obtained at 10K for the HWCVD II series of μc-Si:H thin films deposited at slightly different T_S=330°C and T_F=1710°C with different *SC* (5-25%).

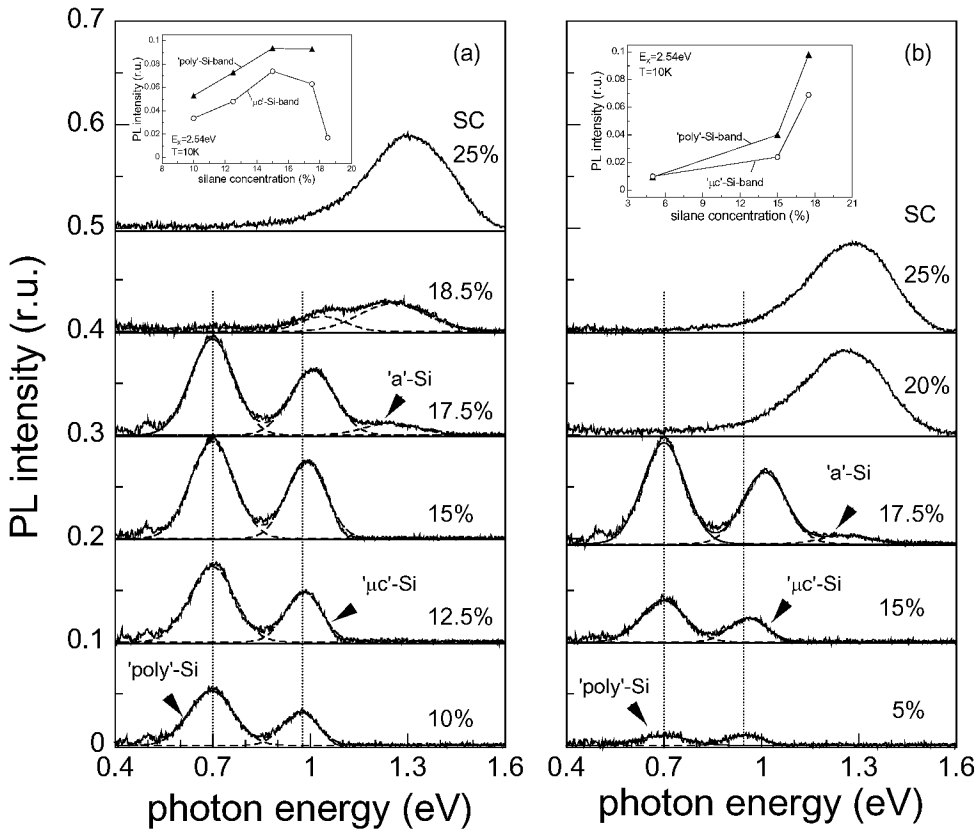

Figure 4.7: (a) PL spectra of two series of μc-Si:H thin films deposited by HWCVD at different substrate and filament temperatures: T_S=310°C and T_F=1730°C (HWCVD I) and (b) T_S=330°C and T_F=1710°C (HWCVD II) with indicated silane concentration. The solid lines are the PL data measured at 10K with an InAs detector, and the dashed lines are fitted curves. Insets (a, b): Dependence of the PL intensity of 'poly'-Si and 'μc'-Si bands on the silane concentration.

All characteristic features, presently observed for the 0.7eV band with increasing *SC* are found also for HWCVD II series: (i) no shift of the maximum of the 'poly'-Si-band, whereas its PL intensity increases dramatically by a factor of more then four with increasing *SC* from 5% to 17.5% and (ii) the same ratio between 'poly'-Si and 'μc'-Si bands, respectively, until the 'a'-Si-band dominates the PL spectra at the highest *SC* values of 20% and 25% (see the inset in Figure 4.7(b)). The films deposited at *SC* of 17.5% from the both HWCVD series show quite similar multi-component structures at the same photon energies.

The luminescence spectra of the third investigated series of μc-Si:H films prepared by PECVD at T_S=325°C with various *SC* from 9% to 17% are shown in Figure 4.8, for comparison. All three emission bands with maxima at ~0.7eV ('poly'-Si), ~1.01-1.03eV ('μc'-Si) and ~1.26eV ('a'-Si) were identified for films with *SC* between 9% and 13%.

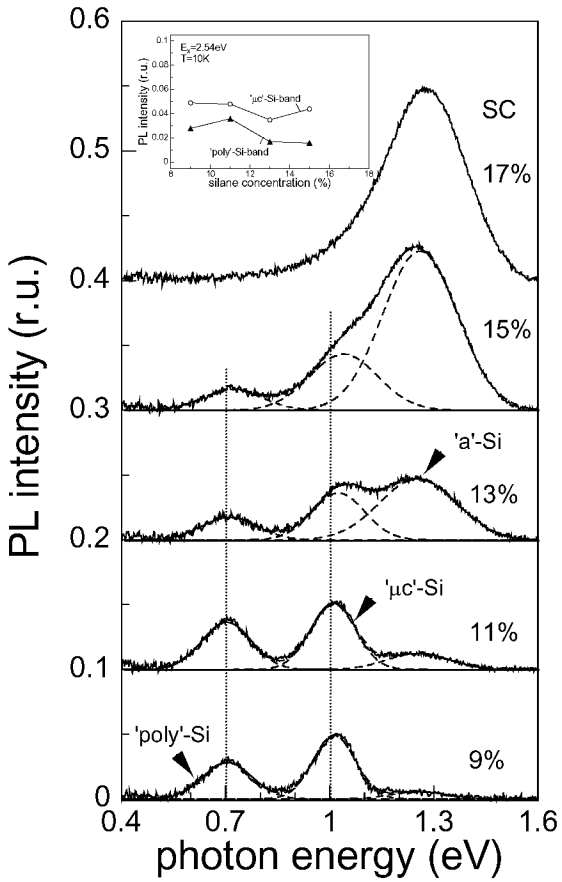

Figure 4.8: PL spectra of μc-Si:H thin films prepared by PECVD at high substrate temperature of 325°C and *SC* between 9% to 17%. The solid lines are the measured PL data, and the dashed lines are the fitted curves. Inset: Dependence of the PL intensity of the 'poly'-Si-band and 'μc'-Si-band on the silane concentration.

For material with a *SC* of 15%, which reveals a PL spectrum dominated by the signal at 1.26eV, still there is a small contribution from the 0.7eV band and the the 'μc'-band. Whereas for *SC*=17% the PL spectrum is entirely dominated by the 1.26eV band. We first examine properties of the 'poly'-Si-band. Upon increasing *SC*, the spectral maximum of this band remains at 0.7eV and a half-width of about 0.17eV. This behaviour is similar to HWCVD material, although a slight difference in the PL intensity and the width are seen. The dependence of the luminescence intensity of the 'poly'-Si-band and the 'μc'-Si-band on the silane concentration is shown in the inset in Figure 4.8. With increasing silane concentration, the luminescence intensity of the two bands does not show a strong increase, as was found for HWCVD material (compare insets in Figure 4.7(a, b)). Instead, the 'poly'-Si-band reveals a maximum intensity in films with low *SC* (9-11%), and it decreases when the 'a'-Si-band become significant at *SC* of 13% and 15%.

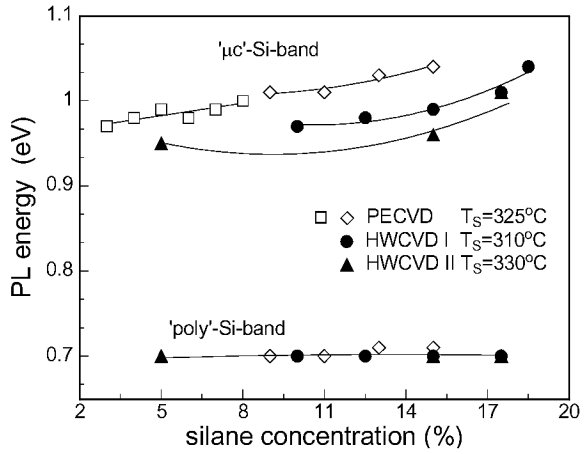

Figure 4.9: PL energy of the 'μc'-Si- and 'poly'-Si-bands vs. silane concentration for the three sample series as in Figures 4.7 and 4.8. Additional points (□) are added originating from the PL results obtained by Ge detector for another PECVD series, deposited at T_S=325°C with *SC* from 3% to 8%.

Similar behaviour was observed for 'μc'-Si-band, but at *SC* of 15% the signal from the 'μc'-band do not decrease and is slightly higher than that from sample with *SC*=13%. The ratio between 'poly'-Si-band and 'μc'-Si-band is almost constant and is different compared to that observed for HWCVD material, i.e. the PL intensity of the 'μc'-Si-band is higher than the intensity of the 'poly'-Si-band up to *SC* of 15%.

The influence of the deposition parameters, such as *SC* and T_S on the luminescence peak energy of the 'μc'-Si- and 'poly'-Si bands for the three series of samples is summarized in Figure 4.9. Additional points (open squares) are added, originating from the PL results obtained by Ge detector for another PECVD series, deposited at T_S=325°C with *SC* (3-8%). A different deposition chamber (p-chamber) of the deposition system was used for the preparation of this μc-Si:H films. The contribution from the 0.7eV peak is clearly visible for all samples from this PECVD series. Since Ge detector cannot resolve this PL band, InAs detector was used. In Figure 4.9 the 'poly'-Si-band maintains spectral maximum at about 0.7eV for all series studied. In contrast, the 'μc'-Si-band shows an increase of the PL peak energy with increasing silane concentration. The PECVD series of μc-Si:H thin films prepared with *SC* from 9% to 17% (see Figure 4.8) exhibits higher values for the μc-Si:H PL peak energy compared to both HWCVD series. This is in line with observed higher luminescence intensity. The second PECVD sample series prepared at the same T_S with different *SC* (3-8%) shows slightly lower energies of the 'μc'-band. These PL energies are comparable to the energies observed for the HWCVD (T_S=310°C) series. Increasing the substrate temperature up to 330°C for the HW-material leads to lower PL energy of the 'μc'-band and comparable FWHM of about 0.16eV. No correlation between the width and the PL peak energy of the luminescence spectra was found, i.e. a broad width corresponds to low energy of the PL band.

In summary, an additional PL band centred at 0.7eV was observed at high T_S, irrespectively of the preparation method. This PL band was not detected for material deposited at low substrate temperature. It is preliminarily assigned to defect-related transitions similar as in polycrystalline silicon.

4.4 Structural Inhomogeneity Along the Growth Direction

In the recent years, the optical and microstructural investigations gave a strong evidence for structural inhomogeneity along the growth axis of the μc-Si:H grown on glass, i.e. at the interface between the substrate and film, voids reach material is found at low *SC* and high amorphous volume fractions at high *SC* (see Figure 2.1) (Finger et al. 1997, Luysberg et al. 1997, Houben et al. 1998a). A previous study, performed by photoluminescence spectroscopy, reveals the sensitivity of the method to probe an amorphous volume fraction at the front surface or at the film/substrate interface by making use of the good spectral separation of the PL bands, but no systematic study was made (Carius et al. 1997).

The present section provides a detailed photoluminescence investigation of the structural inhomogeneity along the growth direction for two previously studied series of μc-Si:H films prepared by VHF-PECVD (PECVD I, T_S=200°C) and HWCVD (HWCVD I, T_S=310°C) process at various silane concentrations (see Sections 4.1, 4.2 and 4.3). The films are measured using two different ways of illumination: from the front surface, i.e. the free surface and from the rear interface, i.e. through the glass substrate to illuminate the film at the substrate / interface.

Figure 4.10 compares PL spectra taken at 10K from the front surface (solid lines) with that from the rear interface (dashed lines) of 3.5μm thick μc-Si:H thin films grown by PECVD I (T_S=200°C) on glass substrate at different *SC*. The photon energy for excitation was 2.54eV and the corresponding penetration depth was about 0.2μm. Therefore, the photoluminescence experiment probe only a thin layer of the film near the surface or interface. The photoluminescence signal from the surface layer is dominated by the 'μc'-Si-band and no PL from the amorphous band at about 1.35eV with halfwidth of about 0.37eV was found up to *SC* of 6% (compare Figure 4.2(a)). Whereas the top two PL spectra from Figure 4.10 show only a broader 'a'-Si-band. However, in the interface layer near the substrate, the photoluminescence signal from the amorphous phase is already seen in the samples with *SC* between 4% and 6%, i.e. the PL spectra reveal dual-band features. As the contribution from the 'a'-Si-band is becoming significant with increasing silane concentration from 5% to 6%, the luminescence from the μc-Si-phase decreases and a strong signal from the amorphous phase dominates the spectra at *SC* of 7% and 8%. Since we probed much larger thickness than the transition zone (0.03-0.05μm) (see Figure 2.1) the differences between the PL spectra from the surface and the interface excitation of the samples grown with *SC* of 5% and 6% are striking. This shows the structural inhomogeneity along the growth direction with considerable amorphous regions at the interface between the substrate and film, similar to that previously observed in the TEM pictures (Luysberg et al. 1997, Houben 1998).

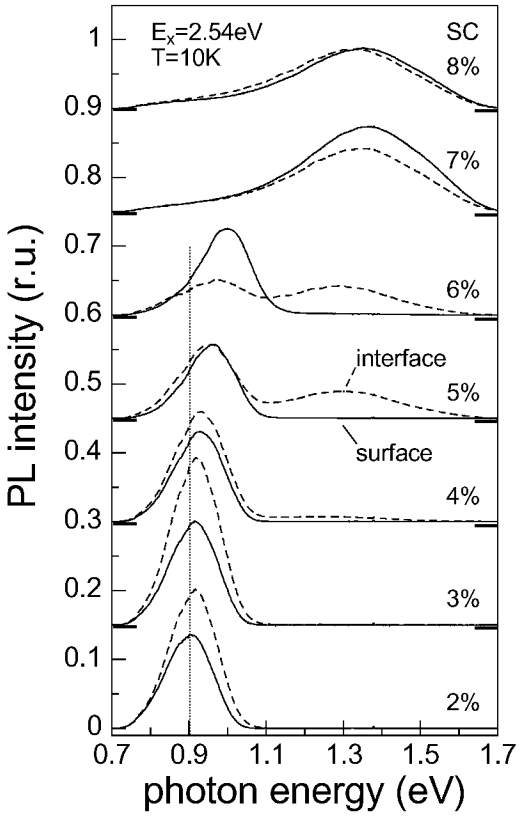

Figure 4.10: Comparison of the photoluminescence spectra, obtained from the front surface (solid lines) and from the rear interface (dashed lines) excited with photon energy of 2.54eV. The μc-Si:H films prepared by PECVD I with various *SC* (2-8%) at T_S=200°C were 3.5μm thick (compare Figure 4.2(a)). The PL spectra are taken at 10K with a Ge detector and shifted vertically for clarity.

The luminescence energy and the width of the 'μc'-Si-band of the investigated PECVD I sample series are summarized in Figure 4.11 for illumination from the front and through the substrate side. In both cases, the PL band related to the microcrystalline phase shifts towards higher energies with increasing *SC*. However, the PL peak energy position shows stronger shift on the surface than at the interface layers when the *SC* varies between 2% and 6%. It starts from lower energies of 0.9eV and increases up to ~1.0eV. A weaker increase of the PL energy (0.91-0.96eV) is observed at the interface layers. For the same increase of the *SC*, the halfwidth of the luminescence spectra of the surface layers remains almost constant at ~0.15eV. In contrast, a deviation of the width of the PL spectra from the interface layer at high *SC* is indicated, i.e. a broadening of the 'μc'-Si-band when the *SC* is higher than 3%.

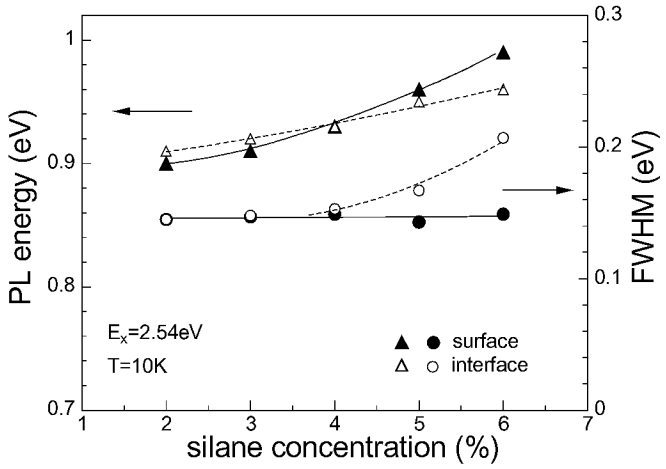

Figure 4.11: Plot of photoluminescence energies (filled and open triangles) and linewidths (filled and open circles) of the 'μc'-Si-band vs. silane concentration for the same sample series shown in Figure 4.10, obtained for the two different ways of illumination: from the front surface (filled symbols) and rear interface (opened symbols).

We will now compare, the photoluminescence spectra from the surface and interface of μc-Si:H films prepared at high T_S by HWCVD (HWCVD I, T_S=310°C) at various *SC* (Figure 4.12(a)). The data measured on the surface were presented already in Figure 4.7(a). The luminescence measurements were performed almost at the same experimental conditions like those from Figure 4.11. The only difference was the use of InAs detector instead of a Ge detector to extend the spectral range down to 0.41eV, to detect the 'poly'-Si-band. All luminescence spectra from the rear interface layer exhibit an 'a'-Si-band with slightly different features compared to those in Figure 4.10, i.e. a PL band at about 1.25eV with a FWHM of about 0.27eV. The PL spectra from the front surface layers reveal a signal from the amorphous phase for $SC \geq 17.5\%$. The 'μc'-Si and 'poly'-Si bands from the interface layer shows quite similar behaviour with increasing *SC* from 10% to 15%, compared to those observed for the surface layer, e.g. (i) the μc-Si:H PL band at about 0.97eV shifts to higher energies by about 0.03eV with slightly different intensity, (ii) the 'poly'-Si-band with similar PL intensity, maintains the spectral maximum at about 0.7eV and FWHM holds also constant values. As *SC* increases further from 17.5% to 25%, the luminescence intensity of the 0.7eV band from the interface layer is strongly reduced and disappears at a *SC* value of 25%. The signal related to the 'μc'-Si-band is superimposed by the 'a'-Si-band for $SC \geq 17.5\%$ (compare Figure 4.8).

In Figure 4.12(b) the Raman spectra at room temperature for interface and surface excitation with photon energy equal to 2.54eV for the same μc-S:H films as in Figure 4.12(a) are shown. The Raman spectra are normalized to the height of the narrow peak at 520cm^{-1} related to crystalline phase and are shifted vertically for clarity. A correlation between the Raman and PL spectra from the interface layer is obvious.

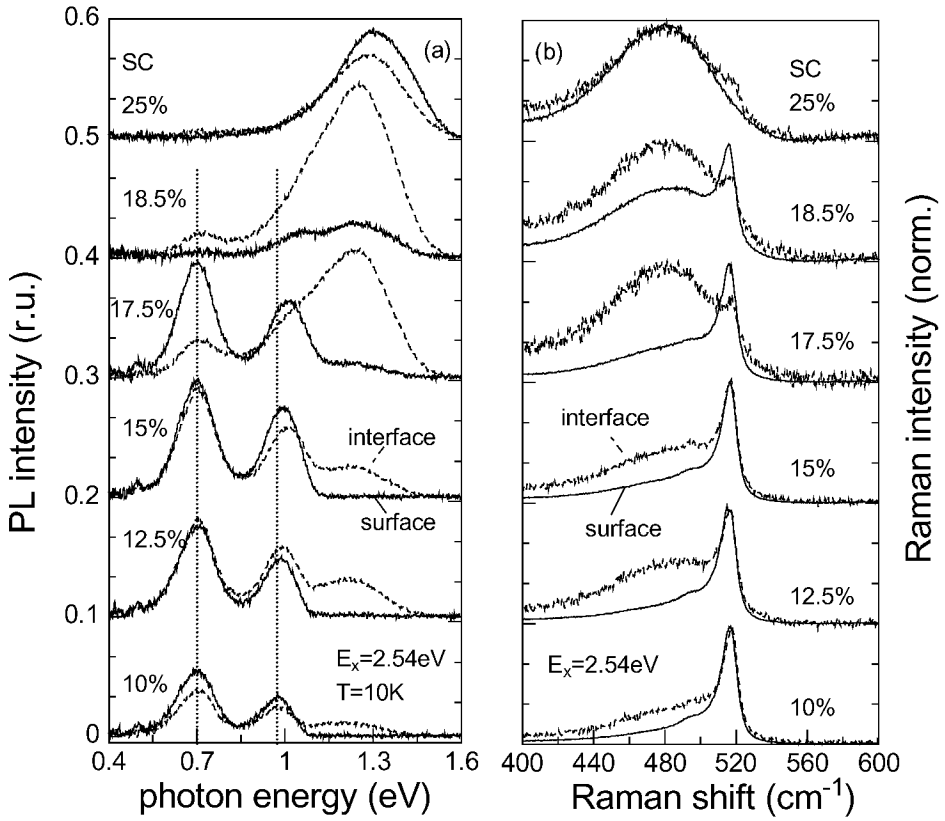

Figure 4.12: Photoluminescence (a) and Raman (b) spectra for front surface (solid lines) and rear interface (dashed lines) excitation with photon energies of $E_x = 2.54\,\text{eV}$ for the same 1μm thick HWCVD I μc-Si:H sample series as in Figure 4.7(a). The films were prepared at T_S=310°C and T_F=1730°C with the indicated values of *SC*.

All Raman spectra show a significant contribution from the band at 480cm^{-1}, characteristics for the amorphous phase. The corresponding PL spectra reveal an 'a'-band at about 1.25eV. At the highest *SC* (17.5-25%), a small contribution from the c-Si band at 520cm^{-1} is found in the Raman spectra, while the PL signal from the microcrystalline phase is hardly seen in the corresponding PL spectra. Three Gaussian functions peaked at 0.71eV, 1.08eV and 1.27eV were used to fit the PL spectrum from the interface layer of the sample prepared at *SC* of 17.5%, while for sample with *SC*=18.5% was difficult to obtain the correct features of the 'μc'-Si-band (data not shown in Figure 4.12(a)).

The influence of the different directions of illumination on the PL energy of the 'μc'-Si and 'poly'-Si bands for the investigated HWCVD I (T_S=310°C) series is demonstrated in Figure 4.13. Filled and open symbols correspond to illumination from the front surface and from the rear interface, respectively.

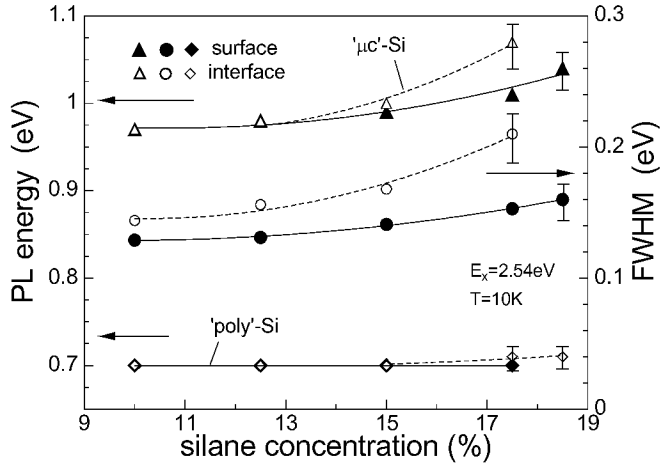

Figure 4.13: PL energy of the 'μc'-Si-band (filled and open triangles) and 'poly'-Si-band (filled and open rhombus) together with the width of the 'μc'-Si-band (filled and open circles) as a function of the *SC* for the same sample series as in Figure 4.12. Filled and open symbols correspond to illumination from the front surface and rear interface excitation, respectively.

There is an increase of the PL energy of 'μc'-Si-band with increasing *SC*, starting at the same PL energy (0.97eV) and rising differently for the two ways of illumination. In contrast to lower PL energy of about 1.04eV reached for illumination from the front surface (filled triangles). For illumination from the rear interface (open triangles), the PL peak energy increases up to about 1.08eV.

The dependence of the full width at half-maximum on the silane concentration for the 'μc'-Si-band is also displayed in Figure 4.13. Illumination from the rear interface (open circles) leads to a slightly larger FWHM (~0.15eV) and a stronger increase above *SC* of 15%, as compare to illumination from the surface (filled circles), i.e. the halfwidth remains almost constant values of about 0.13eV and slightly increases at the highest *SC*. Apart from the weak increase of the PL energy of the 'poly'-Si-band above *SC*=15% for illumination from the rear interface, it maintains the spectral maximum at about 0.7eV for the two kinds of illumination. For the sample prepared at *SC* of 18.5%, the illumination from the front surface quenches the transitions due to defects ('poly'-Si-band) while for illumination through the substrate it is still visible (see Figure 4.13).

4.5 Separation of Microcrystalline from Amorphous Photoluminescence Bands

The PL peak position of 'μc'-Si-band in material with predominantly amorphous structure could not be determined under the experimental conditions used in the previous sections.

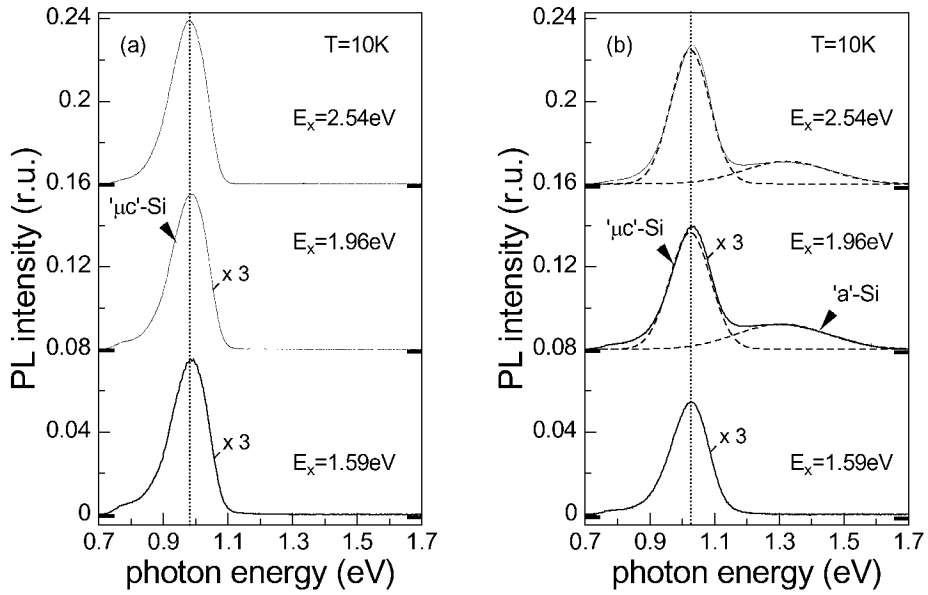

Figure 4.14: Photoluminescence spectra of μc-S:H films prepared by PECVD II (T_S=230°C) at silane concentrations of (a) 3% and (b) 7%, exited by different photon energies E_x of 1.59eV, 1.96eV and 2.54eV. All PL spectra are shifted vertically for clarity. Note that in (b), the solid lines are the measured PL data and the dashed lines are the fitted curves.

In order to reduce the contribution of the amorphous band, an excitation using photon energy of 1.59eV has been performed. The data presented in this section refer to high quality films produced by PECVD at a low substrate temperature of 230°C and were already presented (see Figure 4.2(b)) for excitation at 2.54eV. Here, we will study the photoluminescence spectra from the same PECVD sample series (denoted as PECVD II) by using excitation energies of 1.96eV and 1.59eV, for comparison. The PL measurements were carried out at temperature of 10K and only the excitation energy was changed.

Figure 4.14(a) presents typical photoluminescence spectra of an μc-Si:H film prepared at a *SC* of 3% for different excitation energies. Upon increasing the excitation energy from 1.59eV to 2.54eV, the PL band identified in Section 4.1 as μc-Si-band maintains it spectral maximum at about 0.98eV and the linewidth hold also a constant value of about 0.13eV. The photoluminescence intensity is found to increase at high excitation energy, following the increase of the absorption coefficient α for microcrystalline silicon (see Figure 2.4). For the material prepared at a high *SC* of 7%, the emission band characteristic for the amorphous phase can be seen. In Figure 4.14(b) typical PL spectra of this material, taken at different excitation energies are shown. It can be seen that illumination at energies above the band gap, excites both 'μc'-Si and 'a'-Si bands. The luminescence spectra exited with photons of energy E_x equal to 1.96eV and 2.54eV reveal two emission band and can be fitted with Gaussian functions peaked at 1.02eV and 1.32eV.

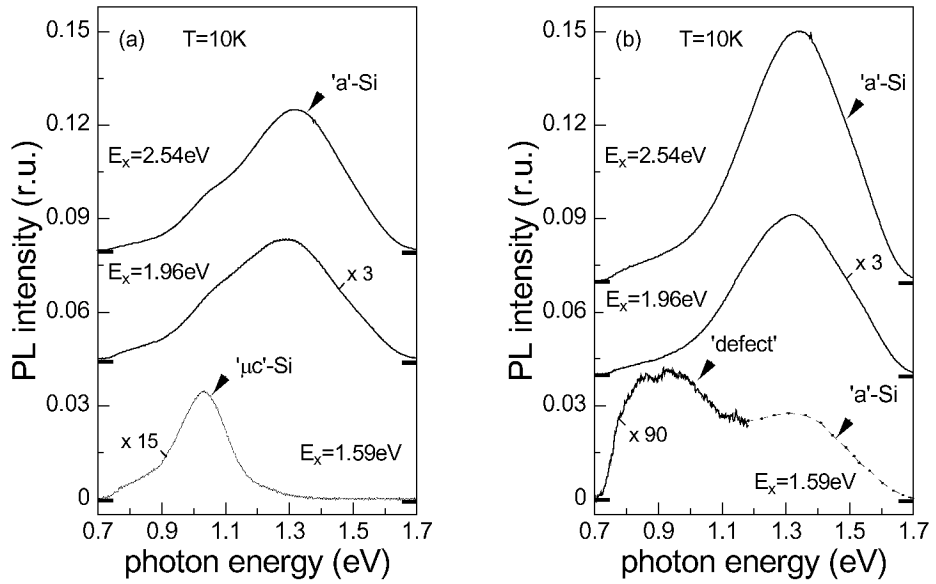

Figure 4.15: PL spectra of two highly amorphous samples prepared at silane concentrations of 8% by PECVD II (T_S=230°C) (a) and of 7.5% by HWCVD (T_S=185°C) (b) for excitation with three different photon energies. Two significantly different PL bands, indicated as 'μc'-Si (a) and 'defect' (b) bands are observed at low excitation energy (E_x = 2.54 eV) for the two samples. Note that all PL spectra are shifted vertically for clarity.

Since, the main feature relevant to the present work is to suppress the 'a'-Si-band, the low excitation energy of 1.59eV is used. The luminescence spectrum obtained at this excitation energy, exhibits the 'μc'-Si-band only. The following can be considered as a common features upon change of the excitation energy: (i) there is no shift of the 'μc'-Si-band with increasing excitation energy and the linewidth remains constant (ii) the luminescence intensity is found to increase by a factor of three with increasing E_x, as expected from the values of the absorption coefficient in microcrystalline silicon.

Figure 4.15 displays PL spectra of two highly amorphous films deposited at different conditions, exited by various excitation energies. For these samples, the Raman spectra (see Figure 4.6(c, a)) indicate a change from highly amorphous structure with small contribution from the microcrystalline phase for the 8% sample (PECVD I, T_S=230°C) to a microstructure that is purely amorphous for the 7.5% sample (HWCVD, T_S=185°C). In Figure 4.15(a) the two spectra for 2.54eV and 1.96eV show a main PL peak near 1.3eV ('a'-Si-band), which has been already attributed to tail-to-tail transitions in the amorphous phase (see Section 2.4.1) and a weak hump at low energy. The 1.59eV spectrum indicates that the absorption in the sub-gap region for a-Si:H does not excite the tail-to-tail transitions in the amorphous phase, but excites preferentially the transitions in the microcrystalline phase.

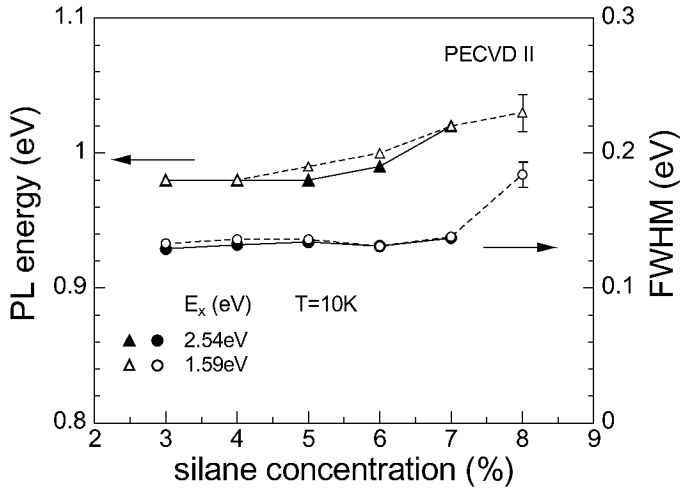

Figure 4.16: Photoluminescence energy (filled and open triangles) and the spectral width (filled and open circles) of 'μc'-Si-band vs. silane concentration for μc-Si:H films deposited by PECVD II at T_S=230°C. The samples are exited by high energy (2.54eV) (see Figure 4.3) and low energy (1.59eV) photons. The PL measurements are performed at 10K.

The corresponding 'μc'-Si-band reveals a maximum at about 1.03eV and halfwidth of about 0.18eV. In contrast, the PL spectrum of the purely amorphous silicon film (*SC*=7.5%) excited by low energy (1.59eV) photons shows a dual peak structure with significantly different lineshape and width, and a decrease of the intensity (the lowest curve in Figure 4.15(b)). In addition to the 'a'-Si-band, a second band at about 0.9eV with a linewidth of about 0.35eV dominates the PL spectrum. Illumination at $E_x \geq 1.59$eV excites only the 'a'-Si-band (top two PL spectra in Figure 4.15(b)) and not the 0.9eV band. This low energy PL is attributed to transitions of carriers from the band tail states to defect states ('defect' PL) (Street and Biegelsen 1980, Wilson and Kerwin 1982). A dual peak structure in undoped a-Si:H with features quite similar to that reported here was previously observed for excitation with 1.16eV photons (Ulber et al. 1995).

Figure 4.16 shows the summarized results on the luminescence peak energy and the linewidth of the μc-Si:H emission band exited by low energy (2.54eV) and high energy (1.59eV) photons versus silane concentration. The shift towards higher energies of the 'μc'-Si-band with increasing silane concentration is observed for the both kinds of excitation. By using excitation at 1.59eV, we can separate the 'a'-Si-band from the 'μc'-Si-band in highly amorphous material (see Figure 4.15(a)). Thus the PL peak position of the 'μc'-Si-band is extended up to about 1.03eV. At the end, a good resemblance can be seen in the halfwidth of the 'μc'-Si-band exited by the two different photons. Apart from the slight deviation at low *SC* and the strong increase (up to 0.18eV) at the highest *SC* of 7%, all the 'μc'-Si-bands have widths close to 0.14eV.

4.6 Temperature Dependent Measurements

So far we have mostly dealt with the PL results from the low temperature measurements. At high temperatures thermally activated diffusion of carriers is expected to affect the recombination mechanisms. It is therefore important to study the influence of the temperature on the photoluminescence properties. In the following, a detail investigation of the PL properties at different temperatures (10-200K) for one previously studied (only at 10K) HWCVD sample series (T_S=185°C, T_F=1650°C) is presented (see Figures 4.1, 4.3, 4.4 and 4.5). The PL measurements are performed at the same experimental conditions and only the temperature was varied, i.e. E_x = 2.54 eV and Ge detector.

The photoluminescence spectra of purely μc-Si:H and a-Si:H samples prepared at silane concentrations of 3% and 7.5%, taken at different temperatures are displayed semilogarithmically in Figures 4.17(a) and 4.17(b), respectively. For these samples, the Raman spectra (see Figure 4.5(a)) indicate a change from a highly crystalline structure with only small contribution of the amorphous phase for the sample with *SC* of 3% to a microstructure that is fully amorphous for the sample with *SC* of 7.5%. In general, the PL intensity decreases and the PL peak shifts to lower energies as the temperatures increases for the both types of material. A narrow PL band ('μc'-Si-band) at 0.98eV (at 10K) characterized the PL spectrum for microcrystalline film, while the spectrum for amorphous film consists of two emission bands. The main PL band is at about 1.35-1.4eV ('a'-Si-band) and the PL band at 0.8-0.9eV. The latter band is identified as 'defect' band (see Section 2.4.1), which can be observed by low energy (1.59eV) photon excitation (see Section 4.5) or at high temperatures in undoped or in doped a-Si:H (Rehm et al. 1976, Engemann and Fischer 1977, Nashashibi et al. 1977). Here, has to be pointed out that the PL spectra extend to energies below 0.8eV are beyond the spectral response of the Ge detector. Therefore, the low-energy shoulders of the 'defect' peak cannot be seen in Figure 4.17(b).

Referring to Figure 4.17(a), at temperatures below 40K, there is a slight decrease in the luminescence intensity of the 'μc'-Si-band. Further, the increase of the temperature results in a rapid quenching of the PL intensity by a three orders of magnitude. In contrast, the intensity of the 'a'-Si-band exhibits an enhancement until 40K, but at temperatures beyond this value it gradually becomes smaller.

Figure 4.17(b) displays also the weak temperature dependence of the PL intensity of the defect peak compared to that observed for 'a'-Si-band, i.e. the recombination via defects has weak temperature dependence. A logarithmic scale was chosen for the PL intensity in Figures 4.17(a) and 4.17(b) to demonstrate the shift of the high-energy part of the 'μc'-Si-band as well as the 'a'-Si-band to lower energies with increasing T (10-200K). The luminescence peak energy decreases by a total of about 0.19eV for 'μc'-Si-band compared to stronger decrease by a total of about 0.21eV for 'a'-Si-band. Figure 4.17(a) shows a slight shift to low energy of the entire 'μc'-Si-band below 40K. That implies a slight shrinking (or shift) of the band gap with increasing temperature. A further increase of the temperature leads to shift in the high-energy parts only, whereas the low-energy parts of the PL spectra coincide in the low energy region for spectra obtained at temperatures between 40K and 120K.

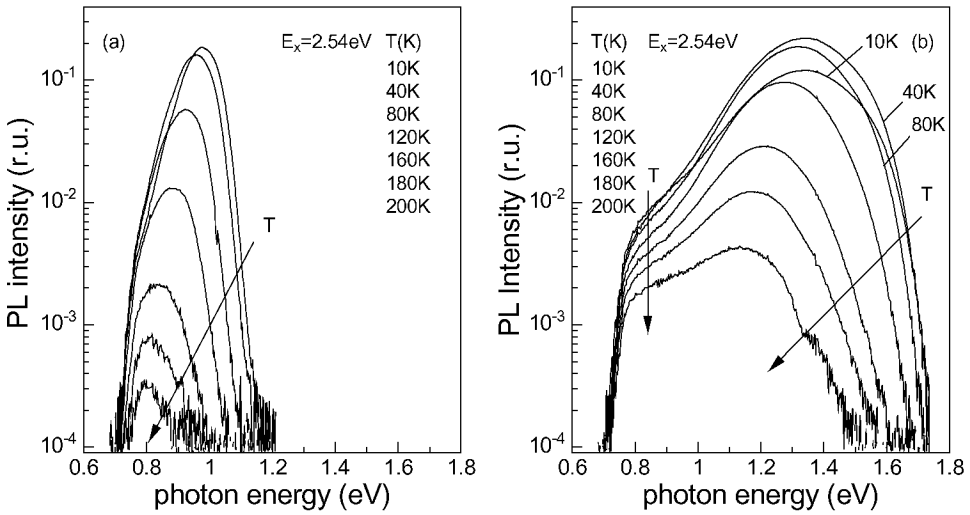

Figure 4.17: Photoluminescence spectra taken at different temperatures between 10K and 200K for purely μc-Si:H and a-Si:H samples prepared by HWCVD at T_S=185°C with silane concentrations of 3% (a) and 7.5% (b).

4.6.1 Temperature Dependence of the Photoluminescence Intensity

This section deals with temperature dependent measurements of the photoluminescence intensity to provide information about the recombination mechanisms responsible for thermal quenching of the luminescence and about the activation energy of the process. In the past, there have been many reports of the temperature dependence of the photoluminescence intensity for hydrogenated amorphous silicon (Engemann and Fischer 1973, Tsang and Street 1979, Austin et al. 1979 and Collins et al. 1980) and for microcrystalline silicon (Bhat et al. 1983b). All find qualitatively similar data, the luminescence intensity has always been found to be a decreasing function of temperature for amorphous silicon as well as for microcrystalline silicon. Although, the values for the activation energy reported are widely different. In fact, no single activation energy is observed in a-Si:H (Street 1981).

The temperature dependence of the photoluminescence intensity in an Arrhenius plot for one investigated series of samples (HWCVD, T_S=185°C) at various *SC* is summarized in Figure 4.18. All films show a decrease of the photoluminescence intensity with increasing temperature. It is obvious that the temperature dependencies of the PL intensity for samples prepared at *SC* between 2% and 4% shows two regions. Below 40K the luminescence intensity reveals almost constant behaviour or a slight decrease. Above this temperature there is a much larger change and the PL intensity quenches rapidly by a factor of three orders of magnitude. For these samples, the Raman spectra (see Figure 4.5(a)) indicate highly crystalline structure with a small contribution of the amorphous phase and the corresponding photoluminescence spectra exhibit only a 'μc'-Si-band (see the example from Figure 4.7(a)).

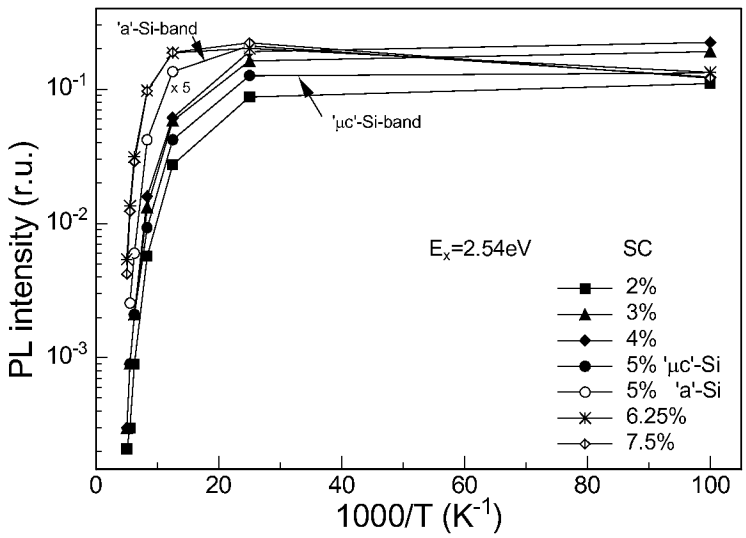

Figure 4.18: Temperature dependence of the luminescence intensity in relative units for HWCVD samples of different silane concentrations. The PL spectra of film prepared at *SC*=5% reveal two emission bands over the temperature range from 10K to 180K. The filled and open circles refer to luminescence intensity of 'μc'-Si and 'a'-Si bands, respectively.

From the data shown in Figure 4.18, it is seen that the PL intensity for material grown at the highest *SC* of 6.25% and 7.5% reveals an increase of the PL intensity below 40K. Followed by almost constant behaviour until 80K and then the PL intensity begins to decrease again. The corresponding Raman spectra of these samples reveal an amorphous structure (see Figure 4.5(a)), while the PL spectra show dual band structure of 'a'-Si-band and 'defect' band.

For the sample prepared at *SC* of 5% the Raman spectrum (see Figure 4.5(a)) reveals almost equal contrubutions of microcrystalline and amorphous phases and the PL spectrum consist of two emission bands. The filled and open circles refer to the luminescence intensity of 'μc'-Si and the 'a'-Si bands, respectively. The PL intensity of the 'μc'-Si-band does not show deviation from the behaviour observed for highly crystalline material. In contrast, the PL intensity of the 'a'-Si-band exhibits quite different behaviour upon an increase of the temperatures. Below 40K the luminescence intensity of the corresponding band increases in a manner similar to that observed in 'fully' amorphous samples. Above this temperature, the intensity of the 'a'-Si-band quenches faster than in purely amorphous films.

In summary, the luminescence signal for highly crystalline samples at low *SC* quenches much faster towards high temperature, compared to the weaker decrease of the PL intensity for amorphous material at high *SC*. No single activation energy was found for μc-Si:H thin films in a manner similar to a-Si:H.

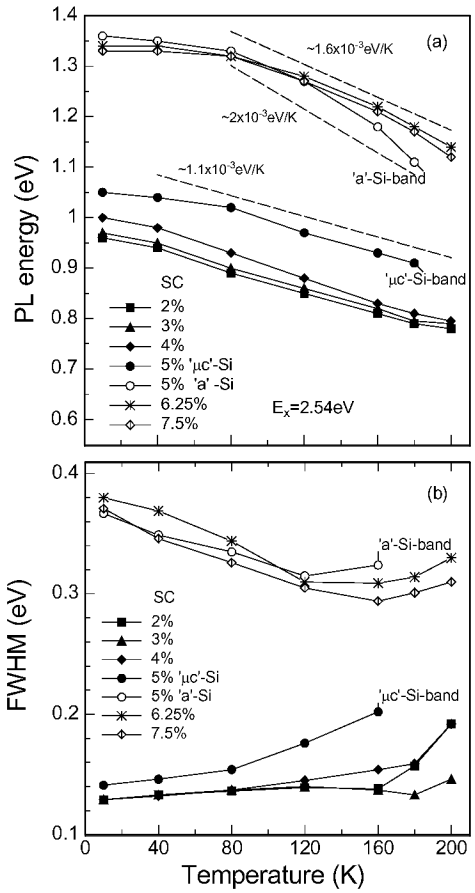

Figure 4.19: Temperature dependences of the luminescence peak energy (a) and spectral width (b) for µc-Si:H thin films prepared by HWCVD at T_S=185°C with indicated values of *SC*. The temperature coefficients for the shift of the 'µc'-Si-band (~1.1×10^{-3}eV/K) and the 'a'-Si band (~1.6×10^{-3}eV/K), and that of the 'a'-Si-band for mixed phase material with *SC*=5% (~2×10^{-3}eV/K) are given.

4.6.2 Temperature Dependence of the Photoluminescence Peak Energy

Further information concerning the distribution of states in µc-Si:H thin films can be gained from the temperature dependence of the luminescence peak energy and the spectral width of the luminescence spectra. The shift of the luminescence peak energy to low energy with increasing temperature is found for all µc-Si:H thin films studied, as also reported by Tsang and Street (1978) and Austin et al. (1979) for hydrogenated amorphous silicon.

Figures 4.19(a) and 4.19(b) contains the plots of the temperature dependence of the luminescence peak energy and the full width at half maximum (FWHM) for the μc-Si:H sample series (HWCVD, T_S=185°C). For highly crystalline samples prepared at low *SC* (2-4%), a continuous shift of the peak energy towards lower energies was observed upon an increase of the temperature. All these films show a similar temperature coefficient of about 1.1×10^{-3}eV/K for the luminescence peak energy above 40K. Compared to highly crystalline samples, the 'μc'-Si-band for mixed phase material (*SC*=5%) reveals the same temperature coefficient above 40K and smaller PL energy shift below this temperature. It can be seen also that, above 80K for highly amorphous films prepared at high *SC* of 6.25% and 7.5% the shift of the peak energy is much stronger with a temperature coefficient of about 1.6×10^{-3}eV/K. The same value of the temperature coefficient was reported by Austin et al. (1979), which is in a good agreement with a value of 1.8×10^{-3}eV/K obtained by Tsang and Street (1979). For mixed phase material prepared at *SC* of 5%, stronger decrease of the PL peak energy of the 'a'-Si-band is found, i.e. the temperature coefficient of about 2×10^{-3}eV/K above 80K (see Figure 4.19(a)).

As was already reported in Section 4.1, the 'μc'-Si-band in samples prepared at low *SC* have a FWHM of 0.13-0.14 at low temperature, compared with the width of 0.3-0.4eV for the 'a'-Si-band in samples prepared at high *SC*. This comparison of spectral widths is shown in Figure 4.19(b) over a range of temperatures from 10K to 200K. The spectral width of 'μc'-Si-band in samples prepared at *SC* values between 2% and 4% remains constant below 120K and increases slightly above this temperature. The width of 'μc'-Si-band in mixed phase material (*SC*=5%) increases much more rapidly with temperature than that in highly crystalline samples at low *SC*. Furthermore, we found that the width of 'a'-Si-band in samples prepared at high *SC* (5-7.5%) decreases with increasing temperature down to values of about 0.27eV, which are typical for pure a-Si:H and then increases slightly above 160K. This decrease of the width is not observed in hydrogenated amorphous silicon. According to Tsang and Street (1978) and Austin et al. (1979) the linewidth of the 'a'-Si-band does not depend on the temperature below 150K, while above this temperature a rapid increase of the width is measured.

Chapter 5

5 Photoluminescence Results on Microcrystalline Silicon Solar Cells

In the preceding chapter has been demonstrated that a lot of information about the changes of the electronic properties of μc-Si:H films upon changes of the silane concentration (and thus the microstructure) can be gained by using photoluminescence spectroscopy. In the present chapter, in full agreement with the observation for nominally undoped μc-Si:H thin films (HWCVD, T_S=185°C), a correlation between microstructure and PL energy with increasing silane concentration is studied for solar cells with very high efficiency of 9% and above, applying similar material as intrinsic layer. Proceeding one step further, a modulation technique is applied in order to avoid spurious PL signal from the glass, TCO and *p*-layer and to probe only those carriers, which are taking part in the photovoltaic process.

The photoluminescence peak energy and the open circuit voltage V_{oc} in solar cells are linked via the carrier distributions in non-equilibrium and the splitting of the quasi-Fermi levels (see Section 2.5, Figure 2.6) (Merdzhanova et al. 2004). A relationship between both quantities together with short circuit current density j_s for μc-Si:H *p-i-n* solar cells is studied as a function of silane concentration and temperature. A comparison with crystalline and amorphous silicon *p-i-n* diodes is also given. Finally, the influence of the optical generation rate g_o on photoluminescence properties and solar cells parameter such as V_{oc} and j_{sc} for the best-performing solar cell from the investigated HWCVD series is addressed.

5.1 Microstructure and Photoluminescence Properties of μc-Si:H Solar Cells

In the following section, a detailed study on the microstructure and electronic properties of μc-Si:H solar cells will be performed by a combination of Raman scattering and PL experiments. The solar cells were fabricated in *p-i-n* deposition sequence on textured ZnO substrates with a ZnO/Ag back reflector. A brief review of the device configuration used throughout this work is given in Section 3.1.3.

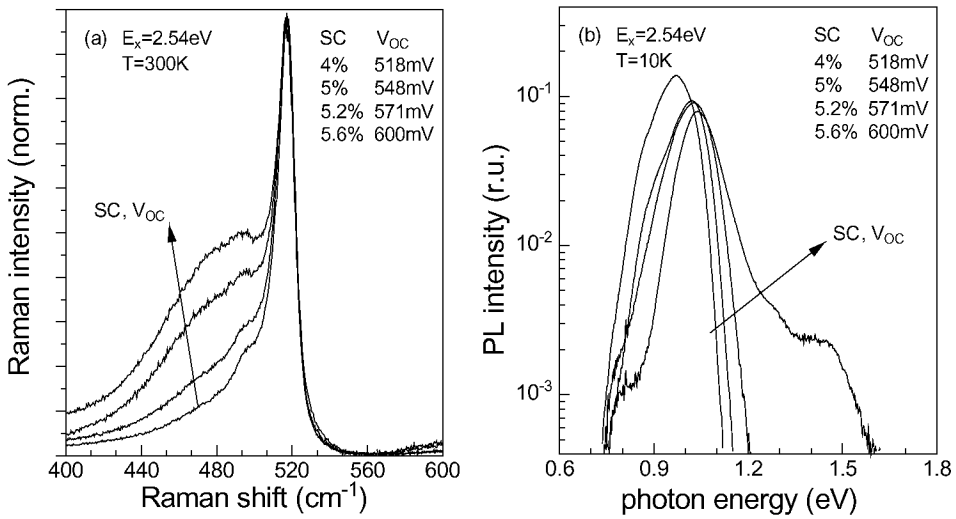

Figure 5.1: Raman spectra (a) and photoluminescence spectra (b) of μc-Si:H solar cells prepared by HWCVD at T_S=185°C at various *SC* or V_{oc}, measured from the top-side after removing the *n*-layer. Photon of energy $E_x = 2.54$ eV is used for excitation of both experiments, performed at the indicated measurement temperatures.

The intrinsic (*i*-) layer was prepared by HWCVD at T_S of 185°C and T_F of 1650°C under various silane concentrations and deposition pressures p_D (4-5Pa). The thickness of the *i*-layer was between 0.85μm and 1μm. Details of the deposition parameters are listed in Table B.5. Figure 5.1 displays the Raman spectra and the PL spectra for the investigated 1μm thick HWCVD series of solar cells. The Raman and PL spectra were excited from the top-side[11] of the solar cell with photon of energy $E_x = 2.54$ eV. Thus, a similar depth of approximately 0.2μm, including part of the *i*-layer is probed. The Raman and PL experiments are carried out, after removing the Ag/ZnO back reflector and the *n*-layer by chemical etching in diluted KOH, to avoid contributions from the *n*-layer.

The Raman spectra (Figure 5.1(a)) show a continuous increase of the amorphous peak at 480cm^{-1} upon increasing *SC* (4-5.6%) or V_{oc} (518-600mV[12]). In particular, at low *SC* values of 4% and 5% or low V_{oc} values of 518mV and 548mV, a small contribution from the amorphous phase is found. It increases significantly for cells with *SC*=5.2% and dominates the Raman intensity for *SC*=5.6%. For this solar cell, the Raman spectrum indicates a microstructure that is highly amorphous with small contribution from the crystalline phase, i.e. the cell prepared at the transition from microcrystalline to amorphous growth. The best efficiency of 8.49% and V_{oc}=600mV at still high fill factor and current density was achieved for this solar cell device, in spite of the lower thickness of 0.85μm (see Klein 2003a, p.89-90).

[11] The term 'top-side' used here for solar cell is defined in respect of deposition sequence. For solar cells with *p-i-n* configuration (see Figure 3.3), the top-side is the Ag/ZnO/*n*-layer, i.e. the free surface.

[12] The values of the open circuit voltage V_{oc} shown in Figure 5.1(a, b) were measured under 1.5AM illumination and were taken from the work of Klein (2003a), Table B.5, p.133.

The photoluminescence spectra of the same series of solar cells (Figure 5.1(b)) reveal similar features like undoped μc-Si:H films. The PL band ('μc'-Si-band) with a maximum at about 0.97eV and half-width of about 0.14eV, characteristic for the microcrystalline phase, shifts continuously to higher energies by about 0.08eV with increasing *SC* or V_{oc}. An additional PL band at about 1.3eV, attributed to the amorphous phase appears in the PL spectrum, but only at the highest *SC* of 5.6% (see Figure 5.1(b)). In spite of the significant contribution from the amorphous phase for sample prepared at *SC*=5.2% (see Figure 5.1(b)), the corresponding PL spectrum shows no PL signal originating from the amorphous phase.

The photoluminescence intensity and the halfwidth of the 'μc'-Si-band remain without significant changes upon increasing silane concentration for all investigated solar cells. Finally, we emphases that the lineshapes of the Raman and PL spectra of solar cells prepared by HWCVD shown in Figure 5.1 are very similar to those of the films shown in Figure 4.5.

5.2 Modulated Photoluminescence Spectra

Photoluminescence spectra on the same thin film *p-i-n* μc-Si:H solar cells as in Section 5.1 were measured now through the glass substrate (*p*-side), applying a modulation technique (see Section 3.3). The use of this technique was necessary in order to eliminate spurious PL signals from the glass, the transparent conductive oxide (TCO) and the *p*-layer and to investigate only those carriers, which are taking part in the photovoltaic process. Therefore, the measurements had to be performed at temperatures where solar cell operation was ensured. The solar cells were continuously excited with the excitation light of full intensity and the applied voltage was switched from 0V to V_{oc}. Thereby the photocurrent changed from I_{sc} (full carrier extraction) to 0mA (no carrier extraction). The recombination rate of the carriers active in the photovoltaic process changed from full recombination to none. Therefore, maximum PL signal is obtained at V_{oc} where full carrier recombination and no extraction in the *i*-layer are expected, whereas the minimum PL signal is obtained at I_{sc} where full carrier extraction and no recombination occurs (see Figure 3.5). By applying this technique it was assured that only the recombination of the relevant carriers are probed. The 1μm thick solar cells investigated here cover the structural composition range from fully crystalline (*SC*=3%) to more then 50% amorphous volume fraction in the intrinsic layer (Klein et al. 2002). The photon energy for excitation was 1.96eV, thus the photoluminescence experiments probe the 1μm thin layer of the solar cells.

In Figure 5.2 modulated luminescence spectra, obtained at 150K for these solar cells at various *SC* are shown on a logarithmic intensity scale, as example. For the lowest silane concentration values of 3%, the PL spectra reveal a broad emission band with the maximum at about 0.86eV and a halfwidth of about 0.14eV, which was already identified as 'μc'-Si-band. Interference fringes modify the shape of the luminescence spectra for solar cells with *SC* between 4% and 5.2%. The indicated open circles and dashed line refer to tentatively corrected spectra. The PL intensities of the modulated spectra for these solar cells prepared at deposition pressure p_D of 5Pa show slightly low values very likely due to reduced optical absorption, back reflection and light trapping.

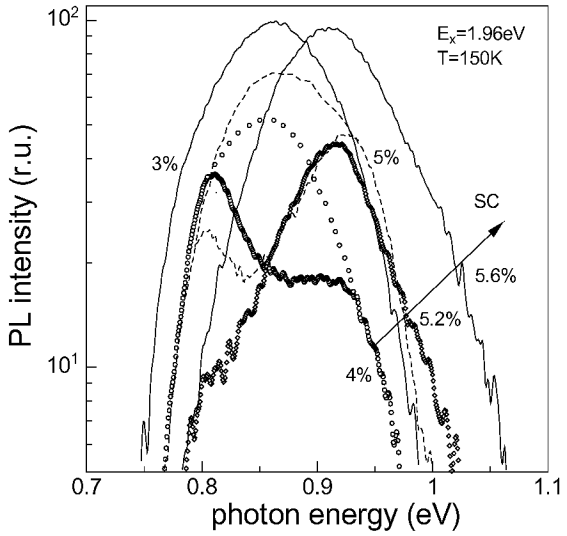

Figure 5.2: Modulated PL spectra of solar cells with *i*-layers prepared by HWCVD at different silane concentrations and deposition pressures, measured at 150K. Note the logarithmic intensity scale and tentatively corrected interference fringes for solar cells with *SC* of 4% and 5%. For solar cell with *SC* of 5.2% the interference fringes are not corrected for clarity.

Ignoring the fringe pattern in these samples, the shift of the 'μc'-Si-band towards higher energies (up to 0.91eV) with increasing *SC* from 4% to 5.6% and the absence of any contribution at 1.35eV originating from an amorphous phase is clearly visible. Such a shift is observed for all investigated temperatures (compare Figure 5.3(b)). As a result of the low deposition pressure (p_D=3.5%), the solar cell prepared at *SC* of 3% may have slightly different properties, i.e. a small deviation from the trend and an improved efficiency.

However, the modulated PL intensity and the spectral width of the 'μc'-Si-band are very similar for all solar cells. It should be noted here, that (i) the conventional PL spectra (data not shown) look almost identical and (ii) surprisingly a contribution of the amorphous volume to the PL spectrum is absent in both types of measurements for the sample with *SC*=5.6%, despite of the high amorphous volume fraction of more than 50%. In summary, we can conclude that with increasing *SC*, the 'μc'-band shifts continuously to higher energies for all μc-Si:H solar cells studied, whereas its modulated PL intensity and width are hardly affected, in agreement with previous observations for the undoped μc-Si:H films.

5.3 Influence of the Silane Concentration

In this paragraph, we provide a study of the influence of the silane concentration on the open circuit voltage V_{oc} and photoluminescence peak energy at different temperatures for the HWCVD μc-Si:H solar cells prepared at T_S=185°C.

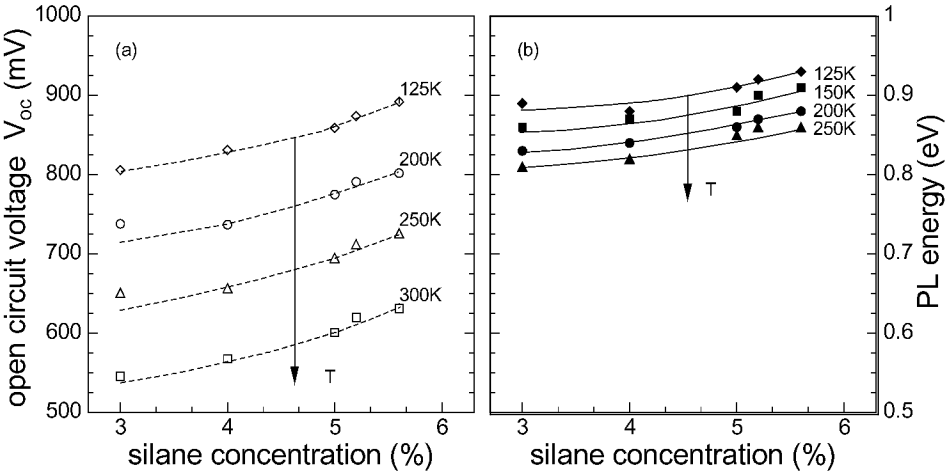

Figure 5.3: Dependence of (a) the open circuit voltage V_{oc} and (b) the energy of modulated photoluminescence spectra on the silane concentration at indicated temperatures for the same HWCVD series of solar cells as in Figure 5.2. Note the same energy scale for V_{oc} and modulated PL energy and additional measured V_{oc} values at 300K.

In Figures 5.3(a) and 5.3(b), the measured V_{oc} values are compared to PL energies of the modulated spectra for the HWCVD series of solar cells (see Figure 5.2) as a function of silane concentration for temperatures from 125K to 250K. Increasing the silane concentration from 3% to 5.6% causes a continuous increase of the open circuit voltage. Such an increase of open circuit voltage with increasing silane concentration was observed at room temperature, irrespective of the preparation method (Vetterl et al. 2000, Klein et al. 2002). Here we obtained higher V_{oc} values at 300K compared to those measured under AM1.5 illumination in the work of Klein (2002), due to higher optical generation rate ($1\times10^{20}cm^{-3}s^{-1}$) used. An increase of open circuit voltage of about 90mV upon change of silane concentration from 3% to 5.6% is found for all temperatures between 125K and 300K. The same parallel shift, but weaker (~50meV) as compared to V_{oc} is observed for the modulated PL peak energy with increasing *SC* (3-5.6%) for all temperatures between 125K and 250K (see Figure 5.3(b)). Figure 5.3 shows different temperature range for the two experiments and missing PL measurements at 300K due to weak PL signals and high effect of the noise there. The observed parallel shift for the both quantities with increasing temperature from 125K to 225K by about 150mV for open circuit voltage V_{oc} and by about 80mV for modulated PL energy is also shown in Figure 5.3. Detailed investigation on the temperature dependencies of V_{oc} and PL energies of the modulated spectra for this HWCVD series of μc-Si:H solar cells will be outlined in Section 5.4.2.

5.4 Temperature Dependence

Temperature dependences of short circuit current density j_{sc}, open circuit voltage V_{oc} and modulated PL peak energy are investigated.

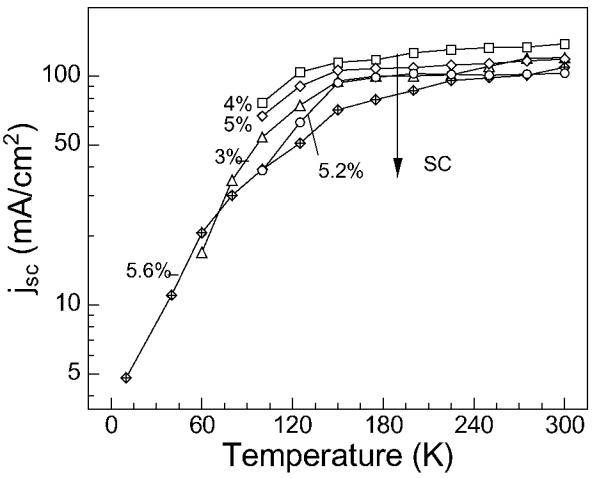

Figure 5.4: Influence of the measurement temperature on the short circuit current density j_{sc} obtained at maximum optical generation rate g_o (1×10^{20}cm^{-3}s^{-1} at $E_x = 1.96$ eV) for the solar cells with 3% ≤ *SC* ≤ 5.6%. The solar cells were prepared at T_S=185°C and T_F=1650°C with *i*-layer deposited by HWCVD.

The first paragraph includes temperature dependence of short circuit current density studied in relation to PL intensity of modulated spectra for μc-Si:H *p-i-n* solar cells with intrinsic layers prepared by HWCVD (T_S=185°C) at various silane concentrations. Next, the relationship between open circuit voltage V_{oc} and peak energy of the modulated PL spectra for the same HW solar cells is studied as a function of temperature. In the last part of this section, temperature dependences of j_{sc}, V_{oc} and modulated PL energy for microcrystalline, crystalline and amorphous silicon *p-i-n* solar cells are compared.

5.4.1 Short Circuit Current Density j_{sc} and Photoluminescence Intensity of Modulated Spectra

Figure 5.4 shows the short circuit current density j_{sc} on a logarithmic scale as a function of temperature for the same μc-Si:H *p-i-n* devices as in Figure 5.2. The higher values for the current density of about 100mA/cm^2 than usually measured at AM1.5 illumination (~20mA/cm^2), results from the high generation rate (1×10^{20}cm^{-3}s^{-1} at $E_x = 1.96$ eV) used in the present study. At high temperatures (> 125K), the short circuit current density exhibits slight decrease for all devices, indicating efficient carrier extraction. The j_{sc} measurements for solar cells with *SC* between 4% and 5.2% were restricted at high temperatures (100-300K). For solar cell prepared at *SC* of 4%, the highest values of the current density are observed and a rapid decrease of j_{sc} below 125K. Similar behaviour reveals solar cell with *SC*=5%, while for solar cell with *SC*=5.2%, the current density with significantly low values exhibits a sharp drop, starting already at 150K.

Extended current density measurements towards lower temperatures down to 10K were performed for two devices prepared at the highest *SC* of 5.6% as well as at the lowest *SC* of 3%. For the solar cell with *SC* value of 5.6%, the temperature dependence of short circuit current density shows completely different behaviour with decreasing temperature compare to all the other solar cells i.e. the j_{sc} starts to decrease at approximately 200K and decreases gradually to 5mA/cm^2 at 10K. The current density of sample with *SC* of 3% remains much higher values down to 125K and shows a sharp drop. Therefore, could not be measured at temperatures lower than 60K.

The differences in the j_{sc} values for μc-Si:H solar cells originate from different optical properties such as absorption, back reflection and light trapping for the different samples. Since, the PL intensity of the modulated spectra is also strongly affected by the different optical properties of the samples (see Section 5.2), seems to be difficult to define direct link between the PL intensity and short circuit current density. Thus the absolute values of j_{sc} are not possible to be used as a measure for the quality of the samples.

5.4.2 Open Circuit Voltage and Photoluminescence Energy of Modulated Spectra

Investigation on the relationship between open circuit voltage and energy of the modulated PL spectra is presented in this paragraph for the same HWCVD (T_S=185°C, T_F=1650°C) series of solar cells in the temperature range from 10K up to 300K. In Figure 5.5 a study of the V_{oc} as a function of the temperature for the same sample series as in Figure 5.4 is shown and compared to the energy of the modulated PL spectra. For all μc-Si:H solar cells studied, the temperature dependences of V_{oc} and modulated PL energy revealed the same increase of the both quantities ($\Delta V_{oc}, \Delta E_{\mathrm{mod}.pl}$) towards low temperature down to 100K. The same parallel shift of V_{oc} and modulated PL energy upon silane concentration is observed at all temperatures, i.e. V_{oc} and modulated PL energy increases with increasing *SC*.

Figure 5.5(a) shows the same $V_{oc}(T)$ dependences down to 100K for solar cells prepared at *SC* from 4% to 5.2%. While, the solar cell with *SC*=3% starts at the lowest value (~550mV) at 300K and rises towards low temperature, showing a strong bend over into saturation at about 150K. For the highest *SC* of 5.6%, V_{oc} shows the highest value (~960mV) at 10K and bends over at the lowest temperature. For these two samples, the Raman spectra indicate a change from a highly crystalline structure with only small contribution of the amorphous phase for the sample with *SC*=3% to a microstructure that is highly amorphous with small contribution from the crystalline phase, for the sample with *SC*=5.6% (see e.g. Figure 5.1(a)).

In Figure 5.5(b) the energy of the modulated PL band is presented as a function of the temperature for comparison. The highly crystalline solar cell with the lowest V_{oc} values exhibits the lowest modulated PL peak energies and the highly amorphous cell with the highest V_{oc} values shows the highest modulated PL energies. Therefore, the trend of V_{oc} and modulated PL peak energy with decreasing temperature is similar but the magnitudes of the increase of the PL energy are by far less than those of the open circuit voltage.

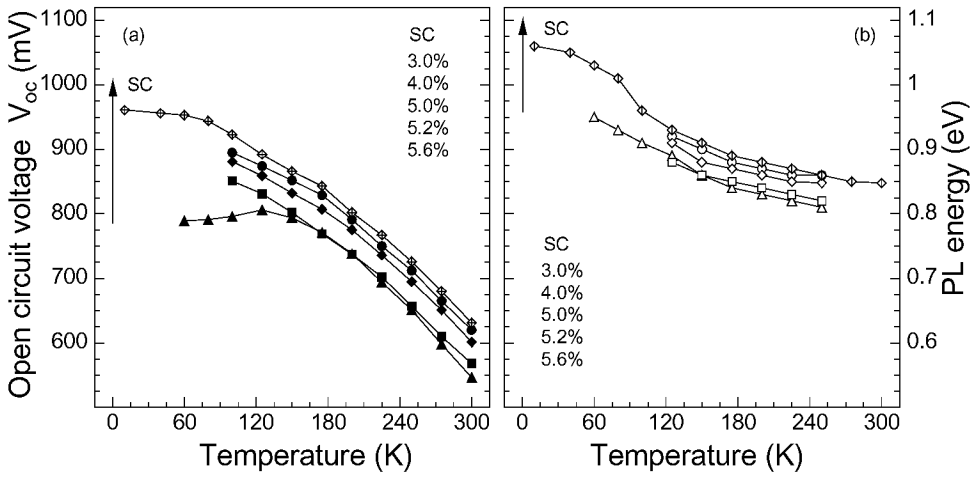

Figure 5.5: Open circuit voltage V_{oc} (a) and PL energy of modulated spectra (b) as a function of the temperature for the same devices as in Figure 5.4. Note the same energy scale for V_{oc} and PL energy of modulated spectra.

At high temperature, the modulated PL energies are much larger than the values of the open circuit voltage for all investigated solar cells and the shift is much weaker compared to the shift of V_{oc}. Therefore, at low temperature down to 100K, the difference between V_{oc} and modulated PL energy gets smaller as compared to that at high temperature. Below ~100K, the differences between V_{oc} and modulated PL energy for samples with *SC* of 3% and 5.6% are slightly bigger compared to that for solar cells with *SC* (4-5.2%). The reason is discussed in Section 6.2 in the framework of the occupation of states at and below the band edges according to quasi-equilibrium distribution. The strongly reduced carrier extraction at lower temperatures reported previously (see Section 5.4.1), seems to be also linked to the observed bend over of the open circuit voltage V_{oc} shown in Figure 5.5(a).

5.4.3 Comparison with Crystalline and Amorphous Silicon Solar Cells

In this paragraph, investigations on the temperature dependencies of short circuit current density j_{sc}, open circuit voltage V_{oc} and PL energy of modulated spectra for crystalline (c-Si) and hydrogenated amorphous silicon (a-Si:H) diodes are presented for comparison to those reported for microcrystalline (μc-Si:H) *p-i-n* solar cells (see e.g. Figures 5.4 and 5.5). As an example for crystalline silicon solar cell, a commercially available c-Si *p-i-n* diode (Hamamatsu) was investigated. The intrinsic layer was 250μm thick. The amorphous silicon solar cell was prepared by PECVD (T_S=185°C) at silane concentration value of 40% and the discharge power was 3.5W. The cell was deposited in *p-i-n* deposition sequence on asahi-u substrate with Ag back contact and 0.6μm thick intrinsic layers.

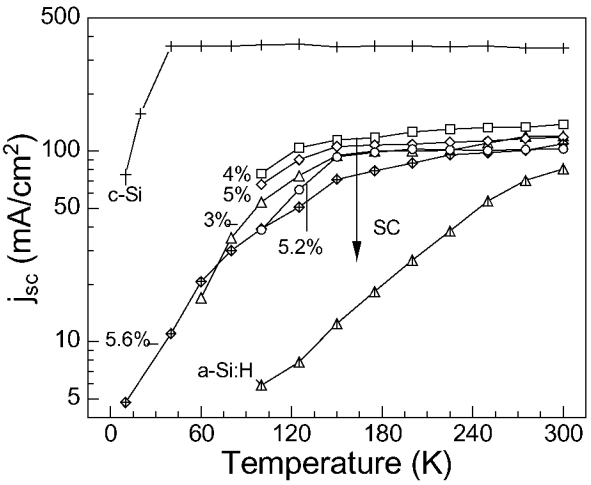

Figure 5.6: Dependence of the short circuit current density j_{sc} on the temperature, obtained at maximum optical generation rate g_o (1×10^{20}cm^{-3}s^{-1} at $E_x = 1.96$ eV) for the same µc-Si:H solar cells as in Figure 5.4, compared to a crystalline (c-Si) and an amorphous silicon (a-Si:H) solar cell.

Figure 5.6 compares the $j_{sc}(T)$ dependencies of investigated µc-Si:H solar cells as in Figure 5.4 with those for crystalline and amorphous silicon diodes. For all temperatures, the current density of the c-Si *p-i-n* diode is significantly higher than the one of the a-Si:H *p-i-n* device. The µc-Si:H *p-i-n* solar cells show j_{sc} values, which are between the current densities observed for c-Si and a-Si:H diodes, respectively. The short circuit density of about 360mA/cm^2 obtained for c-Si diode retains constant values upon decreasing temperature until 40K. Below 40K, a rapid decrease of the j_{sc} is seen up to values of about 75mA/cm^2 at 10K. In contrast, the current density for amorphous silicon *p-i-n* type solar cell decreases continuously with decreasing temperature, starting at the highest temperature with the lowest j_{sc} value of about 80mA/cm^2. The j_{sc} drops to 6mA/cm^2 and could not be measured at temperatures lower than 100K. The higher current density values for the c-Si *p-i-n* diode compared to those measured for a-Si:H *p-i-n* diode and for approximately 1µm thick µc-Si:H diodes, are due to significantly higher absorption of photons of energy $E_x = 1.96$ eV for the much thicker crystalline silicon diode.

Figure 5.7(a) compares the $V_{oc}(T)$ dependencies of the same microcrystalline diodes (see Figure 5.5(a)) with those of the crystalline and the amorphous silicon diodes. For the crystalline silicon *p-i-n* diode, V_{oc} is about 600mV at room temperature and rises almost linear up to about 1100mV at 10K, i.e. crystalline silicon diode bends over at the lowest temperature with the highest value of the V_{oc}. Open circuit voltage of the a-Si:H *p-i-n* diode shows the highest value (~900mV) at 300K and increases almost parallel to the $V_{oc}(T)$ of c-Si diode up to about 175K, when V_{oc} bends over. Further decrease of the temperature leads to a decrease of the V_{oc}, accompanied by a rapid decrease of j_{sc} (compare Figure 5.6).

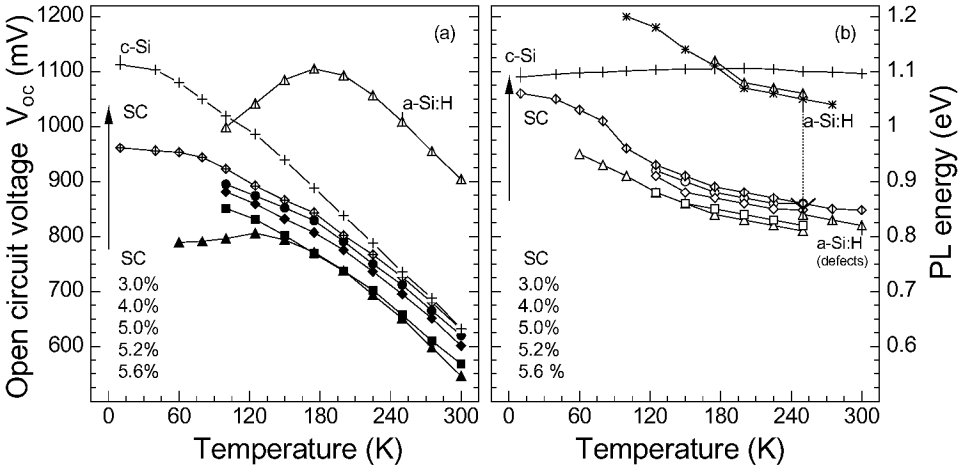

Figure 5.7: Open circuit voltage (a) and PL energy of modulated spectra (b) vs. temperature for the same µc-Si:H solar cells as Figure 5.5(a, b), compared to a crystalline and an amorphous silicon solar cell. Note, that above 250K the PL spectra of the a-Si:H solar cell is dominated from the 'defect'-band at about 0.84eV.

In contrast, for c-Si *p-i-n* diode a very weak band over is observed, which is also attended by a reduced carrier extraction below 40K (see Figure 5.6). It is obvious that with increasing silane concentration, the temperature dependence of V_{oc} for the microcrystalline diodes is getting closer to that of crystalline silicon and not to that of amorphous silicon.

Furthermore, Figure 5.7(b) shows the energy of the modulated PL spectra of crystalline and amorphous silicon diodes vs. temperature, compared to those of the microcrystalline silicon diodes. The modulated photoluminescence spectra of the c-Si *p-i-n* diode reveal a narrow band ('c'-Si-band) with a spectral maximum at about 1.1eV (see Figure 2.5). The PL energy of the modulated spectra maintained a constant value upon a change of the temperature from 10K to 300K. The spectral width of the entire modulated band is of about 0.004eV at 10K and increases to about 0.08eV at room temperature (data not shown). At low temperature, a second broader emission band at about 1.05eV appears, assigned to radiative recombination in the metallic electron-hole droplets (EHD) (Robbins et al. 1984).

Referring to Figures 5.7(b) and 5.2, the modulated PL spectra of µc-Si:H *p-i-n* diodes show the rather broad, featureless 'µc'-Si-band in contrast to c-Si. The peak position of the modulated 'µc'-Si-band for a diode with *SC* of 5.6% rises towards low temperature and bends over at about 1.06eV. This value is quite close to that of c-Si diode. For a-Si:H *p-i-n* diode, in addition to the main modulated band at about 1.12eV at 175K, a second transition at about 0.85eV dominates the modulated PL above 225K (modulated PL spectra not shown). The high energy PL band originates from tail to tail transition. The low energy PL band with a broader linewith than that of the 'µc'-Si-band and weak temperature dependence is attributed to radiative transitions via defect states ('defect'-band) (see Section 2.4.1).

The PL experiment on the a-Si:H solar cell displayed in Figure 5.7(b) is limited by strongly reduced carrier extraction at low temperature (see Figure 5.6). However, the additional PL spectra from this cell recorded by conventional PL technique in the temperature range 175-250K is observed. The conventional PL spectra revel slightly lower values of PL peak energy (stars symbols) compared to the modulated spectra (open triangles). By extension of the temperature range down to 100K, the PL energy of about 1.2eV is observed (see Figure 5.7(b)).

5.5 Effect of the Optical Generation Rate

As already demonstrated in Sections 5.3 and 5.4.2, there is an increase of the PL energy of modulated spectra and open circuit voltage V_{oc} with increasing silane concentration and decreasing temperature. It is also found that the short circuit current density j_{sc} drops at low temperatures. The emphasis here is on a investigation of the influence of the optical generation rate g_o on the photoluminescence properties and solar cells parameters for the best μc-Si:H solar cell from the HWCVD *p-i-n* device, i.e. *SC*=5.6% shown in Figure 5.2. Open circuit voltage, PL energy and of modulated spectrum and short circuit current density are studied as a function of the generation rate for different temperatures.

5.5.1 Open Circuit Voltage and Photoluminescence Energy of Modulated Spectra

Figures 5.8(a) and 5.8(b) illustrates the V_{oc} and the PL data measured at different temperatures as a function of the generation rate over three orders of magnitude. Here, the results for the solar cell with *SC* of 5.6% are presented as an example, since the other solar cells studied exhibit a similar behaviour.

In Figure 5.8(a) at high optical generation rate, above $g_o \geq 1\times10^{20}\,\mathrm{cm^{-3}s^{-1}}$ a logarithmic dependence of the open circuit voltage on the generation rate is shown for temperatures between 100K and 300K, i.e. $\Delta V_{oc} \propto \log g_o$. Below this value of the generation rate a strong deviation from the logarithmic dependence of V_{oc} on g_o is observed at room temperature. The investigated solar cell (*SC*=5.6%) contains high amorphous volume fraction and shows reversible light induced degradation (see Klein et al. 2003 for details). The curve at 300K in Figure 5.8(a) represents the $V_{oc}(g_o)$ in the degraded states, the arrow corresponds to the observed recovering process after annealing at 160°C for 1 hour.

At low temperature (down to 100K) the strong deviation from the logarithmic dependence of the V_{oc} on the g_o is reduced and change of the slope of the curves is observed. Further decrease of the temperature below ~100K leads to bend-over of the curves. At 10K an enhancement of V_{oc} by 30mV for a change of g_o by two orders of magnitude and subsequent slight decrease is observed.

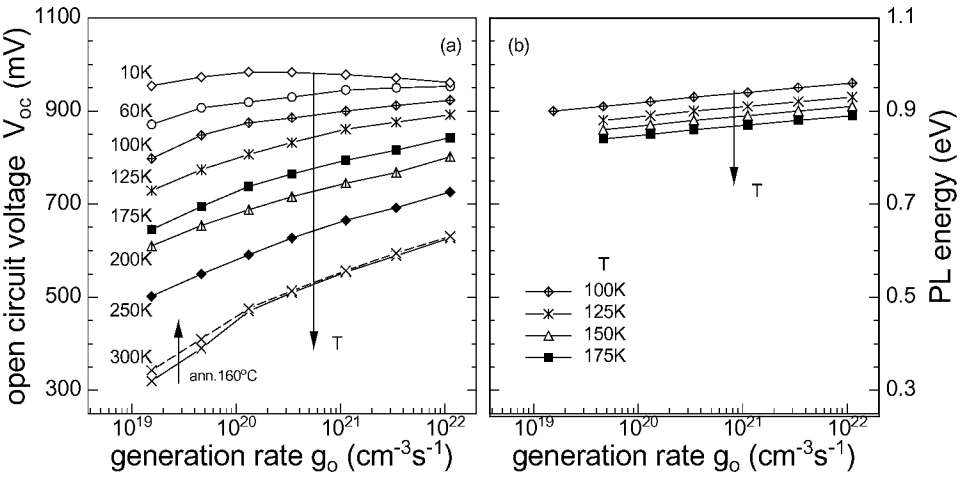

Figure 5.8: Open circuit voltage (a) and energy of modulated photoluminescence spectra (b) at different temperatures vs. optical generation rate in logarithm scale for the solar cell prepared at *SC*=5.6%. Note the same energy scale for V_{oc} and modulated PL energy.

Similar $V_{oc}(g_o)$ dependence exhibit the other solar cell prepared at lower *SC* (3-5.2%) at temperatures below 100K, while above this temperature at low generation rate ($g_o \leq 1\times10^{20}\,\mathrm{cm^{-3}s^{-1}}$) there is no deviation from the logarithmic dependence of the open circuit voltage on the generation rate (data not shown).

In Figure 5.8(b) the energy of the modulated PL band is shown versus generation rate on a logarithmic scale, for comparison. Compare to the V_{oc}, the modulated PL energy is found to be proportional to the logarithm of the generation rate over three orders of magnitude for all temperatures investigated from 100K to175K, i.e. $\Delta E_{pl} \propto \log g_o$. At low generation rate, the energies of modulated PL spectra show significantly higher values than the values of V_{oc} for all temperatures. The differences become smaller at high generation rate, while the shift of the modulated PL energy is much weaker compared to the shift of V_{oc}, e.g. the modulated PL energy shows a weak generation rate dependency as well as a weak temperature dependence (see Figure 5.5(b)).

5.5.2 Short Circuit Current Density j_{sc}

Having presented the $j_{sc}(T)$ dependence at maximum generation rate ($1\times10^{20}\mathrm{cm^{-3}s^{-1}}$ at $E_x = 1.96\,\mathrm{eV}$) for the highly amorphous μc-Si:H thin film solar cell prepared at *SC*=5.6% (see e.g. Figure 5.4), it will now be analysed the effect of a change of the generation rate on the current density. The maximum generation rate was chosen such that it provided a current density of about $100\mathrm{mA/cm^2}$ at room temperature, i.e. about five times the current density of AM1.5 illumination, and was reduced by neutral density glass filters over three orders of magnitude.

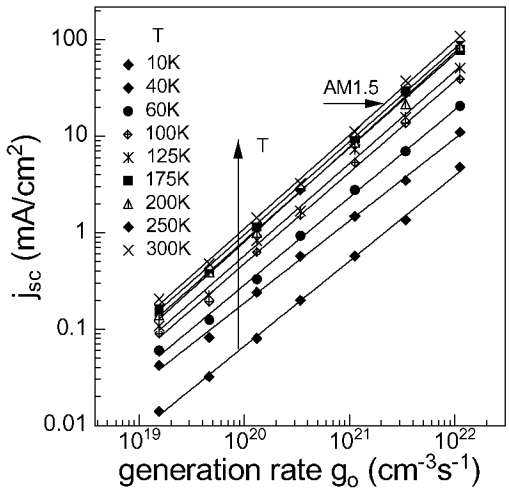

Figure 5.9: The short circuit current density j_{sc} at different temperatures vs. optical generation rate for µc-Si:H solar cell prepared at *SC* of 5.6%in a double logarithmic plot.

Figure 5.9 demonstrates in a log-log plot, an almost power low dependence of the short circuit current density on the photo-generated carriers for all temperatures, i.e. ($j_{sc} \propto g_o^{\gamma}, \gamma \approx 0.9$), i.e. the decrease of j_{sc} as a function of temperature (compare Figure 5.6) does not alter the almost linear dependence of j_{sc} on g_o. For highly amorphous µc-Si:H solar cell (*SC*=5.6%) the slope of the curves is $\gamma < 1$ for all temperatures, instead of expected absolute value of one, but the others solar cells prepared at lower *SC* (3-5.2%) show $\gamma \approx 1$.

Chapter 6

6 Discussion

The last chapter is organised in two main parts: In the first part, the shift of the photoluminescence band ('μc'-Si-band) in microcrystalline silicon to high energy with increasing silane concentration is discussed based on the assumption of band tail states. Then, to determine the slope of the band tail state for the conduction band, a 'carrier thermalization model' developed for a-Si:H is applied to μc-Si:H thin films. Furthermore, crystallinity obtained by Raman spectroscopy is used as a parameter that allows a general discussion of all PL data for sample series prepared by different deposition methods and parameters.

In the second part, a link between the PL peak energy and open circuit voltage V_{oc} in solar cells based on carrier distributions in the band tail states, i.e. the splitting of the quasi-Fermi levels of the electrons and holes will be discussed. The influence of the temperature and optical generation rate on the both quantities is also discussed. Finally, from simulated experimental PL spectra and open circuit voltages for different temperatures, a distribution of band tail states is deduced, by using a simple model.

6.1 Discussion on Photoluminescence Properties of μc-Si:H Thin Films

Throughout this work, the electronic properties of microcrystalline silicon (μc-Si:H) thin films and devices was extensively studied by photoluminescence (PL) spectroscopy to explore the localized band tail states, the defect states and the material quality. Already in the early stages of research on microcrystalline silicon, the PL measurements indicated similarities of microcrystalline and hydrogenated amorphous silicon (see e.g. Section 2.4.1), showing a broad featureless PL band below the band gap and the distribution of recombination lifetimes according to Bhat et al. (1983). Photoluminescence results on μc-Si:H thin films presented in Chapter 4, will therefore be discussed in a framework of a model for recombination processes in a-Si:H (see Figure 2.3).

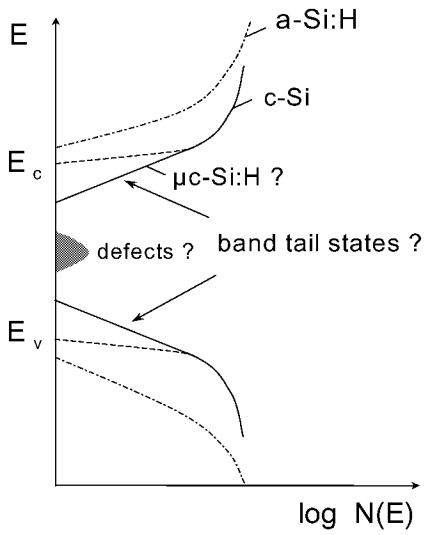

Figure 6.1: Model density of states diagram for microcrystalline silicon (µc-Si:H), illustrating possible localized band tail states and defect states in the gap. For comparison, the density of states diagram for hydrogenated amorphous (a-Si:H) and crystalline (c-Si) silicon are outlined.

Now, the model density of states diagram for µc-Si:H, illustrating the possible localized band tail states and defects in the band gap is introduced for further discussion on the changes of the electronic properties of the material upon changes of the silane concentration (i.e. crystalline volume fraction) and also on the slope of the exponential band tails. In Figure 6.1 the density of states distribution $N(E)$ for µc-Si:H is shown and compared to those of crystalline and hydrogenated amorphous silicon. The bonding disorder in a-Si:H leads to broadening of the density of states distributions to form band tail states, instead of sharp band edges in c-Si. Such band tails of localized states in a-Si:H extended from the band edges into the gap over an energy range of about 0.2eV (conduction band tail) or of about 0.3-0.4eV (valence band tail) (Stutzmann et al. 1987).

From the optical absorption spectra shown in Figure 2.4 it is known that µc-Si:H almost reproduced the absorption coefficient values of c-Si in the above-gap absorption region (above 1.1eV). The density of states distribution for µc-Si:H is suggested to be quite similar to the one in c-Si in this absorption region. However, at energies below the c-Si band gap, evidence of additional states within the gap is provided from the photothermal deflection spectroscopy (e.g. Carius et al. 1997). Evidence for exponential band tails was reported for polycrystalline silicon, caused by the grain boundaries (Werner and Peisl 1985a). From various other experimental data, e.g. electrical transport, electron spin resonance there is additional evidence for localized states in µc-Si:H apart from those of the well-known dangling bond defects (Carius et al. 1997, Fuhs et al. 2000, Reynolds et al. 2003, Finger et al. 2000a).

6.1.1 Blueshift of Photoluminescence Peak Energy

A question of how does the density of states distribution in μc-Si:H change upon change of the silane to hydrogen ration in the gas phase (*SC*) during the film growth is addressed here by investigation of the lineshapes, the energies and the widths of luminescence spectra.

Referring to Figures 4.3 and 4.9, the PL band at about 0.9eV ('μc'-Si-band) shifts continuously to higher energies (up to 1.05eV) with increasing silane concentration for all sample series investigated. Corresponding to the model for a-Si:H, this shift of the 'μc'-Si-band upon *SC* could be a result of (i) a increase of a electron-phonon interaction, leading to a Stokes shift between luminescence and absorption energies as have been proposed in the work of Street (1978a) (ii) a steepening of band tail sates and /or (iii) a decrease of the density of band tail sates with a constant slope (iv) decreasing of a non-radiative recombination via defect states (v) and a shift of the band gap in μc-Si:H and thus the crystallite size, e.g. 'quantum size effect'[13] as will be shown later in Section 6.1.3.

At first, electron-phonon coupling will be discussed as the possible reason for the shift of the luminescence peak energy upon silane concentration. The photoluminescence linewidth ΔE_{pl} can be described by electron-phonon coupling contribution ΔE_{el-ph} and the zero-phonon distribution ΔE_{0-pl} by the expression:

$$\Delta E_{pl}^2 = \Delta E_{0-pl}^2 + \Delta E_{el-ph}^2 = \Delta E_{dis}^2 + \Delta E_{el-ph}^2 \tag{6.1}$$

According to the considerations of Street (1978a) for a-Si:H, the largest contribution to the width of luminescence band comes from the Stokes shift, *W*, due to electron-phonon coupling. The linewidth is defined as the energy difference $E_{04} - E_{pl}$ between the optical gap and the photoluminescence peak energy, i.e. $\Delta E_{pl} \propto W^{1/2} \approx (E_{04} - E_{pl})^{1/2}$. Then, one should expect that the width of the luminescence band change upon change of the silane concentration. Taking into account that the linewidth of 'μc'-Si-band remains without significant changes upon silane concentration for all undoped μc-Si:H thin films studied (see Figures 4.3 and 4.13). The prediction of a predominant electron-phonon coupling contribution to the width of the 'μc'-Si-band can be ruled out. Therefore, it is reasonable assumption that the width of the luminescence band is given by the zero-phonon distribution, i.e. the disorder. It is therefore directly related to the slope of the band tails.

The steepening of band tail sates and /or the decrease of the density of band tail sates with a constant slope is pointed out as the second and the third possible reasons for the shift of the PL band to higher energies with increasing silane concentration. The rather constant width or a slight broadening of the PL band in μc-Si:H, means that a steepening of the band tail is not very likely.

[13] 'Quantum size effect' may occur in very small size crystallites embedded in amorphous phase leading to increase of the band gap.

Instead, in this work is proposed that the shift of the 'μc'-Si-band is caused by a decrease in the density of band tail states. This will lead to increase of the PL peak energy in relation to a shift of the carrier distributions towards higher energies as will be shown in Section 6.1.3.

6.1.2 Temperature Dependent Measurements

In the previous paragraph it has been demonstrated that the width of the luminescence band is given by the zero-phonon distribution, identified with the disorder. It is therefore, directly related to the slope of the band tails. To determine the slope of exponential band tail states, more quantitatively. In the following, we attempt to apply the 'carrier thermalization model' developed for a-Si:H (see Section 2.4.1) to μc-Si:H thin films prepared by HWCVD at T_S=185°C. The model considered a temperature dependent demarcation level, $E_d(T)$ at which the probability for radiative recombination equals to probability for non-radiative thermal excitation. Defined in this way E_d can be used to explain the temperature dependence of both, the intensity (Section 4.6.1) and the peak energy position (Section 4.6.2) of the PL band in μc-Si:H. In the model for a-Si:H, it has been assumed that with increasing temperature, only electrons trapped at the conduction band tail states are thermally exited to more mobile states from where they can diffuse away non-radiatively, while the holes are deeply trapped at the valence band tail states (see Street 1981 and reference therein).

At first, the results on the temperature dependence of the PL intensity (see e.g. Section 4.6.1) are discussed. As shown in Figure 4.18 the luminescence intensity is found to be a decreasing function of temperature for all investigated μc-Si:H films prepared by HWCVD at T_S=185°C. The luminescence signal of the 'μc'-Si-band quenches much faster starting at lower temperatures compare to that observed for the 'a'-Si-band. Like in amorphous silicon, thermal excitation of carriers trapped in shallow states and subsequent diffusion to defect states is proposed as the reason for the quenching of the PL intensity also for μc-Si:H films. The more rapid quenching of the photoluminescence originating from μc-Si:H as compared to a-Si:H pointed to shallower trap states, e.g. a steeper band tail.

However, for more quantitative discussion, the temperature dependence of the PL intensity is used to determine the slope of the band tail. According to Eq.2.3, i.e.

$$I(T) = I_o\left(1 + A\exp\left(\frac{T}{T_o}\right)\right)^{-1}$$

a logarithmic plot of $(I_o / I - 1)$ vs. temperature shown in Figure 6.2 provided the characteristic temperature T_o, which is related to the slope of the band tail. Where I_o is the temperature independent PL intensity at low temperature where the thermal excitation of electrons is negligible. We use I_o as a fitting parameter for obtaining the best straight line following Collins et al. (1980), i.e. for films with low temperature saturation one normalized I to I_o, the zero temperature extrapolation of the data in the saturation regime. In this way obtained values for I_o are outlined in Table 6.1.

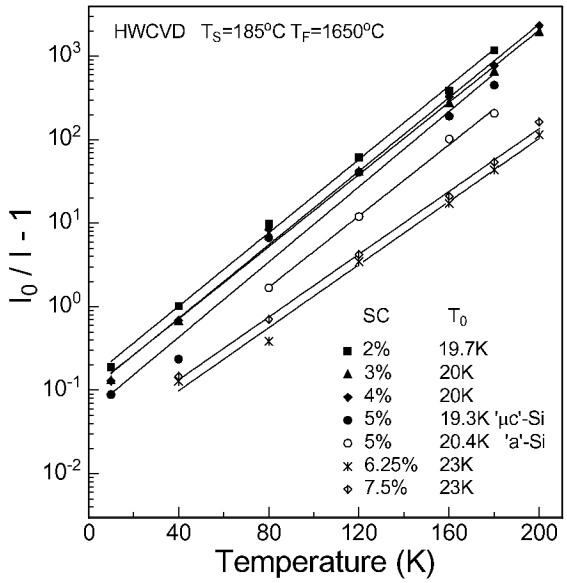

Figure 6.2: Temperature dependence of total PL intensity fitted to Eq.2.3 for μc-Si:H undoped films deposited by HWCVD at T_S=185°C with indicated values of the silane concentration and characteristic temperature T_o.

The slope of the band tail is described by the T_o, derived directly from the slope of the curves displayed in Figure 6.2. The values for T_o, deduced from the best fit to Eq.2.3 for μc-Si:H thin films deposited by HWCVD at varies silane concentration are listed in Table 6.1. For highly crystalline films prepared at low *SC* between 2% and 5%, the derived characteristic temperatures is $T_o \approx 20$K. Similar values of about 23K for the T_o are obtained in highly amorphous films (*SC* > 6.25%). Corresponding to the model for a-Si:H, the T_o is related to the slope of conduction band tail, E_o by Eq.2.6, i.e.

$$T_o = E_o / k \ln(v_o \tau_r)$$

By using a reasonable value of the average radiative lifetime $\tau_r \approx 10^{-3}$s for μc-Si:H (see Bhat et al. 1983a), one obtains quite similar value of the band tail for highly crystalline and predominantly amorphous films, i.e. $E_o \approx 0.035$ eV and $E_o \approx 0.039$ eV, respectively. The latter is comparable with the observed value of 0.04eV for the conduction band tail (CB-band tail) in a-Si:H (Street 1981).

Having estimated the slope of the single tail in μc-Si:H by adopting the model for a-Si:H, the question of how steep are the CB-band tail and the valence band tail (VB-band tail) in μc-Si:H is of importance. The slope of the both tails determines the full width at half maximum of the PL spectrum.

Samples	*SC (%)*	I_o	$T_o (K)$	$E_o (eV)$ *PL int. dep.*	$E_o (eV)$ *PL peak shift*	k *(eV/K)*
01C190	2	0.039	19.7	0.034	0.019	9.9×10^{-4}
01C188	3	0.066	20.1	0.035	0.02	1×10^{-3}
01C187	4	0.078	20	0.034	0.03	1.38×10^{-3}
01C185 'μc'-Si	5	0.045	19.3	0.033	0.021	1.09×10^{-3}
01C185 'a'-Si	5	0.014	20.4	0.035	0.036	1.8×10^{-3}
01C184	6.25	0.07	23	0.039	0.035	1.5×10^{-3}
01C180	7.5	0.077	23.1	0.039	0.037	1.6×10^{-3}

Table 6.1: Overview of the fitting parameter to the Eq.2.3 obtained for μc-Si:H thin films deposited by HWCVD at T_S=185°C. The slope of the band tail can be calculated once from temperature dependence of PL intensity (Eq.2.6) and second from the shift of the PL peak energy (Eq.2.8).

In hydrogenated amorphous silicon the broader VB-band tail of about 0.03-0.04eV determines the halfwidth of the luminescence spectrum, considering strong electron-phonon interaction suggested from Street (1978a) (see e.g. Section 2.4.1). Therefore, one way of explanation is (i) that the CB-band tail in μc-Si:H is similar to the CB-band tail in a-Si:H or (ii) VB-band tail is similar to CB-tail in a-Si:H or (iii) both, the CB-band tail and VB-band tail in μc-Si:H are similar to CB-band tail in a-Si:H. The possible answer of this question will be given in our model calculation (see e.g. Section 6.2.1) based on electron and hole distributions in the CB- and VB- band tail states with a constant slope.

Another way to determine the slope of the band tail is to apply 'carrier thermalization model' to describe the temperature dependence of the PL peak position. In Figure 4.19(a) the shift of the PL peak energy towards lower energies with increasing temperature was shown for all μc-Si:H films prepared by HWCVD at T_S=185°C. A temperature coefficient, k of about 1.1×10^{-3} eV/K for the shift of luminescence peak energy above 40K is deduced for highly crystalline samples prepared at low *SC* values between 2% and 4%. For highly amorphous films prepared at high *SC* of 6.25% and 7.5% the shift of the peak energy is much stronger and has a temperature coefficient of about 1.6×10^{-3}eV/K above 80K (the data for k are listed in Table 6.1). The same value of the temperature coefficient was reported by Austin et al. (1979), which is in a good agreement with value of 1.8×10^{-3}eV/K (Tsang and Street 1979). According to the model, the values of the characteristic temperature T_o and $(-dE_d/dT)$ are connected to the slope of the band tail, E_o by Eq.2.8, i.e.

$$\frac{dE_d}{dT} = -\frac{E_o}{T_o}$$

Again, a fairly good agreement between calculated slope of the band tail from the temperature dependence of the PL intensity (Eq.2.6) and the one obtained from the shift of the PL peak energy upon temperature (Eq.2.8) was found for highly amorphous samples, i.e. $E_o \approx 0.039$eV derived from Eq.2.6 and $E_o \approx 0.036$eV from Eq.2.8.

For highly crystalline material, the E_o values derived from the temperature dependence of PL intensity suggested less steeper band tail states of about 0.035eV, compared to the values of about 0.022eV obtained from the shift of the PL peak energy to low energy with increasing temperature. The discrepancy could be explained in the following way: for microcrystalline silicon the distributions of electrons and holes in the conduction and valence band tail states are very likely involved in the non-radiative process, which quench the PL intensity and shift the PL peak to low energy. Therefore, the model assumption adopted from a-Si:H, saying that only one type of carriers, namely electrons are thermally exited with rise of the temperature is likely not valid for microcrystalline silicon.

In Figure 4.19 the FWHM of the 'μc'-Si-band does not depend on the temperature up to 120K, than slightly increase. A broadening of the 'μc'-Si-band at high temperature is explained in terms of a broadening of the carrier distributions. At low temperature, it can be assumed that the deeper states have a constant occupation probability, i.e. the carrier distribution is proportional to density of states, as $(\exp(-E/kT))$. With increasing temperature the distribution of carriers in the shallower states above E_d can be approximated by a Bolzman distribution, e.g. $N(E)\exp[-(E-E_d)/kT]$ for electrons. The width of 'a'-Si-band in samples prepared at high *SC* (5-7.5%) decreases with increasing temperature up to values of typically 0.27eV for pure a-Si:H and then increases slightly above 160K. This decrease of the width is not observed in hydrogenated amorphous silicon, for which below 150K the linewidth does not depend on the temperature and increases rapidly above this temperature (Tsang and Street 1978, Austin et al. 1979). Structural inhomogeneity along the growth direction is very likely the reason for the unexpected decrease of the width of the 'a'-Si-band at lower temperatures, observed for μc-Si:H films.

6.1.3 Crystallinity in Relation to Photoluminescence Peak Energy

Microcrystalline silicon is an inhomogeneous mixture of amorphous regions and crystalline regions, which consists of small crystallites, clustered to columns or grains of different sizes (see Figure 2.1). As described in Section 3.5.1, Raman intensity ratio I_C^{RS} is used as a semi-quantitative measure for the crystalline volume fraction of the material. I_C^{RS} is defined as the ratio of the integrated Raman intensity of the crystalline phase to the total scattering intensity in accordance to Eq.3.7, i.e.

$$I_C^{RS} = \frac{I_{520} + I_{505}}{I_{520} + I_{505} + I_{480}}$$

The Raman intensity ratio shall not be identified with the 'real' crystalline volume content, but it has been shown to be a useful quantity in determining trends in the crystallinity of μc-Si:H sample series in the deposition parameter space.

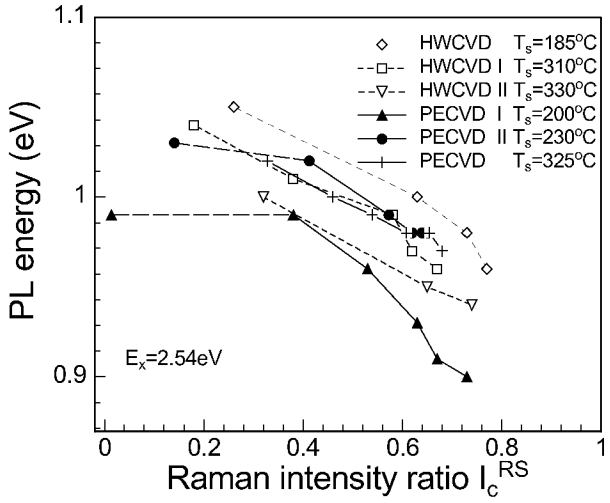

Figure 6.3: Photoluminescence energy of 'μc'-Si-band measured by photoluminescence vs. integrated intensity ratio I_C^{RS} obtained by Raman spectroscopy for samples prepared by different deposition methods and substrate temperatures. Laser wavelength of 488nm ($E_x = 2.54\,\text{eV}$) was used for excitation of the PL spectra, as well as for the Raman spectra.

This has been demonstrated in the work of Vetterl et al. (2002), where I_C^{RS} is shown to be a common parameter when the conductivity increases for all μc-Si:H films prepared by PECVD at different substrate temperatures.

In Figures 4.3, 4.9, 4.11, 4.13, 4.16 it is shown that with increasing silane concentration the 'μc'-Si-band shifts continuously to higher energies for all μc-Si:H films studied, irrespectively from the preparation method, the substrate temperature, the way of illumination (front surface and rear interface) and the photon energies of excitation. However, for sufficient comparison and further discussion on differently prepared μc-Si:H films, the Raman intensity ratio will be used.

In Figure 6.3 PL peak energy vs. I_C^{RS} is shown for all sample series studied, prepared by different deposition methods and substrate temperatures. The use of Raman intensity ratio, instead of silane concentration provides a better ordering of the data, even when the data points do not fall in a single line, i.e. the films with similar crystalline volume fraction exhibit different PL energies. A general trend is found for all films investigated, i.e. the PL peak energy increases with decreasing crystalline volume fraction. For all HWCVD series, the PL peak energy shifts continuously towards higher energies with decreasing I_C^{RS}, while for PECVD I, II series the continuous increase of the PL energy is followed by a constant behaviour of the PL energy at the highest crystalline volume fraction. It is difficult to determine the PL peak position for this material due to the dominant contribution of the 'a'-Si-band in the PL spectra (see Figure 4.15(a)).

In order to reduce the contribution of the amorphous band, an excitation at 1.59eV has been performed (see Section 4.5). The corresponding PL spectrum for PECVD II (T_S=230°C) sample (see Figure 4.15(a)) revel a rather broad halfwidth of about 0.18eV and less steeper slope of the low energy part of the PL spectrum as compared to the other µc-Si:H films from this series, indicating not fully microcrystalline material. Similar PL properties were found for the sample with the highest I_C^{RS} prepared by PECVD I (T_S=200°C) (see Table B.4).

The reason for the shift of the PL energy to higher energies with decreasing crystalline volume fraction is not a smaller size of the crystallites embedded in amorphous phase leading to the increase of the band gap of the material, i.e. 'quantum size effect'. Since the highest energies found in Figure 6.3 are still below the band gap of crystalline silicon, there is no indication for 'quantum size effect', as proposed from Kaan Kalkan et al. (2000). Also the analysis of the absorption spectra of many series do not give any evidence for the shift of the gap in µc-Si:H with decreasing crystalline volume fraction.

The increase of the PL peak energy upon change of the crystalline volume fraction can also be a result of decreasing non-radiative recombination via defect states as was proposed in the work of Bhat et al. (1983b). Referring to Figure 4.4, the PL intensity remains without significant changes upon changes of the crystallinity, i.e. the PL intensities are very similar for all films. Thus, decreasing non-radiative recombination via defect states cannot cause the shift of the PL peak energy to higher energies with decreasing I_C^{RS}. Besides the present work, the shift of the luminescence band with varying crystalline volume fraction is also reported for µc-Si:H deposited by HWCVD (T_S=240°C) (Yue et al. 2000, Han et al. 2000). The PL intensity increases two orders of magnitude with decreasing crystallinity, thus the non-radiative recombination via defect states cannot be excluded.

Figure 6.4 shows the spin density N_S obtained by ESR measurements as a function of I_C^{RS} for the two sample series prepared by different deposition methods and substrate temperatures, as in Figure 6.3. Almost constant values of the spin densities are found with increasing I_C^{RS} up to about 0.7 for all films from the both series, except at the lowest I_C^{RS} value for PECVD I (200°C) series. Therefore, below $I_C^{RS} < 0.7$ the shift of the PL peak energy upon change of I_C^{RS} for HWCVD I (310°C)[14] as well as for PECVD I (see Figure 6.3) cannot be caused by the non-radiative recombination via defects. Above I_C^{RS} value of about 0.7, the spin density increases for PECVD I series, while the PL energy drops (see Figure 6.3), indicating that a part of the shift can be due to non-radiative recombination. For HWCVD I, the N_S values remained constant and PL energy increase with decreasing I_C^{RS}, thus the contribution of non-radiative recombination to the shift of PL energy can be excluded. Another effect might have a dominant contribution to the shift of the luminescence energy.

[14] In this work we distinguish between HWCVD I series prepared at T_S=310°C and HWCVD II at T_S=330°C (see Table B.2), while in the work of Finger et al. (2002) and Klein et al. (2003) the same films are combined in one series denoted as HWCVD (T_S=330°C).

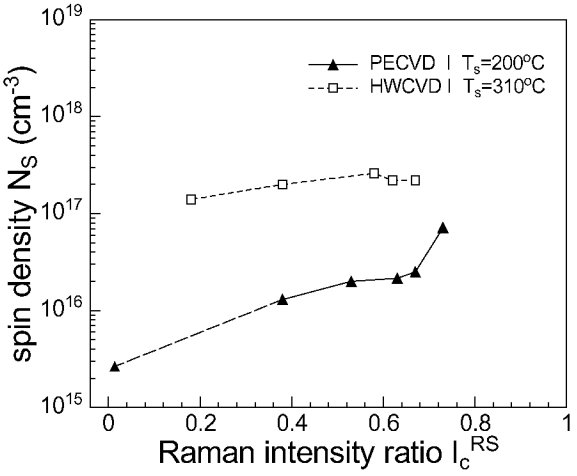

Figure 6.4: Spin densities measured by ESR as a function of Raman intensity ratio I_C^{RS} of two sample series prepared by different deposition methods and substrate temperatures as in Figure **6.3**. The spin density data are taken from Baia Neto et al. (2002), Finger et al. (2002) and Klein et al. (2003).

Now, the effect of the substrate temperature on the PL peak energy will be discussed. An increase of substrate temperature in HW material (see Figure 6.3) leads to decrease of the PL energy and increase of N_S up to about $10^{17}cm^{-3}$ as shown in Figure 6.4. No similar correlation with the substrate temperature was found for μc-Si:H films prepared by PECVD. The spin densities of films deposited by PECVD II (T_S=230°C) and PECVD (T_S=325°C) are not known. For HW films, the shift of the PL peak energy could be due to non-radiative recombination, but since the PL intensity for films at high T_S is the same (in the factor of 2) as that in low T_S, another effect might have a dominant contribution to the shift here, too.

In the model of density of states distribution in μc-Si:H (see Figure 6.1), the density of states distribution is given by the superposition of density of states distribution similar to that in c-Si in the upper part and the additional band tail sates as in a-Si:H in the lower part. The shift of the PL peak energy to higher energies with decreasing I_C^{RS} (increasing *SC*) can be interpreted assuming steepening of the band tail states and /or decease of the density of band tail states with a constant slope. As the halfwidth of the 'μc'-Si-band remanded constant values or slightly increases with increasing *SC* (see Figure 4.3), the steepening of the band tail states can be excluded. Figure 6.5 shows the model density of states distributions in μc-Si:H, demonstrating a reduced density of states distribution and a shift of the carrier distribution towards higher energies with decreasing crystalline volume fraction (or increasing silane concentration). However, the small effect of N_S on the shift of the PL peak energy cannot completely be ruled out, but the major contribution to the shift very likely is due to change of the band tail states.

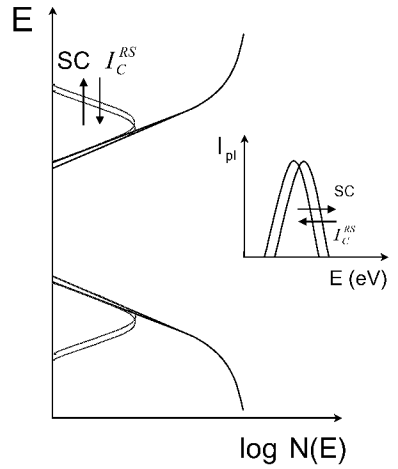

Figure 6.5: Schematic density of states distributions in μc-Si:H, indicating a reduced density of states distribution and a shift of the carrier distribution towards higher energies with decreasing I_C^{RS} (or increasing *SC*).

Referring to Figures 4.7 and 4.8, the occurrence of an additional broader PL band ('poly'-Si-band) centred at 0.7eV only for films prepared at high T_S is strongly related to the high spin density observed for these material (see Figure 6.4). In Figure 4.9 the 'poly'-Si-band maintains a spectral maximum at about 0.7eV with increasing *SC* (or decreasing crystalline volume fraction), compare to the observed shift of the 'μc'-Si-band to higher energies. The 0.7eV band reveals very similar PL peak position and linewidth to that of previously observed in polycrystalline silicon (Savchouk et al. 1995, Koshka et al. 1996). Therefore this emission band is preliminarily assigned to defect-related transitions as in polycrystalline silicon.

6.2 Discussion on Solar Cells - Link between PL Energy and V_{oc}

The relationship between PL energy and open circuit voltage V_{oc} in solar cells is discussed in this section. Before starting with a discussion, general experimental findings and arising problems related to improvement in the material and device quality of μc-Si:H solar cells are outlined. Previous work on μc-Si:H solar cells with intrinsic layers prepared by PECVD and HWCVD have shown, a very similar electronic and device properties, such as the increase in V_{oc}, plus the decrease in short circuit current density and in the dark conductivity with increasing *SC* (i.e., decreasing I_C^{RS}) (Vetterl et al. 2002, Klein et al.2003). These effects are not understood, and particularly the high V_{oc} of more than 590mV obtained for a HWCVD cell, while retaining a high current density, is of current interest (Klein et al. 2003).

It has been attempted to interpret these effects in terms of a shift of the effective mobility gap from 1.15eV for highly crystalline material to 1.35eV for a cell close to the transition to amorphous growth (Brammer et al. 2000). However, a careful analysis of the absorption spectra of many sample series does not give any evidence for such a shift in this energy range. Barriers between crystalline regions could cause a similar effect, but would affect the carrier mobility rather than the carrier density.

Applying the model of density of states distribution in μc-Si:H proposed in Figure 6.1, the PL-band ('μc'-Si-band) at low temperature (PL energy and width of the spectrum) is attributed to radiative tunnelling transitions of electrons and holes trapped in their respective band tails.

If the excess carriers occupy the states at band edges and below them according to a quasi-equilibrium distribution within the time scale of the experiment (i.e. for temperatures which are not too low) the distributions can be characterized by quasi-Fermi-levels (see e.g. Section 2.5). The splitting of the quasi-Fermi levels determines the open circuit voltage V_{oc} in solar cells (see Eq.2.20). Therefore, a study of relationship between V_{oc} and PL peak energy as a function of temperature (see Section 5.4.2) and optical generation rate (see Sections 5.5.1) can provide information on the density of states. In this work, one HWCVD series of thin film *p-i-n* μc-Si:H solar cells is investigated. By using modulation technique it was assured that only the recombination of the relevant carriers is probed and thus a direct link between energy of modulated PL spectra and V_{oc} is given.

The effect of the silane concentration on the energy of modulated PL spectra and V_{oc} measured at different temperatures for μc-Si:H solar cells is discussed at first. Referring to Figure 5.5 the increase of the energy of modulated PL spectra and V_{oc} with increasing silane concentration is observed for all temperatures investigated. The constant width and a very similar PL intensity of the modulated PL band upon change of *SC* (see Figure 5.2) indicated that the increase of it energy position is not caused by a decreasing defect density. This is consistent with the very similar short circuit current j_{sc} values for all the samples (see Figure 5.4). Instead, the increase of the PL peak position with increasing *SC* can be interpreted assuming, a reduced density of the localized states, which leads to a shift of the carrier distribution towards higher energies as shown in Figure 6.5.

The discussion of the increase of V_{oc} with increasing silane concentration has to take into account the effect of the temperature on the splitting of the quasi-Fermi levels. By comparison of $V_{oc}(T)$ dependence of the μc-Si:H *p-i-n* devices prepared at various *SC* with that of the c-Si *p-i-n* diode (see Figure 5.7(a)), one gets further evidence that the increase of V_{oc} with increasing *SC* is likely caused by a decrease of the density of band tail states. Figure 5.7(a) shows that with increasing *SC*, the $V_{oc}(T)$ dependency of the microcrystalline diodes is getting closer to that of crystalline silicon. This can be interpreted by a reduction of the states below the band gap of crystalline silicon, as this effect allows the quasi-Fermi levels to shift closer to the band edges and thereby giving rise to an increase of V_{oc}.

A study of the temperature dependences of V_{oc} and the energy of modulated PL band for μc-Si:H solar cells with different *SC* revealed the same parallel shift of both quantities with increasing *SC* for all temperatures investigated (see Figure 5.5).

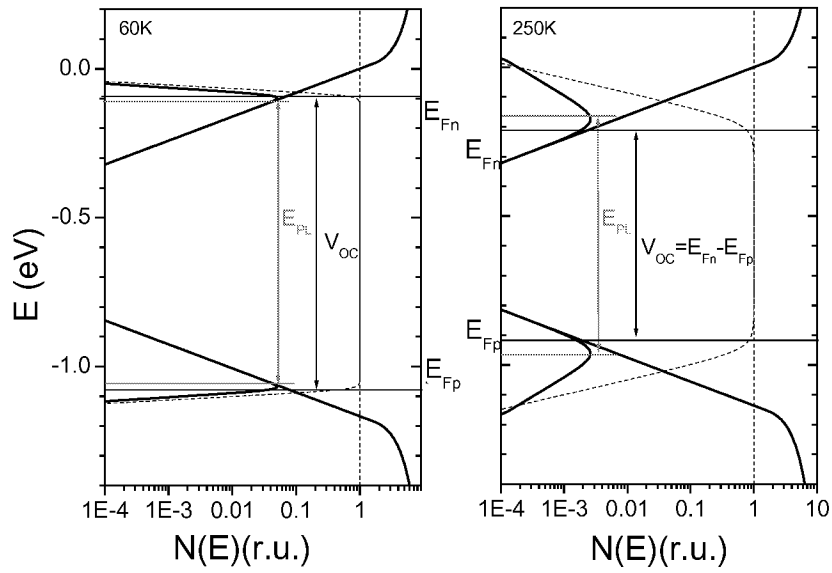

Figure 6.6: Schematic density of states diagram together with Fermi-Dirac statistical distribution function (dashed lines), showing the change of the carrier distributions in band tails states and the splitting of the quasi-Fermi levels for electrons and holes at two indicated temperatures.

The open circuit voltage and the energy of modulated PL band are found to increase towards low temperature for all μc-Si:H solar cells as shown in Figure 5.5. The magnitude of the increase of the PL energy is by far less than those of the open circuit voltage. At high temperature, the modulated PL energies are much larger than the values of the V_{oc} for all μc-Si:H solar cells and while the shift is much weaker compared to the shift of the V_{oc}, at lower temperatures the differences becomes smaller. The reason is discussed in the following: the important point is the probability for the occupation of states in the conduction and valence band tail given by quasi-Fermi levels and the transition (recombination) of carriers between 'real states' determines the energy of modulated PL band. Therefore upon decreasing temperature (i) the strong increase of V_{oc} is assigned to a strong shift of quasi-Fermi levels to higher energies and (ii) the weaker increase of the energy of modulated PL band is due to much weaker change of the carrier distributions in the band tail states (see Figure 6.6). Referring to Figure 5.7(a) the shift of quasi-Fermi levels to higher energies with decreasing temperature is inhibited by the band tails. An increasing deviation between $V_{oc}(T)$ of μc-Si:H solar cells and that of c-Si diode is observed towards lower temperatures (see Figure 5.7(a)). It is accompanied by a strongly reduced carrier extraction found for μc-Si:H solar cells as compared to c-Si diode (see Figure 5.4), i.e. current density j_{sc} decrease rapidly when the bend-over of V_{oc} sets in. Carriers trapped at the band tails is suggested as the possible reason for short diffusion or drift length leading to observed current density behaviour. It is tempting to identify here, the carrier transport as a limiting factor at low temperatures.

Finally, the influence of the optical generation rate on the V_{oc} and on the energy of modulated PL spectra at different temperatures is discussed (see Figure 5.8). The results for the best-performing solar cell (*SC*=5.6%), which contains high amorphous volume fraction, are discussed in more details, since the other solar cells studied exhibited similar behaviour. In Figure 5.8(a) a logarithmic dependence of the open circuit voltage on the generation rate is found at high generation rate, above $g_o \geq 1\times10^{20}\,\mathrm{cm^{-3}s^{-1}}$ for all temperatures between 100K and 300K, i.e. $\Delta V_{oc} \propto \log g_o$ for $j_{sc} \propto g_o$ as shown in Figure 5.9. The logarithmic dependence of V_{oc} on g_o is expected, according to:

$$V_{oc} \propto \ln\left(\frac{j_{ph}}{j_0(T)}\right) \tag{6.2}$$

if the short circuit current density j_{sc}, which is proportional to the g_o, is much larger than the $j_0(T)$. The saturation current density depends on properties including the band gap, temperature and defect density. At room temperature for generation rate below $g_o \leq 1\times10^{20}\mathrm{cm^{-3}s^{-1}}$, a strong deviation from the logarithmic dependence of the V_{oc} on the g_o is found, which is recovered after annealing at 160°C for 1 hour (see Klein et al. 2003 for details). This indicates light induced degradation of the material during the experimental cycles of illumination and annealing, which increases the saturation current density. The reduced V_{oc} at low generation rate can be improved by minimising the $j_0(T)$, i.e. with decreasing temperature the j_0 decreases. At low temperature (down to 100K) the strong deviation from the logarithmic dependence of the V_{oc} on the g_o is reduced and change of the slope of the curves is observed. Further decrease of the temperature below 100K leads to bend-over of the curves. The reason might be a change of the diode quality factor n, i.e. transfer from low-level injection (LLI) to high-level injection (HLI) regions (see Section 2.5.1) or the exponential increase of density of state distributions to higher energies with increasing generation rate at lower temperatures can limited the increase of the quasi-Fermi levels, i.e. the increase of the V_{oc} with increasing the number of photo generated carries at lower temperatures is likely determined by the localized band tail states.

The modulated PL energy is found to be proportional to the logarithm of the generation rate over three orders of magnitude for all temperatures investigated, i.e. $\Delta E_{pl} \propto \log g_o$. Referring to Figure 5.8, the energy of the modulated PL spectra and V_{oc} show similar behaviour upon increasing the number of photo generated carries as well as decreasing temperature. The reason of much weaker shift of energy of modulated PL band to higher energies compare to the strong increase of V_{oc} with increasing number of photo generated carriers is the weak change of carrier distributions when the density of states distribution increases exponentially in contrast to the strong shift of quasi-Fermi levels to higher energies starting at lower voltages determined by the dark current density (compare Figure 5.5).

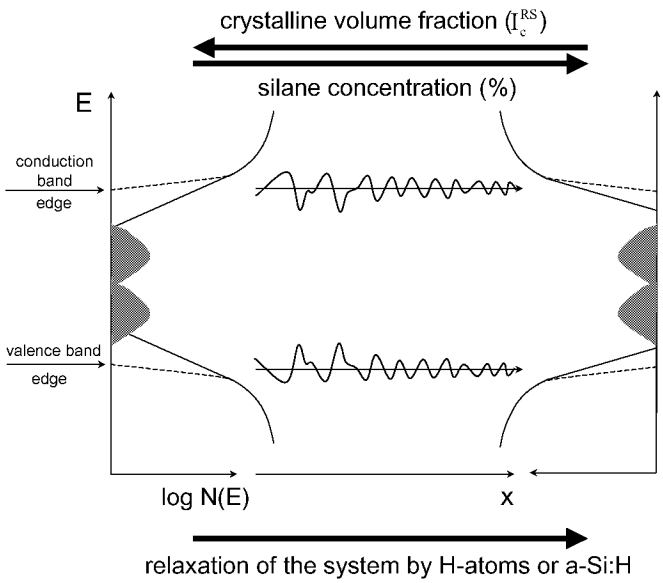

Figure 6.7: Density of states scheme and energy space diagram for microcrystalline silicon, demonstrating a model of fluctuations of the band edges and reduced density of band tail states with increasing silane concentration or decreasing crystalline volume fraction, respectively.

In conclusion, the increase of the PL energy and V_{oc} with increasing silane concentration (or decreasing crystalline volume fraction) is attributed to the shift of the carrier distributions and thus the quasi-Fermi levels to higher energies. This can be interpreted assuming a decrease of the density of band tail states. As the short circuit current density is found to be almost constant for the investigated solar cells, the band tail states do not act as a recombination centres but act as a traps at room temperature. However, microcrystalline silicon is an inhomogeneous material (see Figure 2.1) consisting of crystalline grains containing structural defects like stacking faults, grain boundary regions and an amorphous phase. Therefore, it is expectable that the band tail states are inhomogeneously distributed on a length scale of several nm, in contrast to the more homogeneous distribution in amorphous silicon. Also the transport and the recombination processes might be very different from the homogeneous distribution of band tail states throughout the material. To date one can only speculate about the microscopic effects that lead to the band tail states. Strain disorder at grain boundaries, structural defects could be the cause. In order to visualize the change of the band tails as a function of the silane concentration (or the crystalline volume fraction) the schematic density of states diagram together with energy space diagram are shown in Figure 6.7. It demonstrates a model of fluctuations of the band edge and the reduced density of band tail states due to presence of hydrogen or hydrogenated amorphous silicon. If one imagines that due to the enhance hydrogen content, strained bonds will be broken and saturated by hydrogen or hydrogenated amorphous silicon the lattice relaxation could be improved.

6.2.1 Comparison between Model Calculated and Experimental Results

In order to get a more quantitative relation between the experimental results and the proposed density of states distribution, a simple model was used to simulate photoluminescence spectra and open circuit voltage V_{oc} in μc-Si:H solar cells as a function of temperature. The model is based on carrier distributions in quasi-equilibrium conditions, i.e. carrier distributions that can be described by Fermi-Dirac statistic and the recombination between the two carrier distributions determines PL band (energy and width of the spectrum). In the model symmetric density of states distributions for electrons and holes are assumed in Appendix A (see Figure A.1). The density of states distribution for the electrons $N_n(E)$ in the conduction band is derivative and it is assumed to be a steady function of the energy.

To account for the tail states, energy $E = \overline{E}$ is defined. Above this energy the density of states for electrons follows the density of states similar to that in crystalline silicon and below which exponentially decreasing band tail states are assumed, thus $N_n(E)$ is described by two functions (see Eq.A.8):

$$N_n(E) = \begin{cases} N_{0n}\sqrt{\dfrac{2eE}{E_{0n}}}, & \text{if } E > \dfrac{E_{0n}}{2} \\ N'_{0n}\exp\left(\dfrac{E}{E_{0n}}\right), & \text{if } E \le \dfrac{E_{0n}}{2} \end{cases} \tag{6.3}$$

where N_{0n} and N'_{0n} are constant pre-factors and E_{0n} is the slope of the band tail states. The basic physics and formulas used in these model calculations can be found in Section 2.5 and Appendix A.

For simplicity, we describe non-equilibrium conditions by quasi-equilibrium. The increase of carrier distributions above their equilibrium values n_0 and p_0 ($\Delta n >> n_0$ and $\Delta p >> p_0$) therefore leads to splitting of the Fermi level into two quasi-Fermi levels for electrons and holes, i.e. E_{Fn} and E_{Fp} respectively (see Figure 2.6). The product of the excess carrier density distributions *np* determines the energy difference between the quasi-Fermi levels (see Section 2.5), which is identical to the open circuit voltage V_{oc} in solar cells, i.e.

$$np \propto \exp\left(\frac{E_{Fn} - E_{Fp}}{kT}\right)$$

This assumption is fulfilled at high temperature, where quasi-equilibrium is established. It requires strong interactions between trap states and band tail states.

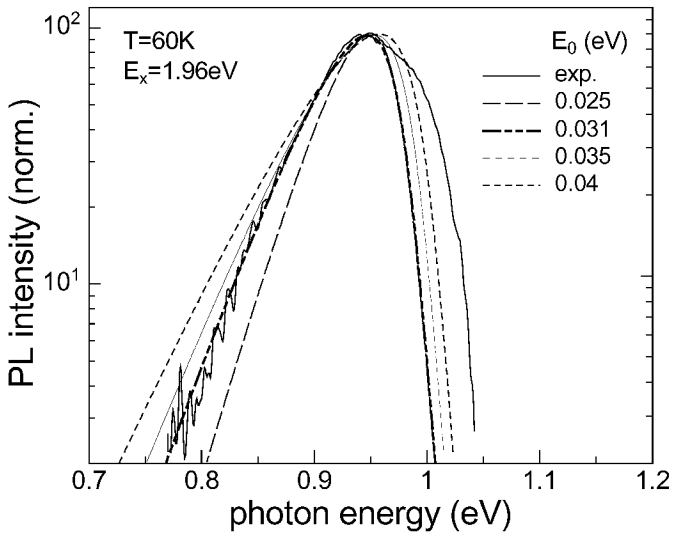

Figure 6.8: PL spectrum taken at 60K for solar cell prepared by HWCVD (T_S=185°C) at *SC* of 3% (solid line) fitted with different values of the slope of band tail states $E_o \approx 0.025\text{-}0.04$eV. The calculated PL spectra are normalized to the height of the experimental PL spectrum.

At low temperature, quasi-thermal equilibrium with deep states cannot be established, as the interactions with band states become weak and the relaxations in the localized tail states are dominated by tunnelling processes. Therefore, deviations between calculated from the model and experimental results are expected. Finally, the PL spectra are calculated as the total sum over equally weighted radiative transitions with energy E_{PL} between carriers from the band tail states (see Eq.A.18):

$$I_{PL} \propto \sum_{E_i=E_{initial}}^{E_{final}} N_n(E) f_n(E) N_p(E-E_{PL}) f_p(E-E_{PL})(E_{i+1}-E_i) \tag{6.4}$$

where $N_n(E)f_n(E)$ and $N_p(E-E_{PL})f_p(E-E_{PL})$ are density distribution of electrons in conduction band tail states and holes in valence band tails states, respectively (see Appendix A).

To get more quantitative value for the slope of the band tails, the PL energy position and the width of the experimental PL spectra taken at different temperatures are matched by the numerically calculated PL spectra from Eq.6.4 by using a values of the slope between 0.025 and 0.04eV. The open circuit voltage V_{oc} is calculated within the model assumption for quasi-equilibrium conditions, as the difference between the quasi-Fermi levels for electrons and holes, i.e. $V_{oc} \propto E_{Fn} - E_{Fp}$.

A first guess for the slope of the exponential band tail states can be obtained from the low energy part of photoluminescence spectrum, as the occupation of these states is constant.

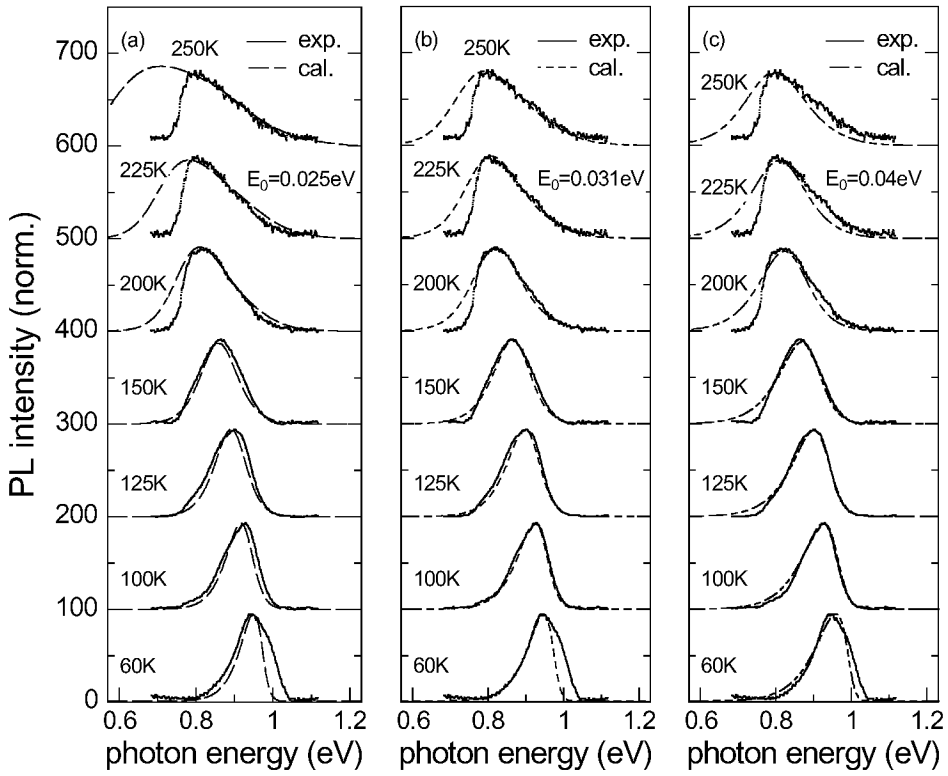

Figure 6.9: Experimental PL spectra (solid lines) taken at different temperatures for a solar cell prepared by HWCVD (T_S=185°C) at *SC*=3%, together with spectra calculated from Eq.6.3 (dashed lines) by using reasonable values for the slope of the band tails of (a) 0.025eV, (b) 0.031eV and (c) 0.04eV. The calculated PL spectra are normalized to the height of the experimental PL spectrum and all PL spectra are shifted vertically for clarity.

In Figure 6.8 a logarithmic intensity scale was chosen to fit the low energy part of PL spectrum taken at 60K for solar cell prepared by HWCVD (T_S=185°C) at *SC* of 3%. The numerically calculated PL spectra are obtained from Eq.6.4 by using values of the slope between 0.025eV and 0.04eV and are normalized to the height of the experimental PL spectrum. A value of 0.025eV for the slope of the band tail states is obviously too low and does not reproduce the experimental PL spectrum reasonably, i.e. steep slope results in a too narrow PL spectrum. The best agreement between calculated and experimental PL spectra in the low energy region is obtained by using a slope of 0.031eV for the band tails. A value of 0.035eV is still reasonable to describe the slope at the low energy part of the experimental PL spectrum. Further increase of the slope gives a strong deviation at lower energies and results in a broader linewidth of the PL spectrum calculated from Eq.6.4. All calculated PL spectra show deviation from the experimental one at higher energies due to the fact that quasi-equilibrium conditions are very likely not established at 60K.

The effect of the temperature and the choice of the slope of the band tails on the PL peak position and the linewidth for the same device as in Figure 6.8 are studied next. Figure 6.9 shows spectra calculated from Eq.6.4 for different temperatures between 60K and 225K by using the same values for the slope $E_o \approx 0.025$, 0.031 and 0.04eV to fit the PL peak energy and the width of experimentally obtained PL spectra. All PL spectra are shifted vertically for clarity. Irrespective of the choice of the slope of the band tails, the calculated spectra reproduced the shift of the PL band to lower energies with increasing temperature. Also the halfwidths of calculated spectra are getting broader upon increasing of the temperature in line with the experimental observations.

Figure 6.9(b) reveals that the best agreement between the numerical model and experiment in the whole temperature range is obtained by using value of 0.031eV for the slope of the band tails. As discussed previously, the calculated spectrum by using $E_o = 0.031\,\mathrm{eV}$ reveals a deviation at the high energy and good agreement at the low energy part as compared to the experimental PL spectrum (at 60K). For temperatures between 100K and 150K the emission spectra calculated from the model reproduce the lineshape, energy position and linewidht of the experimentally obtained spectra, quite reasonably. At high temperatures the experimental PL spectra, which are extended to energies below 0.8eV are beyond the spectral response of the Ge detector. The PL peak energies of calculated PL spectra are slightly shifted to lower energies (see Figure 6.11(b)) and their linewidths are getting broader when compared with experimental PL spectra. By using a less steeper slope of 0.025eV for exponential band tails states, a deviation in the high energy part is observed between calculated and experimental PL spectra, taken at temperatures above 200K (see Figure 6.9(c)). Steepening of the band tail states at high temperatures (see Figure 6.9(a)) leads to broader halfwidth of the calculated spectra. The reason might be that a simple exponential function used in Eq.6.3 is not sufficient to describe the density of localized tails states distributions in microcrystalline silicon.

In Figure 6.10 the PL spectra taken at different temperatures for a solar cell prepared at high *SC* of 5.6% is shown. For this sample the PL spectrum (at 150K) reveals a higher PL peak energy of about 0.91eV compare to that observed for sample prepared at low *SC* of 3% (see Figure 5.2). With increasing silane concentration, the shift of the 'μc'-Si:H towards higher energies is indicated for all temperatures (compare Figure 6.9). Despite, the interference fringes that modify the shape of PL spectra slightly, the best agreement between theory and experiment is obtained by using the same value of 0.031eV for the slope of the band tails as for sample with *SC*=3%. This suggests that steepening of the of the band tail states with increasing silane concentration is not the cause for the higher PL energy. Since the PL intensity is found to be very similar for both solar cells (see Figure 5.2), the strong influence of non-radiative recombination can also be ruled out. The shift of the PL band to high energies with increasing *SC* is therefore interpreted assuming a decrease of the localized band tail states with a constant slope of 0.031eV.

In Figure 6.11 calculated and experimental values of V_{oc} and PL peak energy as a function of temperature are summarized for two solar cells prepared by HWCVD at *SC* of 3% and 5%.

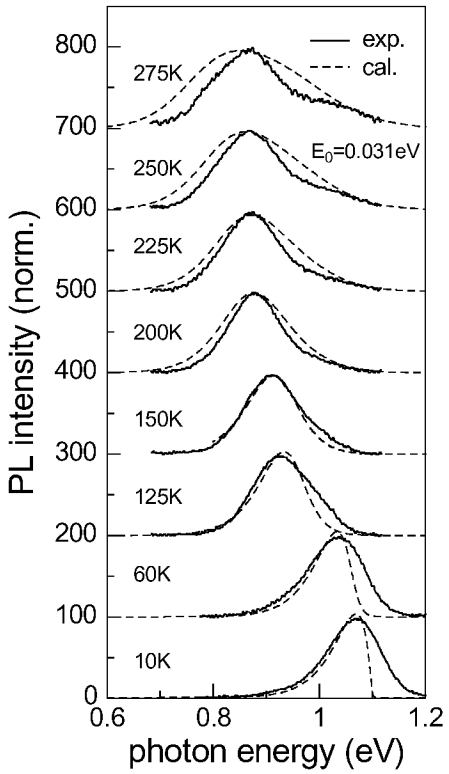

Figure 6.10: Experimental PL spectra (solid lines) at different temperatures for solar cell prepared by HWCVD (T_S=185°C) at *SC*=5.6% and numerical spectra (dashed lines) calculated from Eq.6.4 by using $E_o = 0.031\,\text{eV}$. All PL spectra are shifted vertically for clarity.

The trend with increasing silane concentration is well established but the calculated V_{oc} are higher than the experimental values by about 80mV for all temperatures. We do not have explanation for this difference between model calculations and experiment, yet. The temperature dependencies of the calculated and the experimental values of V_{oc} are well described for both solar cells. Upon decreasing temperature, the numerically calculated V_{oc} increases, while the experimental V_{oc} bends over into saturation likely related to reduced carrier extraction for both solar cells (see Figure 5.4). At low temperature, the difference between calculated and experimental V_{oc} becomes larger, because the quasi-thermal equilibrium cannot be established. The interactions with band states become weak and the relaxations in the localized tail states are dominated by tunnelling processes. It is not clear how the V_{oc} is defined there, as the splitting of the quasi-Fermi level obviously does not follow Fermi-Dirac statistics.

In Figure 6.11(b) calculated and experimental values of PL peak energy vs. temperature are shown for comparison. For the both solar cells, the calculated PL spectra by using the same value of 0.031eV for the slope of band tail states reproduce quite reasonably the PL energy positions of the experimental spectra at all temperatures.

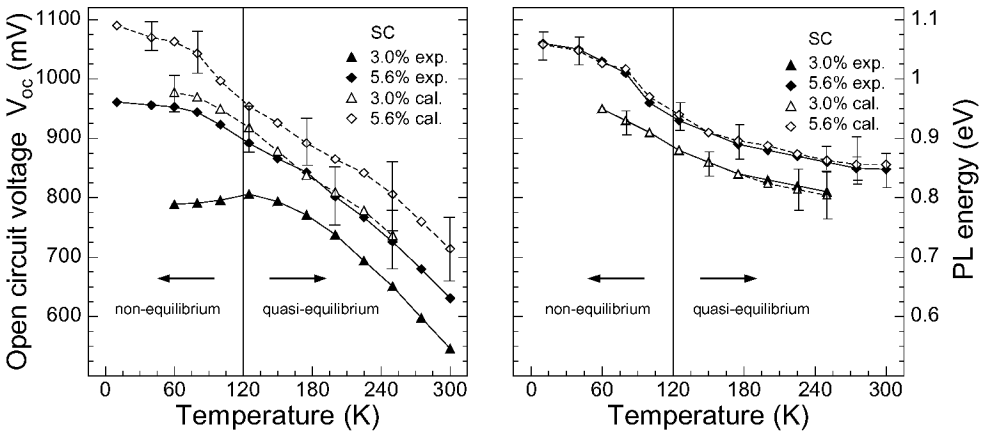

Figure 6.11: Comparison between calculated (open symbols) and experimental (filled symbols) values of the open circuit voltage V_{oc} (a) and the PL energy (b) vs. temperature for two solar cells prepared at *SC* of 3% and 5.6% (compare with Figure 5.5). Numerical calculated results for the two devices are obtained by using a 0.031eV value for the slope of the band tail states.

In summary, the density of states distribution in μc-Si:H given by: (i) the density of states distribution similar to that in c-Si in the upper part and (ii) the exponential density of states distribution for localized sates with a value of 0.031eV for the slope in the lower part, described all data well. From the transient photocurrent measurements (TOF) by using a multiple-trapping model, the same value of the slope of the valence band tail (~0.031eV) was obtained (Dylla et al. 2004).

Chapter 7

7 Summary and Conclusions

The electronic properties of microcrystalline silicon thin films and solar cells with different structural composition were studied by photoluminescence spectroscopy. In particular, the changes of the electronic properties of this material upon changes of the silane concentration were addressed in this work by investigation of the lineshape, energy and linewidth of the luminescence spectrum. For μc-Si:H thin films, the luminescence spectra with almost Gaussian shape reveal a rather broad featureless band ('μc'-Si-band). The maximum peak energy of the 'μc'-Si-band is between 0.9-1.05eV and the linewidth is of about 0.13-0.15eV. Compare to the sharp spectral line with a maximum at about 1.1eV of the narrow PL band of crystalline silicon and the broader featureless band ('a'-Si-band) lying between 1.25eV and 1.4eV with a width of 0.25-0.35eV observed for amorphous silicon, the 'μc'-Si-band show similarities with the 'a'-Si-band, i.e. the broader and featureless PL band below the band gap and the distribution of recombination lifetimes. In conjunction with other experimental results, e.g. photothermal deflection spectroscopy, electrical transport, electron spin resonance it is concluded that the 'μc'-Si-band can be assigned to radiative tunnelling transitions of electrons and holes trapped in their respective band tail states, similar to amorphous silicon.

With increasing silane concentration the 'μc'-Si-band shifts continuously to higher energies for all μc-Si:H thin films investigated, irrespectively of the preparation method (PECVD and HWCVD), the substrate temperature, the way of illumination (front surface and rear interface) and the photon energies of excitation. The photoluminescence intensity and the linewidth of the luminescence spectra do not reveal significant differences upon increasing silane concentration. However, for comparison of differently prepared films in the present work the Raman intensity ratio I_C^{RS}, obtained by Raman spectroscopy was used instead of silane concentration. The use of Raman intensity ratio provides a better ordering of the data, even when the data points do not fall in a single line, i.e. the films with similar crystalline volume fraction exhibit different absolute values of the PL peak energy. The data of all sample series, prepared by different deposition methods and substrate temperatures show a clear trend, i.e. the PL energy increases with decreasing crystalline volume fraction (or increasing silane concentration). As the shift of the PL energy to higher energies with decreasing crystallinity is not accompanied by an increase of the PL intensity of the investigated films.

The shift cannot be caused by the decreasing non-radiative recombination via defect states. This is valid below $I_C^{RS} < 0.7$ and it is in line with almost constant values of the spin density N_S obtained by the electron spin resonance measurements. Above I_C^{RS} value of about 0.7, the spin density increases, whereas the PL energy drops indicating that part of the shift of the PL peak energy could be due to non-radiative recombination. If the non-radiative recombination via defects cannot cause the shift of the PL energy to higher energies upon decreasing I_C^{RS}, another effect might have a dominant contribution to the shift. An increasing substrate temperature at a constant I_C^{RS} leads to a decrease of the PL energy and increase of the spin density of the HW material. For HW films, the shift of the PL peak energy could be due to non-radiative recombination, but since the PL intensity for films at high T_S is the same (in the factor of 2) as that in low T_S, another effect might have a dominant contribution to the shift here, too.

According to the model of density of states distribution in μc-Si:H, the density of states distribution is given by the superposition of density of states distribution similar to that in c-Si at higher energies and the additional band tail sates as in a-Si:H at lower energies. The increase of the PL peak energy of 'μc'-Si-band with decreasing crystalline volume fraction (or increasing *SC*) can be interpreted, assuming a steepening of the band tail states and /or a decease of the density of band tail states with a constant slope. As the halfwidth of the 'μc'-Si-band remanded constant values or slightly increases with increasing *SC*, the steepening of the band tail states can be excluded. It is proposed, that the shift of the 'μc'-Si-band to higher energies with decreasing I_C^{RS} is caused by reduced density of the localized band tail states, which lead to a shift of the carrier distributions towards higher energies. However, the small effect of N_S on the shift of the PL peak energy cannot completely be ruled out, but the major contribution to the shift very likely is due to change of the band tail states.

Samples prepared at high substrate temperature exhibit an additional PL band ('poly'-Si-band) centred at about 0.7eV with linewidth slightly broader than the 'μc'-Si-band. The occurrence of this additional PL band is strongly related to the high spin density observed for these samples. This emission band reveals a very similar PL peak position and a linewidt to the one previously observed in polycrystalline silicon. Therefore the 0.7eV band is preliminarily assigned to defect-related transitions as in polycrystalline silicon. The 'poly'-Si-band maintains a spectral maximum at 0.7eV with decreasing I_C^{RS} in contrast to observed shift of the 'μc'Si-band to higher energies.

From the temperature dependence of the PL intensity and the PL peak energy, a slope of the exponential band tail sates of the conduction band can be deduced by applying a 'carrier thermalization model' created for amorphous silicon. Different values for the slope of the conduction band tail states are derived from the PL intensity quenching, i.e. $E_o \approx 0.035$ eV and from the shift of the PL peak energy to lower energies with increasing temperature, i.e. $E_o \approx 0.022$ eV.

Therefore, a simple model assuming that only one type of carriers (electrons) are thermally exited with increasing temperature that holds for a-Si:H is obviously not sufficient in case of microcrystalline silicon. Both distributions of electrons in the conduction band tail states and holes in the valence band tail states are likely involved in the non-radiative process, quenching the PL intensity and shifting the PL peak to lower energies.

By using a new technique an information on the carrier distributions is obtained by monitoring the splitting of the quasi-Fermi-levels of electrons and holes via open circuit voltage V_{oc} and the PL energy in µc-Si:H solar cells. A relationship between these quantities was studied as a function of silane concentration, temperature and optical generation rate. In order to investigate only those carriers, which are taking part in the photovoltaic process, a modulation technique was applied. By using this technique it was assured that only the recombination of the relevant carriers is probed and thus a direct link to V_{oc} is given.

The increase of the V_{oc} and the energy of the modulated PL spectra with increasing silane concentration are attributed to reduced density of the localized states, which for a constant carrier density leads to a shift of the carrier distribution to higher energies. The observed increase of the V_{oc} and the PL peak energy with decreasing temperature is assigned to an increasing carrier concentration due to an increasing carrier lifetime. This will also cause a shift of the carrier distribution towards higher energies. The reason for the smaller shift of the PL energy of modulated spectrum as compared to the V_{oc} with decreasing temperature is the difference between carrier distributions, i.e. the energy distribution of occupied states and the probability of occupation of states. The increase of the V_{oc} with decreasing temperature starts at lower voltages determined by the dark current density and the optical generation rate and shows stronger increase as compare to PL peak energy due to a strong shift of quasi-Fermi levels to higher energies and the weak change of carrier distributions in the band tails.

Compare to $V_{oc}(T)$ dependence of the c-Si *p-i-n* diode, the temperature dependence of V_{oc} of the µc-Si:H *p-i-n* diodes prepared at different silane concentration is getting closer to that of c-Si when the *SC* increases. At low temperature, the deviation between the V_{oc} of µc-Si:H solar cells and that of the c-Si diode increases. The open circuit voltage of c-Si diode bends over into saturation at values close to the band gap of c-Si, while the highest V_{oc} value for µc-Si:H solar cells is significantly below the band edges. Therefore, we can concluded that at high density of states in µc-Si:H the strong shift of the quasi-Fermi levels to higher energies upon decreasing temperature as well as the weak increase of the carrier distributions are limited by the band tail states, i.e. the shift of the V_{oc} and the PL peak energy is determined by the band tail states. The limitation of the V_{oc} in µc-Si:H solar cells is accompanied by a strongly reduced carrier extraction at low temperature, i.e. current density j_{sc} decrease rapidly when the band-over of V_{oc} sets in. It is tempting to identify here, the carrier transport as a limiting factor at low temperatures. Trapping in band tail stats is suggested as a possible reason for short diffusion or drift length leading to observed current density behaviour.

The influence of the optical generation rate on the V_{oc} and the energy of modulated PL spectra at different temperatures were also studied. A logarithmic dependence of the V_{oc} on the g_o was found at high optical generation rate for temperatures between 100K and 300K.

This is expected if the short circuit current density j_{sc}, which is proportional to the generation rate, is much larger than the saturation current density j_0. Deviation from the logarithmic dependence of the open circuit voltage on the generation rate is found at room temperature for low generation rate. This indicates light indicated degradation of the material during the experiment, which increases the saturation current density. The reduced V_{oc} at low generation rate can be improved by minimising the saturation current density, i.e. with decreasing temperature the j_0 decreases. At low temperature (down to 100K) the strong deviation from the logarithmic dependence of the V_{oc} on the g_o is reduced and change of the slope of the curves is observed. Further decrease of the temperature below 100K leads to bend-over of the curves. The reason might be a change of the diode quality factor n, i.e. transfer from low-level injection (LLI) to high-level injection (HLI) regions or the exponential increase of density of state distributions to higher energies with increasing number of photo generated carriers at lower temperatures can limited the increase of the quasi-Fermi levels, i.e. the increase of the V_{oc} with increasing the g_o at lower temperatures is determined by the localized band tail states. In contrast to the behaviour of the V_{oc}, the modulated PL energy is found to be proportional to the logarithm of the generation rate over three orders of magnitude for all temperatures studied. The energy of modulated PL spectra and V_{oc} show similar behaviour upon increasing number of photo-generated carries as well as upon decreasing temperature. The reason of much weaker shift of the energy of modulated PL band to higher energies compared to the strong increase of the V_{oc} with increasing g_o-rate is already discussed in terms of a weak change of carrier distributions in the band tail slates in contrast to the strong shift of quasi-Fermi levels to higher energies.

A simple physical model was proposed to simulate photoluminescence spectra and open circuit voltages in μc-Si:H solar cells as a function of temperature. In the model is assumed symmetric density of states distribution for electrons and holes in the conduction and the valence band tail states. The model is based on carrier distributions in quasi-equilibrium conditions, i.e. carrier distributions described by a Fermi-Dirac statistics and the recombination between the two carrier distributions determines PL band. These assumptions are fulfilled at high temperature, where quasi-equilibrium is established. It requires strong interactions between trapped states and band tail states, resulting in the splitting of the quasi-Fremi levels for electrons and holes. The temperature dependences of the open circuit voltage V_{oc} and the PL peak energy derived from the model calculations and from the experiment were compared for two solar cells with different structural properties. The good agreement between the model calculations and experimental results for the two devices is obtained by using the same E_o of 0.031eV for the slope of the both exponential band tail states. At high temperature the trend with increasing silane concentration is well established, i.e. the V_{oc} increases with increasing *SC* for all temperatures, but a constant difference of about 80mV is observed between the calculated and the experimental values of V_{oc}. The reason for this difference is not clear, yet. A deviation between calculated and experimental V_{oc} is found at low temperature, because the quasi-thermal equilibrium cannot be established.

The interactions with band states become weak and the relaxation in the localized band tail states are dominated by tunnelling processes. It is not clear how the V_{oc} is defined at low temperature, as the splitting of the quasi-Fermi level obviously does not follow Fermi-Dirac statistics.

In conclusion, the density of states distribution in μc-Si:H given by the density of states distribution similar to that in c-Si in the upper part and the exponential density of states distribution for localized band tail states as in a-Si:H in the lower part with a value for the slope of about 0.031eV, described the experimental data reasonably well. The photoluminescence results obtained in this work give evidence for a decrease of the density of band tail states at a constant slope with decreasing crystallinity. This results in the observed changes of the electronic properties for μc-Si:H films and solar cells. The reason of the band tail states and their reduction is not clear but strain in the crystalline phase might play a critical role. An improved structural relaxation due to hydrogen or hydrogenated amorphous silicon might be the cause of the reduced density of localized band tail states for material prepared towards the transition to amorphous growth.

Appendix A

A Simulation of PL Spectra Based on Simple Model

The basic formulas used in the simple numerical model to simulate photoluminescence spectra and open circuit voltage V_{oc} in μc-Si:H solar cells are outlined below. Figure A.1 shows symmetric density of states for electrons and holes, which is assumed in the model. The upper part of density of states distributions for electrons in conduction band suggested in Figure A.1 is defined similar to that in crystalline silicon, while the lower part follows exponentially decreasing band tail states. The density of states distribution for electrons is therefore defined by two functions:

$$N_{n1}(E) = N_{0n}\sqrt{\frac{E}{E'_n}} \tag{A.1}$$

$$N_{n2}(E) = N'_{0n}\exp\left(\frac{E}{E_{0n}}\right) \tag{A.2}$$

where N_{0n} and N'_{0n} are constant pre-factors, E'_n and E_{0n} are fixed defined energies for the density of states in Eq.A.1 and A.2, respectively. The latter is identified with the slope of the exponential band tail states. The density of states is assumed to be continuous with a continuous slope at all energies, E. Therefore, an energy $E = \overline{E}$ is defined where the transition from density of states given by Eq.A.1 to Eq.A.2 occurs, defined by a system of equations:

$$\begin{aligned} N_{n1}(\overline{E}) &= N_{n2}(\overline{E}) \\ \frac{d}{dE}N_{n1}(\overline{E})\Big|_{E=\overline{E}} &= \frac{d}{dE}N_{n2}(\overline{E})\Big|_{E=\overline{E}} \end{aligned} \tag{A.3}$$

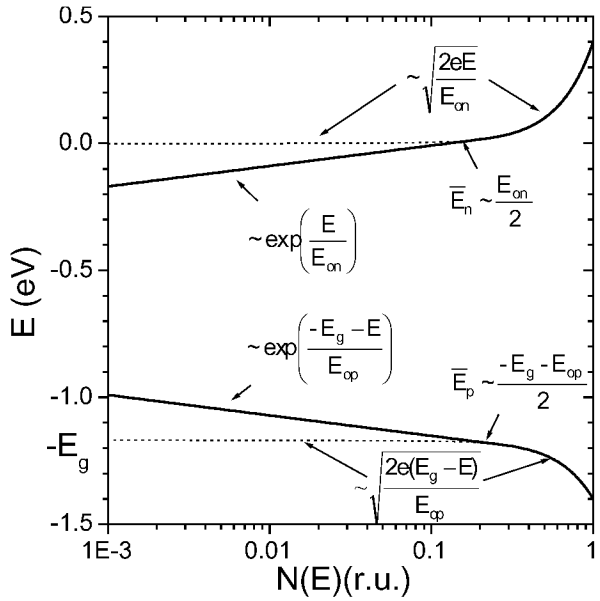

Figure A.1: Schematic density of states diagram, showing symmetric density of states for electrons and holes calculated from Eqs.A.8 and A.9 by using value of 0.031eV for the slope of exponential band tail states and the value of the band gap for c-Si at 0K is $E_g(0)$=1.17eV.

Solving the system of equations:

$$N_{0n}\sqrt{\frac{\overline{E}}{E'_n}} = N'_{0n}\exp\left(\frac{\overline{E}_n}{E_{0n}}\right)$$
$$\frac{d}{dN}N_{0n}\sqrt{\frac{E}{E'_n}}\bigg|_{E=\overline{E}} = N'_{0n}\exp\left(\frac{E}{E_{0n}}\right)\bigg|_{E=\overline{E}} \qquad \text{(A.4)}$$

leads to

$$N_{0n} = N'_{0n}\ ;\ \ \overline{E}_n = \frac{E_{0n}}{2};\quad E'_n = \frac{E_{0n}}{2e} \qquad \text{(A.5)}$$

For simplicity $N_{0n}=N'_{0n}=1$ is assumed. The density of states distribution for holes in the valence band is defined in analogy to that of electrons but the energy axis is shifted by $-E_g$ (see Figure A.1):

$$N_n = N_{0p}\sqrt{\frac{E_g - E}{E'_p}}$$
$$N_p = N'_{0p}\exp\left(\frac{E_g - E}{E_{0p}}\right) \tag{A.6}$$

Solving the system of equations in an analogue way yields to:

$$N_{0p} = N'_{0p}\,;\quad \overline{E}_p = -E_g - \frac{E_{0p}}{2};\quad E'_p = \frac{E_{op}}{2e} \tag{A.7}$$

Finally, the density of states for the electrons in the conduction band can be written in the form:

$$N_n(E) = \begin{cases} N_{0n}\sqrt{\dfrac{2eE}{E_{0n}}}, & \text{if } \mathrm{E} > \dfrac{E_{0n}}{2} \\ N'_{0n}\exp\left(\dfrac{E}{E_{0n}}\right), & \text{if } \mathrm{E} \le \dfrac{E_{0n}}{2} \end{cases} \tag{A.8}$$

The density of states distribution for the holes in the conduction band has the final form:

$$N_p(E) = \begin{cases} N_{0p}\sqrt{\dfrac{2e(E_g - E)}{E_{0p}}}, & \text{if } \mathrm{E} < -E_g - \dfrac{E_{0p}}{2} \\ N_{0p}\exp\left(\dfrac{(E_g - E)}{E_{0p}}\right), & \text{if } \mathrm{E} \ge -E_g - \dfrac{E_{0p}}{2} \end{cases} \tag{A.9}$$

The model is based on carrier distributions in quasi-equilibrium conditions, i.e. the distribution of the electrons and holes are described by Fermi-Dirac statistics. The increase of carrier distributions above their equilibrium values n_0 and p_0 ($n_0, p_0 << \Delta n = \Delta p \propto g_o$) leads to splitting of the Fermi level into two quasi-Fermi levels for electrons and holes, i.e. E_{Fn} and E_{Fp}, respectively. For the electrons, the Fermi-Dirac statistical distribution function f_n, determines the probability of occupation of an allowed electron state for any given energy E and temperature T. The f_n is given by:

$$f_n(E,T) = \frac{1}{\exp\left(\dfrac{E - E_{Fn}}{kT}\right) + 1} \tag{A.10}$$

Where k the Bolzmann constant and E_{Fn} is the quasi-Fermi level of electrons. The Fermi-Dirac statistical distribution function f_p for the holes follows the expression:

$$f_p(E,T) = 1 - \frac{1}{\exp\left(\frac{E - E_{Fp}}{kT}\right) + 1} \tag{A.11}$$

with the quasi-Fermi level of the holes $E_{Fp.}$ Then, the density distribution for electrons $n_{n\_}$ in the conduction band can be obtained as the product of the density of states distribution and Fermi-Dirac distribution function:

$$n_{n\_}(E,T)dE = N_n(E) f_n(E,T)dE \tag{A.12}$$

The density distribution for holes $p_{p\_}$, i.e. missing electrons, is:

$$p_{p\_}(E,T)dE = N_p(E)(1 - f_p(E,T))dE \tag{A.13}$$

The total number of electrons n_n and holes p_p per unit volume in the conduction and valence band can be found by performing the integration of Eqs.A.12 and A.13:

$$n_n = \int N_n(E) f_n(E,T)dE \tag{A.14}$$

$$p_p = \int N_p(E)\ (1 - f_p(E,T))dE \tag{A.15}$$

The temperature dependence of the optical gap of c-Si is taken into account. The variations of the band gap with the temperature can be expressed by:

$$E_g(T) = E_g(0) - \frac{\alpha T^2}{(T + \beta)} \tag{A.16}$$

The value of the band gap for c-Si at 0K is $E_g(0) = 1.17\,\text{eV}$ and $\alpha = 4.73 \times 10^{-4}\,\text{eV/K}$, $\beta = 636\,\text{K}$ are empirical parameter listed by Varshni (1967).

In the model is assumed that the PL band (energy and width of the spectra) originates from radiative tunnelling transitions of electrons and holes trapped in the conduction and valence band tails states. The electron-phonon interactions are neglected. Finally, the calculation of photoluminescence spectra included integration over equally weighted radiative transitions with energy E_{PL} between carriers from the band tail states in accordance to:

$$I_{PL} \propto \int N_n(E) f_n(E) N_p(E - E_{PL}) f_p(E - E_{PL})dE \tag{A.17}$$

Where $N_n(E)f_n(E)$ and $N_p(E-E_{PL})f_p(E-E_{PL})$ are density distribution of electrons in conduction band tail states and holes in valence band tails states, respectively. As the integral from Eq.A.17 cannot be solved analytically, it is transformed into the sum for numerical calculation, corresponding to:

$$I_{PL} \propto \sum_{E_i=E_{\text{initial}}}^{E_{final}} N_n(E)f_n(E)N_p(E-E_{PL})f_p(E-E_{PL})(E_{i+1}-E_i) \tag{A.18}$$

The sum in Eq.A18 is calculated with energy steps $E_{i+1}-E_i \cong 1\text{meV}$. E_{initial} and E_{final} are taken at energies where the carrier distribution is already several orders of magnitude lower or higher than the carrier distribution at the quasi-Fermi level. Calculated PL spectra with lower precision ($E_{i+1}-E_i \cong 10\text{meV}$) already show no visible deviation to that calculated with higher precision. Therefore, it is concluded that the error between calculated sum from Eq.A.18 and the solution of the integral in Eq.A.17 can be neglected.

Appendix B

B Deposition Parameters, Raman and Photoluminescence Properties of Films and Solar Cells

During this work, six well characterized, very high quality sample series of nominally undoped μc-Si:H films prepared by HWCVD and PECVD at different silane concentrations and substrate temperatures were studied by photoluminescence spectroscopy. The deposition parameters used for the preparation of these series of samples are summarized in Table B.1 and Table B.2. Furthermore, the photoluminescence and Raman properties of all thin films investigated are outlined in Table B.3 and Table B.4. At the end, the deposition parameters, together with Raman and I-V properties for investigated in this work μc-Si:H solar cells, prepared by HWCVD are listed in Table B.5.

B.1 Thin Film Deposition Parameters

HWCVD						
Sample	$SC\ (\%)$	$T_S(°C)$	$T_F(°C)$	$p_D\ (Pa)$	$d_i\ (\mu m)$	$r_D\ (Å/s)$
01C190	2	185	1650	5	0.35	0.39
01C188	3				0.36	0.6
01C187	4				0.38	0.79
01C185	5				0.38	0.88
01C184	6.25				0.35	0.97
01C180	7.5				0.35	1.17
HWCVD I						
01C013	10	310	1730	5	1	2.76
01C017	12.5				0.98	3.25
01C012	15				1.14	3.8
01C014	17.5				1.09	4.33
01C018	18.5				1.05	4.61
01C039	25				0.91	5.06

HWCVD II						
01C029	5	330	1710	5	0.86	1.37
01C038	15		1730		1.5	4.17
01C024	17.5				1	3.97
01C021	20				1.01	4.66
01C033	25				0.92	6.13

Table B.1: Overview of deposition parameters used for the deposition of material samples, prepared by HWCVD method.

PECVD I					
Sample	SC (%)	T_S (°C)	p_D (Pa)	d_i (μm)	r_D ($\AA/s$)
00B501	2	200	40	3.25	0.63
00B493	3			3.05	0.94
00B489	4			3.46	1.2
00B483	5			2.49	1.15
00B487	6			3.48	1.61
00B497	7			3.94	1.56
00B509	8			3.52	1.63
PECVD II					
00C451	3	230	40	0.22	0.47
00C450	4			0.33	0.91
00C449	5			0.3	0.85
00C452	6			0.56	1.87
00C453	7			0.37	2.03
00C454	8			0.37	2.44
PECVD					
00C458	3	325	40	0.42	0.88
00C456	4			0.39	1.09
00C457	5			0.29	0.8
00C455	6			0.45	1.51
00C459	7			0.29	1.61
00C460	8			0.28	1.84
01C028	9			0.3	1.64
01C026	11			0.42	2.31
01C036	13			0.44	2.46
01C032	15			0.46	2.58
01C035	17			0.48	3.19

Table B.2: Overview of deposition parameters used for the deposition of material samples, prepared by PECVD method.

B.2 Photoluminescence and Raman Proprieties of Thin Films

HWCVD T_S=185°C										
PL		2.54eV			1.96eV			1.59eV		
Sample	I_C^{RS}	E_{PL} (eV)	I_{PL} (r.u.)	*FWHM* (eV)	E_{PL} (eV)	I_{PL} (r.u.)	*FWHM* (eV)	E_{PL} (eV)	I_{PL} (r.u.)	*FWHM* (eV)
01C190	0.77	0.96	0.111	0.13	0.97	0.014	0.13	0.97	0.014	0.13
01C188	0.73	0.98	0.192	0.13	0.98	0.019	0.13	0.98	0.02	0.13
01C187	0.63	1	0.187	0.13	1	0.019	0.13	1	0.018	0.13
01C185	0.26	1.05	0.139	0.14	1.06	0.016	0.15	1.05	0.011	0.13
01C184	0	1.35	0.14	0.39	1.33	0.017	0.42	1	0.001	0.28
01C180	0	1.34	0.122	0.37	1.32	0.017	0.4	1.28	0.0005	0.38
HWCVD I T_S=310°C										
01C013	0.67	0.96	0.11	0.13	0.97	0.016	0.13	0.97	0.021	0.13
01C017	0.62	0.97	0.095	0.13	0.97	0.041	0.14	0.97	0.05	0.13
01C012	0.58	0.99	0.099	0.14	0.99	0.049	0.14	0.99	0.06	0.14
01C014	0.38	1.01	0.081	0.14	1.01	0.037	0.17	1.01	0.037	0.15
01C018	0.18	1.05	0.117	0.19	1.04	0.049	0.17	1.04	0.026	0.19
01C039	0	1.26	0.066	0.34	1.23	0.054	0.33	1.07	0.004	0.28
HWCVD II T_S=330°C										
01C029	0.74	0.94	0.113	0.13	0.95	0.018	0.13	0.95	0.021	0.13
01C038	0.65	0.95	0.072	0.14	0.96	0.05	0.14	0.95	0.054	0.15
01C024	0.32	1	0.085	0.14	1	0.053	0.15	1	0.051	0.15
01C021	0.03	1.23	0.073	0.33	1.2	0.077	0.33	1.08	0.009	0.34
01C033	0	1.24	0.074	0.33	1.2	0.086	0.33	1.09	0.011	0.33

Table B.3: Overview of photoluminescence and Raman properties for material samples, prepared by HWCVD method. The PL results are obtained by using of Ge detector at 10K for excitation with different photon energies of 1.59eV, 1.96eV and 2.54eV.

PECVD I T_S=200°C										
PL		2.54eV			1.96eV			1.59eV		
Sample	I_C^{RS}	E_{PL} (eV)	I_{PL} (r.u.)	*FWHM* (eV)	E_{PL} (eV)	I_{PL} (r.u.)	*FWHM* (eV)	E_{PL} (eV)	I_{PL} (r.u.)	*FWHM* (eV)
00B501	0.73	0.9	0.136	0.15	0.91	0.09	0.14	0.92	0.114	0.14
00B493	0.67	0.91	0.151	0.15	0.92	0.074	0.14	0.92	0.104	0.14
00B489	0.63	0.93	0.131	0.15	0.93	0.082	0.15	0.93	0.11	0.15
00B483	0.53	0.96	0.108	0.14	0.96	0.081	0.14	0.96	0.11	0.14
00B487	0.38	0.99	0.126	0.15	1	0.087	0.15	0.99	0.11	0.15
00B497	0.01	1.36	0.123	0.37	1.33	0.064	0.39	0.99	0.003	0.23
00B509	0	1.35	0.088	0.38	1.32	0.069	0.38	1.14	0.002	0.3
PECVD II T_S=230°C										
00C451	0.64	0.98	0.079	0.13	0.98	0.025	0.13	0.98	0.025	0.13
00C450	0.65	0.98	0.097	0.13	0.98	0.029	0.13	0.98	0.032	0.14
00C449	0.62	0.98	0.098	0.13	0.99	0.029	0.14	0.99	0.032	0.14
00C452	0.57	0.99	0.107	0.13	1	0.033	0.13	1	0.04	0.13
00C453	0.41	1.02	0.065	0.14	1.02	0.019	0.15	1.02	0.018	0.14
00C454	0.14	1.3	0.045	0.38	1.26	0.013	0.44	1.03	0.002	0.18
PECVD T_S=325°C										
00C458	0.68	0.97	0.07	0.13	0.97	0.024	0.13	0.97	0.027	0.13
00C456	0.65	0.98	0.075	0.13	0.98	0.028	0.13	0.98	0.034	0.13
00C457	0.6	0.99	0.094	0.14	0.99	0.033	0.14	0.99	0.038	0.14
00C455	0.61	0.98	0.103	0.14	0.98	0.03	0.14	0.98	0.036	0.14
00C459	0.54	0.99	0.052	0.14	0.99	0.017	0.15	0.99	0.016	0.14
00C460	0.52	1	0.048	0.16	1	0.014	0.17	0.99	0.012	0.15
01C028	0.5	1.01	0.18	0.14	1.01	0.024	0.14	1.01	0.024	0.14
01C026	0.46	1	0.213	0.15	1	0.028	0.16	1	0.026	0.15
01C036	0.33	1.02	0.153	0.18	1.02	0.031	0.16	1.02	0.022	0.17
01C032	0.26	1.02	0.147	0.21	1	0.014	0.21	1.02	0.011	0.19
01C035	0.03	1.24	0.217	0.31	1.22	0.045	0.3	1.05	0.004	0.3

Table B.4: Overview of photoluminescence properties for material samples, prepared by PECVD method. The PL results are obtained by using of Ge detector at 10K for excitation with different photon energies of 1.59eV, 1.96eV and 2.54eV.

B.3 Solar Cells Deposition Parameters, Raman and I-V Proprieties

	HWCVD								
Sample	SC (%)	T_S (°C)	T_F (°C)	p_D (Pa)	d_i (μm)	I_C^{RS}	η (%)	V_{oc} (mV)	j_{sc} (mA/cm^2)
03C085	3	185	1650	3	1	0.6	6.95	493	21.12
01C202	4			5	1	0.65	7.66	518	21.7
01C201	5			5	1	0.56	8	548	21.3
01C213	5.2			5	1.2	0.37	8.07	571	20.17
01C239	5.6			4	0.85	0.25	8.49	598	19.92

Table B.5: Overview of deposition parameters, Raman and I-V properties of μc-Si:H solar cells prepared by HWCVD. The table show the silane concentration (SC), the substrate and the filament temperatures (T_S and T_F), the deposition rate (r_D), the thickness of the solar cell (d_i), the Raman intensity ratio (I_C^{RS}), the efficiency (η), the open circuit voltage (V_{oc}) and the short circuit current density (j_{sc}).

Bibliography

AMBROS, S. (1991), *Recombination in amorphem Silizium (a-Si:H) und amorphen Silizium-Germanium Legirungen (a-$Si_{1-x}Ge_x$:H)*, Ph.D. thesis, Rheinisch-Westfälische Technische Hochschule Aachen.

ASHCROFT, N. W., AND MERMIN N. D. (1976), *Solid States Physics*, W. B. Saunders Company.

AUSTIN, I. G., NASHASHIBI T. S., SEARLE T. M., LE COMBER P. G. AND SPEAR W. E. (1979), Photoluminescence and lifetime studies on plasma discharged a-Si, *Journal of Non-Crystalline Solids* **32**, 373.

BAIA NETO, A. L., LAMBERTZ A., CARIUS R., FINGER F. (2002), Relationships between structure, spin density and electronic transport in 'solar-grade' microcrystalline silicon films, *Journal of Non-Crystalline Solids* **299-302**, 274.

BECK, N., MEIER J., FRIC J., REMES Z., PORUBA A., FLUCKIGER R., POUL J., SHAH A., AND VANĚČEK M. (1996), Enhanced optical absorption in microcrystalline silicon, *Journal of Non-Crystalline Solids* **198-200**, 903.

BELL, R. J. (1972), *Introductory Fourier Transform Spectroscopy*, Academic press, New York.

BERGFELD, S. (2003), private communication.

BHAT, P. K., AUSTIN I. G., AND SEARLE T. M. (1983), Luminescence life time distributions in μc-Si and glow discharge and sputtered a-Si:H, *Journal of Non-Crystalline Solids* **59-60**, 381.

BHAT, P. K., DIPROSE G., SEARLE T. M., AUSTIN I. G., LECOMBER P.G., AND SPEAR W. E. (1983a), Plasma deposited microcrystalline and amorphous silicon-a comparative study of photoluminescence, *Physica* **117B&118B**, 917.

BHAT, P. K., RHODES A. J., SEARLE T. M., AUSTIN I. G., AND ALLISON J. (1983b), The 0.9 defect luminescence band in sputtered and other form of plasma-deposited a-Si:H, *Philosophical Magazine B* **47**, L99.

BÖER, K. W. (1990), Survey of Semiconductor Physics: Electrons and Other Particles in Bulk Semiconductors, Van Nostrand Reinhold, New York.

BÖER, K. W. (1995), Survey of Semiconductor Physics, *Vol. II: Barriers, Junctions, Surfaces* and Devices, Van Nostrand Reinhold, New York.

BRAMMER, T., BUNTE E., STIEBIG H., FINGER F., WAGNER H. (2000), Comparative study of microcrystalline silicon pin and nip diodes, *Proceedings of the 16th E. C. Photovoltaic Solar Energy Conference*, Glasgow, Scotland, 545.

CARDONA, M. (1982), *Light Scattering in Solids*, Springer, Berlin.

CARIUS, R., FINGER F., BACKHAUSEN U., LUYSBERG M., HAPKE P., OTTE M., AND OVERHOF H. (1997), Electronic properties of microcrystalline silicon, *Materials Research Society Symposium Proceedings* **467**, 283.

CARIUS, R., MERDZHANOVA T., FINGER F., KLEIN S., VETTERL O. (2003), A comparison of microcrystalline silicon prepared by plasma enhanced chemical vapour deposition and hot wire chemical vapour deposition: electronic and device properties, *Journal of Material Science: Materials in Electronics*, **14**, 625.

CARIUS, R., MERDZHANOVA T., FINGER F. (2003a), Electronic properties of microcrystalline silicon investigated by photoluminescence spectroscopy on film microcrystalline silicon and devices, *Materials Research Society Symposium Proceedings* **762**, A4.2.

CHELIKOWSKY, J. R., AND COHEN M. L. (1976), Nonlocal pseudopotential calculations for the electronic structure of eleven diamonds and zinc-blende semiconductors, *Physical Review B* **14**, 556.

COLLINS, R. W., PAESLER M. A., AND PAUL W. (1980), The temperature dependence of photoluminescence in a-Si:H alloys, *Solid State Communications* **34**, 833.

COLLINS, R. W., PAESLER M. A., MODDEL G., AND PAUL W. (1980a), Photoluminescence in sputtered amorphous Si:H alloys, *Journal of Non-Crystalline Solids* **35&36**, 681.

COLLINS, R. W., AND PAUL W. (1981), Model for the temperature dependence in a-Si:H and related materials, *Physical Review B* **25**, 5257.

CURTINS, H., WYRSCH N., AND SHAH A. V. (1987), High rate deposition of amorphous hydrogenated silicon: effect of plasma excitation frequency, *Electronics Letters* **23**, 228.

DASGUPTA, A., LAMBERTZ A., VETTERL O., FINGER F., CARIUS R., ZASTROW U. AND WAGNER H. (2000), P-layers of microcrystalline silicon thin film solar cells, *Proceedings of the 16th E. C. Photovoltaic Solar Energy Conference*, Glasgow, UK, 557.

DEPINNA, S. P., HOMEWOOD K., CAVENETT B. C., AUSTIN I. G., SERLE T. M., WILLEKE G., KINMOND S. (1983), O.D.M.R. investigations of recombination in μc-Si:H, *Philosophical Magazine B* **47**, L57.

DIEHL, F., SCHRÖDER B., AND OECHSNER H. (1998) Light scattering and enhanced optical absorption in hot wire microcrystalline silicon, *Journal of Applied Physics* **84 (6)**, 3416.

DOYLE, J. R., DOUGHTY D. A., AND GALLAGHER A. (1990), Silane dissociation products in deposition discharges, *Journal of Applied Physics* **68 (9)**, 4375.

DUNCAN, W. M., CHANG P. -H., MAO B. -Y, AND CHAN C. -E. (1987), Photoluminescence and microstructural properties of high-temperature annealed buried oxide silicon-on-insulator, *Applied Physics Letters* **51 (10)**, 773.

DUNSTAN, D. J., AND BOULITROP F. (1981), A no-Stokes shift model for the photoluminescence of a-Si:H, *Journal de Physique* **42**, Suppl. 10, C4-331.

DUNSTAN, D. J., AND BOULITROP F. (1984), Photoluminescence in hydrogenated amorphous silicon, *Physical Review B* **30**, 5945.

DYLLA, T., CARIUS R., AND FINGER F. (2002), Electron spin resonance and electronic conductivity in moderately doped n-type microcrystalline silicon as a probe for the density of gap states, *Materials Research Society Symposium Proceedings* **715**, A20.9.

DYLLA, T., FINGER F., AND SCHIFF E. (2004), Hole drift-mobility measurements in microcrystalline silicon, *Materials Research Society Symposium Proceedings* **808**, A8.10.

ENGEMANN, D., AND FISCHER R. (1973), *Amorphous and Liquid Semiconductors*, edited by J. Stuke and W. Brenig (London: Taylor& Francis Ltd.), 947.

ENGEMANN, D., AND FICSHER R. (1977), Photoluminescence in amorphous silicon, *Physica Status Solidi (b)* **79**, 195.

FANG, M., CHEVRIER J., AND DREVILLION B. (1991), In situ investigation of the growth of microcrystalline silicon obtained by alternating deposition and hydrogen-etching sequences, *Journal of Non-Crystalline Solids* **137-138**, 791.

FINGER, F., HAPKE P., LUYSBERG M., CARIUS R., AND WAGNER H. (1994), Improvement of grain size and deposition rate of microcrystalline silicon by use of very high frequency glow discharge, *Applied Physics Letter* **65 (20)**, 2588.

FINGER, F., CARIUS R., HAPKE P., HOUBEN L., LUYSBERG M., AND TZOLOV M. (1997), Growth and structure of microcrystalline silicon prepared with glow discharge at various plasma excitation frequencies, *Materials Research Society Symposium Proceedings* **452**, 725.

FINGER, F., MÜLLER J., MALTEN C., AND WAGNER H. (1998), Electronic states in microcrystalline silicon, *Philosophical Magazine B* **77 (3)**, 805.

FINGER, F., VETTERL O., CARIUS R., LAMBERTZ A., SCHOLTEN C., HOUBEN L., LUYSBERG M. (2000), Microcrystalline silicon solar cells: relationship between material properties and device performance, *Proceedings of the Eleventh International School of Condensed Matter Physics,* Varna, Bulgaria, 26.

FINGER, F., MÜLLER J., MALTEN C., CARIUS R., WAGNER H. (2000a), Electronic properties of microcrystalline silicon investigated by electron spin resonance and transport measurements, *Journal of Non-Crystalline Solids* **266-269**, 511.

FINGER, F., KLEIN S., CARIUS R., DYLLA T., VETTERL O., BAIA NETO A. L. (2002), Defects in microcrystalline silicon prepared with hot wire CVD, *Materials Research Society Symposium Proceedings* **715**, A16.3.

FUHS, W., KANSCHAT P., AND LIPS K. (2000), Bandtails and defects in microcrystalline silicon (μc-Si:H), *Journal of Vacuum Science & Technology B* **18**, 1792.

GALLAGHER, A., DOYLE J., AND DOUGHT D. (1989), Plasma chemistry in silane and silane-germane discharge deposition, *Materials Research Society Symposium Proceedings* **149**, 23.

GREEN, M. A., EMERY K., KING D. L., IGARY S., AND WARTA W. (2002), Solar sell efficiency tables (Version 19), *Progress in Photovoltaics: Research and Applications* **10**, 55.

GROSS, A. (2001), *Solarzellen aus microcrystallinem Silizium: Zum Einfluss der Beleuchtungsrichtung und der Substrattemperatur bei der Deposition der intrinsischen Absorberschicht*, Diploma thesis, Universität Bonn.

HAN, D., YUE G., LORENTZEN J. D., LIN J., HABUCHI H., AND WANG Q. (2000), Optical and electronic properties of microcrystalline silicon as a function of microcrystallinity, *Journal of Applied Physics* **87**, 1882.

HAPKE, P. (1995), *VHF-Plasmaabscheidung von mikrokristallinem Silizium (μc-Si): Einfluss der Plasmaanregungsfrequenz auf die strukturellen und elektrischen Eigenschaften,* Ph.D. thesis, Rheinisch-Westfälische Technische Hochschule Aachen.

HAPKE, P., BACKHAUSEN U., CARIUS R., FINGER F., AND RAY S. (1996), Modulated Hall-effect techniques for the study of transport properties of microcrystalline silicon with different grain size, *Materials Research Society Symposium Proceedings* **420**, 789.

HAYNES, J. R., LAX M., AND FLOOD F. (1959), Analyses of intrinsic recombination radiation from silicon and germanium, *Journal of Physics and Chemistry of Solids* **8**, 392.

HEINTZE, M., WESTLAKE W., AND SANTOS P. (1993), Surface controlled plasma deposition and etching the silicon near the chemical equilibrium, *Journal of Non-Crystalline Solids* **164-166**, 985.

HOUBEN, L. (1998), *Plasmaabscheidung von mikrokristallinen Silizium: Merkmale der Mikrostruktur und deren Deutung im Sinne von Wachstumsvorgängen*, Ph.D. thesis, Heinrich-Heine-Universität Düsseldorf.

HOUBEN, L., LUYSBERG M., HAPKE P., CARIUS R., FINGER F., AND WAGNER H. (1998a), Structural investigations of microcrystalline silicon in the transition from highly crystalline to amorphous growth, *Philosophical Magazine A* **77**, 1447.

JACKSON, W. B., JOHNSON N. M., AND BIEGELSEN D. K. (1983), Density of gap states of silicon grain boundaries determined by optical absorption, *Applied Physics Letters* **43 (2)**, 195.

KAAN KALKAN, A., FONASH S. J., SHANG-CONG CHENG (2000), Band tail photoluminescence in nanocrystalline Si, *Applied Physics Letters* **77**, 55.

KEPPNER, H., MEIER J., FISHER D., AND SHAH A. (1999), Microcrystalline silicon and micromorph tandem solar cells, *Applied Physics A* **69**, 169.

KLEIN, S. (1999), Wasserstoff- and Ultraschallbehandlung von polykristallinem Silizium, Diploma thesis, Universität Stuttgart.

KLEIN, S., FINGER F., CARIUS R., WAGNER H., STUTZMANN M. (2001), Intrinsic amorphous and microcrystalline silicon by hot-wire-deposition for thin film solar cells applications, *Thin Solid Films* **395**, 305.

KLEIN, S., FINGER F., CARIUS R., RECH B., HOUBEN L., LUYSBERG M., AND STUTZMANN M. (2002), High efficiency thin film solar cells with intrinsic microcrystalline silicon prepared by hot wire CVD, *Materials Research Society Symposium Proceedings* **715**, A26.2.

KLEIN, S. (2003), private communication.

KLEIN, S., FINGER F., CARIUS R., DYLLA T., RECH B., GRIMM M., HOUBEN L., AND STUTZMANN M. (2003), Intrinsic microcrystalline silicon prepared by hot-wire chemical vapour deposition for thin film solar cells, *Thin Solid Films* **430**, 202.

KLEIN, S. (2003a), Microcrystalline Silicon Prepared by Hot Wire CVD: Preparation and Characterisation of Material and Solar Cells, Ph.D. thesis, Technischen Universität München.

KLUTH, O., LÖFFEL A., WIEDER S., BENEKING C., APPENZELLER W., HOUBEN L., RECH B., WAGNER H., HOFFMANN S., WASER R., ANNA-SELVER J. A., AND KEPPNER H. (1997) Texture etched Al-doped ZnO: A new material for enhanced light trapping in thin film solar cells, *Proceedings of the 26th IEEE Photovoltaic Specialists Conference, Anaheim*, 715.

KOBLISKA, R., AND SOLIN S. (1973), Raman spectrum of wurtzite silicon, *Physical Review B* **8**, 3799.

KOSHKA, J., OSTAPENKO S., RUF T., AND ZHANG M. (1996), Activation of luminescence in polycrystalline silicon thin films by ultrasound treatment, *Applied Physics Letters* **69 (17)**, 2537.

KUZMANY, H. (1989), *Festkörperspecroskopie*, Springer Publisher Berlin, Heidelberg, New York, London, Paris, Tokyo.

LONG, D. A. (1977), *Raman Spectroscopy*, McGrow-Hill International Book Company, New York.

LUYSBERG, M., HAPKE P., CARIUS R., AND FINGER F. (1997), Structure and growth of microcrystalline silicon: Investigation by TEM and Raman spectroscopy of films grown at different plasma excitation frequencies, *Philosophical Magazine A* **75 (1)**, 31.

MATSUDA, A. (1983), Formation kinetics and control of microcrystalline silicon obtained from reactive plasmas, *Journal of Non-Crystalline Solids* **59-60**, 767.

MATSUMURA, H. (1998), Formation of silicon-based thin films prepared by catalytic chemical vapor deposition (Cat-CVD) method, *Japanese Journal of Applied Physics* **37 (6A)**, 3175.

MEIER, J., DUBAIL S., FISCHER R. F. D., KEPPNER H., AND SHAH A. (1994), Intrinsic microcrystalline silicon (μc-Si:H) – a promising new thin film solar cell material, Proceedings of the 1st World Conference on Photovoltaic Solar Energy Conversion, Hawaii, USA, 409.

MEIER, J., TORRES P., PLATZ R., DUBAIL S., KROLL U., ANNA SELVAN J., PELLA-TON VAUCHER N., HOF C. KEPPNER H., SHAH A., UFERT K. –D., GIANNOULES P., AND KOEHLER J. (1996), On the way towards high efficiency thin film solar cells by the "micromorph" concept, *Material Research Society Symposium Proceeding* **420**, 3.

MERDZHANOVA, T., CARIUS R., KLEIN S., FINGER F., AND DIMOVA-MALINOVSKA D. (2004), Photoluminescence energy and open circuit voltage in microcrystalline silicon solar cells, *Thin Solid Films* **451-452**, 285.

MIDDYA, A. R., LLORET A., PERRIN J., HUC J., MONCEL L., PAREY Y., AND ROSE G. (1995), Fast deposition of polycrystalline silicon films by hot-wire CVD, *Material Research Society Symposium Proceeding* **377**, 119.

MOLENBROEK, E., MAHAN H. A., AND JOHNSONS E. J. (1996), Film quality in relation to deposition conditions of a-Si:H films deposited by the "hot wire" method using highly diluted silicon, *Journal of Applied Physics* **82**, 1909.

NASHASHIBI, T. S., AUSTIN I. G. AND SEARLE T. M. (1977), Photoluminescence in pure and doped amorphous silicon, *Philosophical Magazine* **35**, 831.

NEVILLE, R. C. (1995), *Solar Energy Conversion-The Solar cell*, Elsevier, Amsterdam, Lausanne, New York, Oxford, Shannon, Tokyo.

ODA, S., AND NODA J. (1988), Preparation of a-Si:H films by VHF plasma CVD, *Material Research Society Symposium Proceeding* **118**, 117.

ORENSTEIN, J., AND KASTNER M. (1981), Photocurrent transient spectroscopy: measurement of the density of localized States in a-As_2Se_3, Physical Review Letters **46**, 1421.

OSTAPENKO, S. S., SAVCHUK A. U., NOWAK G., LAGOWSKI J., AND JASTREBSKI L. (1995), Photoluminescence defect diagnostics in poly-Si thin films, *Materials Science Forum* **196-201**, 1897.

OVERHOF, H., AND THOMAS P. (1989), *Electronic Transport in Hydrogenated Amorphous Semiconductors*, Springer, Berlin.

PAESLER, M. A., AND PAUL W. (1980), Photoluminescence in sputtered amorphous silicon-hydrogen alloys, *Philosophical Magazine B* **41**, 393.

PANKOVE, J. POLLAK H., AND SCHNABOLK C. (1980), Optical absorption by gap states in hydrogenated amorphous silicon, *Journal of Non-Crystalline Solids* **35&36**, 459.

PERKOWITZ, S. (1993), Optical Characterization of Semiconductors: Infrared, Raman and Photoluminescence Spectroscopy, Academic Press, London.

PERRIN, J. (1991), Plasma and surface reactions during a-Si:H film growth, *Journal of Non-Crystalline Solids* **137-138**, 639.

PERRIN, J., LEROY O., AND BRODAGE M. (1996), Cross sections, rate constants and transport coefficients in silane plasma chemistry, *Contributions to Plasma Physics* **36**, 3.

PRASAD, K., FINGER F., CURTINS H., SHAH A., BAUMAN J. (1990), Preparation and characterization of highly conductive (100S/cm) phosphorus doped μc-Si:H films deposited using the VHF-GD technique, *Materials Research Society Symposium Proceedings* **164**, 27.

RATH, J. K., TICHELAAR F. D., MEILING H., SCHROPP R. E. I. (1998), Hot-wire CVD poly-silicon films for thin film devices, *Materials Research Society Symposium Proceedings* **507**, 879.

RECH, B., KLUTH O., REPMANN T., ROSCHEK T., SPRINGER J., MÜLLER J., FINGER F., STIEBIG H., AND WAGNER H. (2002), New materials and deposition techniques for highly efficient silicon thin film solar cells, *Solar Energy Material and Solar Cells* **74**, 439.

REHM, W., ENGEMANN D., FISHER R., and STUKE J. (1976), Photoluminescence and photoconductivity of doped amorphous silicon, *Proceedings of the 13th International Conference of Physics of Semiconductors*, edited by F.G. Fumi, p. 525.

REYNOLDS, S., SMIRNOV V., MAIN C., CARIUS R., AND FINGER F. (2003), Localized states in microcrystalline silicon photovoltaic structures studied by post-transit time-of-flight spectroscopy, *Materials Research Society Symposium Proceedings* **762**, 327.

RICHTER, H., WANG Z. P., AND LEY L. (1981), The one phonon Raman spectrum in microcrystalline silicon, *Solid State Communications* **39**, 625.

RICHTER, H. (1983), *Elektronen und Phononen in mikrokristallinem Silizium*, Ph.D. thesis, Universität Stuttgart, unpublished.

ROBBINS, D. J., KUBIAK R. A. A., AND PARKER E. H. C. (1985), Photoluminescence studies of silicon molecular beam epitaxy layers, *Journal of Vacuum Science & Technology B* **3 (2)**, 588.

SAITO, K., SANO M., SAKAI A., HAYASHI R., AND OGAWA K. (2001), High efficiency microcrystalline silicon solar cells at high deposition rates, in: *Technical Digest of the 11th International PVSEC-12*, Jeju (Korea), 429.

SAUER, R., WEBER J., AND STOLZ J. (1985), Dislocation-related photoluminescence in silicon, *Applied Physics A* **36**, 1.

SAUVAIN, A., SHAH A., HUBIN J. (1990), Measurement of ambipolar mobility-lifetime product and its significance for amorphous silicon solar cells, Proceedings of the 21st IEEE Photovoltaic Specialist Conference, Orlando, vol.2, 1560.

SAVCHOUK, A. U., OSTAPENKO S., NOWAK G., LAGOWSKI J., AND JASTRZEBSKI L. (1995), Band-tail photoluminescence in polycrystalline silicon thin films, *Applied Physics Letters* **67**, 82.

SCHROPP, R. E. I., XU Y., IWANICZKO E., ZAHARIES G. A., AND MAHAN A. H. (2002), Microcrystalline silicon for solar cells at high deposition rates by hot wire CVD, *Materials Research Society Symposium Proceedings* **715**, A26.3.

SHIRAI, H., DAS D., HANNA J., AND SHIMIZU I. (1991), A novel preparation technique for preparing hydrogenated amorphous silicon with a more rigid and stable Si network, *Applied Physics Letter* **59**, 1096.

STACHOWITZ, R., SCHUBERT M., AND FUHS W. (1998), Non-radiative distant pair recombination in amorphous silicon, *Journal of Non-Crystalline Solids* **227-230**, 190.

STAEBLER, D. L., AND WRONSKI C. R. (1977), Reversible conductivity changes in discharge amorphous Si, *Applied Physics Letters* **31 (4)**, L292.

STIEBIG, H., KNIPP D., HAPKE P., AND FINGER F. (1998), Three color piiin-detector using microcrystalline silicon, *Journal of Non-Crystalline Solids* **227-230**, 1330.

STREET, R. A., KNIGHTS J. C., AND BIEGELSEN D. K. (1978), Luminescence studies of plasma-deposited hydrogenated silicon, *Physical Review B* **18**, 1880.

STREET, R. A. (1978a), Phonon interaction in the luminescence of amorphous silicon, *Philosophical Magazine* **37**, 35.

STREET, R. A. BIEGELSON D., AND STUKE J. (1979), Defects in bombarded amorphous silicon, *Philosophical Magazine* B **40**, 451.

STREET, R. A., AND BIEGELSEN D. K (1980), Luminescence and ESR studies of defects in hydrogenated amorphous silicon, *Solid State Communications* **33**, 1159.

STREET, R. A. (1981), Luminescence and recombination in hydrogenated amorphous silicon, *Advanced in Physics* **30**, 593.

STREET, R. A. (1991), *Hydrogenated Amorphous Silicon*, Cambridge University Press, Cambridge.

STUTZMANN, M., BIEGELSON D. K., AND STREET R. A. (1987), Detailed investigation of doping in hydrogenated amorphous silicon, *Physical Review B* **35 (11)**, 5666.

SZE, S. M. (1981), *Physics of Semiconductor Devices*, John Wiley & Sons, New York 2nd Edition.

TIEDJE, T., AND ROSE A. (1980), A physical interpretation of dispresive transport in disordered semiconductors, *Solid State Communications* **37**, 49.

TSANG, C., AND STREET R. A. (1979), Recombination in plasma-deposited amorphous Si:H. Luminescence decay, *Physical Review B* **19**, 3027.

TZOLOV, M., FINGER F., CARIUS R., AND HAPKE P. (1997), Optical and transport studies on thin microcrystalline silicon films prepared by very high frequency glow discharge for solar cells applications, *Journal of Applied Physics* **81**, 7376.

ULBER, I., SALEH R., FUHS W., AND MELL H. (1995), Recombination at defects in amorphous silicon (a-Si:H), *Journal of Non-Crystalline Solids* **190**, 9.

USUI, S., AND KIKUCHI M. (1979), Properties of heavily doped gd-Si with low resistivity, *Journal of Non-Crystalline Solids* **34**, 1.

VARSHNI, Y. P. (1967), Band-to-band radiative recombination in groups IV, VI, and III-V semiconductors (I), *Physica Status Solidi* **19**, 459.

VEPŘEK, S., AND MAREČEK V. (1968), The preparation of thin layers of Ge and Si by chemical hydrogen plasma transport, *Solid-State Electronics* **11**, 683.

VEPŘEK, S., SAROTT F. –A., IQBAL Z. (1987), Effect of grain boundaries on the Raman spectra, optical absorption, and elastic light scattering in nanometer-sized crystalline silicon, *Physical Review B* **36**, 3344.

VEPŘEK, S., SAROTT F. –A., RAMBERT S., AND TAGLAUER E. (1989), Surface hydrogen content and passivation of silicon deposited by plasma induced chemical vapor deposition from silan and the implications for the reaction mechanism, *Journal of Vacuum Science & Technology* **A7**, 2614.

VEPŘEK, S. (1990), Chemistry of solid states physics of microcrystalline physics, *Materials Research Society Symposium Proceedings* **164**, 39.

VETTERL, O., CARIUS R., HOUBEN L., SCHOLTEN C., LUYSBERG M., LAMBERTZ A., FINGER F., WAGNER H. (2000), Effect of structural properties of μc-Si:H absorber layers on solar cell performance, *Materials Research Society Symposium Proceedings* **609**, A15.2.

VETTERL, O. (2001), *On the Physics of Microcrystalline silicon Thin film Solar Cells*, Ph.D. thesis, Heinrich-Heine-Universität Düsseldorf. Published as: Berichte des Forschungszentrums Jüluch, No. 3897, ISSN 0944-2952.

VETTERL, O., GROSS A., JANA T., RAY S., LAMBERTZ A., CARIUS R., FINGER F. (2002), Changes in electric and optical properties of intrinsic microcrystalline silicon upon variation of the structural composition, *Journal of Non-Crystalline Solids* **299-302**, 772.

VOGET-GROTE, U., KÜMMERLE W., FISCHER R., AND STUKE J. (1980), The influence of spin defects on recombination and electronic transport in amorphous silicon, *Philosophical Magazine B* **41**, 127.

WERNER, J., AND PEISL M. (1985), Experimental band tails at silicon grain boundaries, *Materials Research Society Symposium Proceedings* **46**, 575.

WERNER, J., AND PEISL M. (1985a), Experimental band tails in polycrystalline semiconductor films, *Physical Review B* **31 (10)**, 6881.

WERNER, J. H. (1989), Band tailing in polycrystalline and disordered silicon, in: J. H. Werner, H. J. Möller, and H. P. Strunk (eds.), *Polycrystalline Semiconductors*, vol. 35 of Spring *Proceedings in Physics*, Springer, Berlin pp. 345-351.

WILSON, B. A., AND KERWIN T. P. (1982), Time-resolved photoluminescence in a-Si:H: sub-band-gap excitation, *Physical Review B* **25 (8)**, 5276.

WÜRFEL, P. (1982), The chemical potential of radiation, *Journal of Physics C: Solid States Physics* **15**, 3967.

YAMAMOTO, K., YOSHIMI M., TAWADA Y., OKAMOTO Y., AND NAKAJIMA A. (2000), Thin film Si solar cell fabricated at low temperature, *Journal of Non-Crystalline Solids* **266-269**, 1082.

YANG, J., BANERJEE A., AND GUHA S. (1997), Triple-junction amorphous silicon alloys solar cells with 14.6% initial and 13% stable conversion efficiencies, *Applied Physics Letters* **70 (22)**, 2975.

YUE, G., LORENTZEN J. D., LIN J., HAN D., AND WANG Q. (1999), Photoluminescence and Raman studies in thin-film materials: transition from amorphous to microcrystalline silicon, *Applied Physics Letters* **75**, 492.

YUE, G., HAN D., MCNEIL L. E., WANG Q. (2000), Characteristics of the low energy photoluminescence in μc-Si films, *Journal of Applied Physics* **88**, 4904.

Acknowledgments

My tenure as a doctoral student was greatly improved by those around me. It is pleasure to offer my sincere thanks to all of them:

First of all, I would like to express my largest gratitude to my supervisors, Prof. Doriana Dimova-Malinovska of the Central Laboratory for Solar Energy and New Energy Sources Sofia for managing my Ph.D. in Bulgarian Academy of Sciences and arranging the official permission to write the manuscript of my thesis in English and Dr. Reinhard Carius for the possibility to make my Ph.D. thesis in the Institut für Photovoltaik (IPV), Forschungszentrum Jülich GmbH.

My deepest thanks belong to Dr. Reinhard Carius for his continuous encouragement and guidance throughout this research work. Without his creativeness and patient way of sharing knowledge, this work would have been impossible. I thank him for the many illuminating discussions and daily work in the labour, which have given me the most interesting insides into the photovoltaic research, and in particular into the photoluminescence spectroscopy. I have learned various things, from him, such as e.g. the way of thinking and the way of proceeding research. Thank you!

I would like to express great thank to Dr. Stefan Klein for providing his excellent μc-Si:H thin films and solar cells for my photoluminescence investigations. Stefan is acknowledged, in particular for carefully reading and correcting the manuscript. Without his aid, many errors would have remained. I would like also to thank Torsten Bronger for his help with the preparation of the cover page of my Ph.D. thesis.

I am very grateful to Markus Hülsbeck, who share with me the same laboratory and was prepared to help me in the technical things always when I was asking him, very often-)) probably. He provide also the Raman data used in this work and was a good friend which make the time spent in the laboratory pleasure to me. I would like to extend my thanks to Josef Klomfaß for the technical support, discussions on the PDS measurements and the help with 'Tech Plot' program.

I wish to thank Dr. F Finger for reading and correcting the manoscript for E-MRS paper. I would like also to thank Dr. O. Vetterl, A. Groß and Dr. L.A. Baia Nato for providing the μc-Si:H thin films prepared by PECVD method.

I especially thank my colleagues from IPV, and particularly the acting head of institute Dr. W. Beyer, Dr. J. Müller, Gunnar Schöpe (for the pleasure to share one office with him), Dr. B. Rech, Dr. O. Kluth, Dr. T. Repmann, T. Dylla (for the discussion on the slope of the band tail states and the friendship), A. Lambertz, Dr. Ch. Roß, F. Pennartz, L. Nießen, Eerke Bunte, N. Senoussaoui Khadir, Dr. T. Brammer, Dr. H. Stiebig and Frau A. Mülheims for the kind collaboration and support.

I would like also to thank my colleagues from CL SENES-Bulgarian Academy of Sciences, especially Marushka Sendova-Vassileva, Mimi Kamenova, Miglena Nikolaeva, Maja and all other colleagues for the nice time spent together at CL SENES.

I am very thankful to my friends in 'Jülich', Julian, Katja, Yanka and Lidia and my friends in Bulgaria, Iveta, Peter and Irena for being always with me in the happiest as well as in the difficult moments in my life. I am truly grateful to your continues support and sincerely friendship.

My wonderful parents, Nikolina Merdzhanova and Radoslav Merdzhanov, and grand parents, who have always been supportive, are generous with love, have good advice and help me find my way. Благодаря Ви, мили мамо и татко!

Finally, I feel incredibly grateful to my boyfriend Dr. Stefan Bergfeld without his love, patience, understanding and friendship this thesis would not be possible. He was always close to me, sometimes propping up my failing strength, sometimes just making me smile. I cannot thank him enough for numerous discussions, for his help with numerical simulation and for carefully reading and correcting the manuscript. Thank you!

The financial support from the Institut für Photovoltaik, Forschungszentrum Jülich giving me the opportunity to work as a Ph.D. student, is gratefully acknowledged.

Publications Related to the Ph.D. Thesis

T. Merdzhanova, R. Carius, S. Klein, F. Finger and D. Dimova-Malinovska, Defect states in microcrystalline silicon probed by photoluminescence spectroscopy, Thin Solid Films, (2005) submitted.

T. Merdzhanova, R. Carius, S. Klein, F. Finger and D. Dimova-Malinovska, A comparison of model calculations and experimental results on photoluminescence energy and open circuit voltage in μc-Si:H solar cells, J. Optoelectron. Adv. Mater., **7(1)** (2005) 485.

R. Carius, T. Merdzhanova, S. Klein and F. Finger, Band tail states in microcrystalline silicon solar cells probed by photoluminescence and open circuit voltage, J. Optoelectron. Adv. Mater., **7(1)** (2005) 121.

T. Merdzhanova, R. Carius, S. Klein, F. Finger and D. Dimova-Malinovska, Photoluminescence energy and open circuit voltage in microcrystalline silicon solar cells, Thin Solid Films, **451-452** (2004) 285.

R. Carius, T. Merdzhanova, F. Finger, S. Klein, O. Vetterl, A comparison of microcrystalline silicon prepared by plasma enhanced chemical vapour deposition and hot wire chemical vapour deposition: electronic and device properties, J. Materials Science: Materials in Electronics, **14** (2003) 625.

R. Carius, T. Merdzhanova, F. Finger, Electronic properties of microcrystalline silicon investigated by photoluminescence spectroscopy on film microcrystalline silicon and devices, Mater. Res. Soc. Symp. Proc., **762** (2003) 321.

Schriften des Forschungszentrums Jülich
Reihe Energietechnik / Energy Technology

1. **Fusion Theory**
   Proceedings of the Seventh European Fusion Theory Conference
   edited by A. Rogister (1998); X, 306 pages
   ISBN: 3-89336-219-3

2. **Radioactive Waste Products 1997**
   Proceedings of the 3rd International Seminar on Radioactive Waste Products
   held in Würzburg (Germany) from 23 to 26 June 1997
   edited by R. Odoj, J. Baier, P. Brennecke et al. (1998), XXIV, 506 pages
   ISBN: 3-89336-225-8

3. **Energieforschung 1998**
   Vorlesungsmanuskripte des 4. Ferienkurs „Energieforschung"
   vom 20. bis 26. September 1998 im Congrescentrum Rolduc und
   im Forschungszentrum Jülich
   herausgegeben von J.-Fr. Hake, W. Kuckshinrichs, K. Kugeler u. a. (1998),
   500 Seiten
   ISBN: 3-89336-226-6

4. **Materials for Advances Power Engineering 1998**
   Abstracts of the 6th Liège Conference
   edited by J. Lecomte-Beckers, F. Schubert, P. J. Ennis (1998), 184 pages
   ISBN: 3-89336-227-4

5. **Materials for Advances Power Engineering 1998**
   Proceedings of the 6th Liège Conference
   edited by J. Lecomte-Beckers, F. Schubert, P. J. Ennis (1998),
   Part I XXIV, 646, X pages; Part II XXIV, 567, X pages; Part III XXIV, 623, X
   pages
   ISBN: 3-89336-228-2

6. **Schule und Energie**
   1. Seminar Energiesparen, Solarenergie, Windenergie. Jülich, 03. und
   04.06.1998
   herausgegeben von P. Mann, W. Welz, D. Brandt, B. Holz (1998), 112 Seiten
   ISBN: 3-89336-231-2

7. **Energieforschung**
   Vorlesungsmanuskripte des 3. Ferienkurses „Energieforschung"
   vom 22. bis 30. September 1997 im Forschungszentrum Jülich
   herausgegeben von J.-Fr. Hake, W. Kuckshinrichs, K. Kugeler u. a. (1997),
   505 Seiten
   ISBN: 3-89336-211-8

8. **Liberalisierung des Energiemarktes**
   Vortragsmanuskripte des 5. Ferienkurs „Energieforschung“
   vom 27. September bis 1. Oktober 1999 im Congrescentrum Rolduc und
   im Forschungszentrum Jülich
   herausgegeben von J.-Fr. Hake, A. Kraft, K. Kugeler u. a. (1999), 350 Seiten
   ISBN: 3-89336-248-7

9. **Models and Criteria for Prediction of Deflagration-to-Detonation Transition (DDT) in Hydrogen-Air-Steam-Systems under Severe Accident Conditions**
   edited by R. Klein, W. Rehm (2000), 178 pages
   ISBN: 3-89336-258-4

10. **High Temperature Materials Chemistry**
    Abstracts of the 10th International IUPAC Conference, April 10 - 14 2000, Jülich
    edited by K. Hilpert, F. W. Froben, L. Singheiser (2000), 292 pages
    ISBN: 3-89336-259-2

11. **Investigation of the Effectiveness of Innovative Passive Safety Systems for Boiling Water Reactors**
    edited by E. F. Hicken, K. Verfondern (2000), X, 287 pages
    ISBN: 3-89336-263-0

12. **Zukunft unserer Energieversorgung**
    Vortragsmanuskripte des 6. Ferienkurs „Energieforschung“
    vom 18. September bis 22. September 2000 im Congrescentrum Rolduc und
    im Forschungszentrum Jülich
    herausgegeben von J.-Fr. Hake, S. Vögele, K. Kugeler u. a. (2000),
    IV, 298 Seiten
    ISBN: 3-89336-268-1

13. **Implementing Agreement 026**
    For a programme of research, development and demonstration on advances fuel cells
    Fuel Cell Systems for Transportation
    Annex X. Final Report 1997 - 1999
    edited by B. Höhlein; compiled by P. Biedermann (2000), 206 pages
    ISBN: 3-89336-275-4

14. **Vorgespannte Guß-Druckbehälter (VGD) als berstsichere Druckbehälter für innovative Anwendungen in der Kerntechnik**
    Prestressed Cast Iron Pressure Vessels as Burst-Proof Pressure Vessels for Innovative Nuclear Applications
    von W. Fröhling, D. Bounin, W. Steinwarz u. a. (2000) XIII, 223 Seiten
    ISBN: 3-89336-276-2

15. **High Temperature Materials Chemistry**
Proceedings of the 10th International IUPAC Conference
held from 10 to 14 April 2000 at the Forschungszentrum Jülich, Germany
Part I and II
edited by K. Hilpert, F. W. Froben, L. Singheiser (2000), xvi, 778, VII pages
ISBN: 3-89336-259-2

16. **Technische Auslegungskriterien und Kostendeterminanten von SOFC- und PEMFC-Systemen in ausgewählten Wohn- und Hotelobjekten**
von S. König (2001), XII, 194 Seiten
ISBN: 3-89336-284-3

17. **Systemvergleich: Einsatz von Brennstoffzellen in Straßenfahrzeugen**
von P. Biedermann, K. U. Birnbaum, Th. Grube u. a. (2001), 185 Seiten
ISBN: 3-89336-285-1

18. **Energie und Mobilität**
Vorlesungsmanuskripte des 7. Ferienkurs „Energieforschung“
vom 24. September bis 28. September 2001 im Congrescentrum Rolduc und im Forschungszentrum Jülich
herausgegeben von J.-Fr. Hake, J. Linßen, W. Pfaffenberger u. a. (2001),
205 Seiten
ISBN: 3-89336-291-6

19. **Brennstoffzellensysteme für mobile Anwendungen**
von P. Biedermann, K. U. Birnbaum, Th. Grube u. a. (2002)
PDF-Datei auf CD
ISBN: 3-89336-310-6

20. **Materials for Advances Power Engineering 2002**
Abstracts of the 7th Liège Conference
edited by J. Lecomte-Beckers, M. Carton, F. Schubert, P. J. Ennis (2002),
c. 200 pages
ISBN: 3-89336-311-4

21. **Materials for Advances Power Engineering 2002**
Proceedings of the 7th Liège Conference
Part I, II and III
edited by J. Lecomte-Beckers, M. Carton, F. Schubert, P. J. Ennis (2002),
XXIV, 1814, XII pages
ISBN: 3-89336-312-2

22. **Erneuerbare Energien: Ein Weg zu einer Nachhaltigen Entwicklung?**
Vorlesungsmanuskripte des 8. Ferienkurs „Energieforschung“
vom 23. bis 27. September 2002 in der Jakob-Kaiser-Stiftung, Königswinter
herausgegeben von J.-Fr. Hake, R. Eich, W. Pfaffenberger u. a. (2002),
IV, 230 Seiten
ISBN: 3-89336-313-0

23. **Einsparpotenziale bei der Energieversorgung von Wohngebäuden durch Informationstechnologien**
von A. Kraft (2002), XII, 213 Seiten
ISBN: 3-89336-315-7

24. **Energieforschung in Deutschland**
Aktueller Entwicklungsstand und Potentiale ausgewählter nichtnuklearer Energietechniken
herausgegeben von M. Sachse, S. Semke u. a. (2002), II, 158 Seiten, zahlreiche farb. Abb.
ISBN: 3-89336-317-3

25. **Lebensdaueranalysen von Kraftwerken der deutschen Elektrizitätswirtschaft**
von A. Nollen (2003), ca. 190 Seiten
ISBN: 3-89336-322-X

26. **Technical Session: Fuel Cell Systems of the World Renewable Energy Congress VII**
Proceedings
edited by D. Stolten and B. Emonts (2003), VI, 248 pages
ISBN: 3-89336-332-7

27. **Radioactive Waste Products 2002 (RADWAP 2002)**
Proceedings
edited by R. Odoj, J. Baier, P. Brennecke and K. Kühn (2003), VI, 420 pages
ISBN: 3-89336-335-1

28. **Methanol als Energieträger**
von B. Höhlein, T. Grube, P. Biedermann u. a. (2003), XI, 109 Seiten
ISBN: 3-89336-338-6

29. **Hochselektive Extraktionssysteme auf Basis der Dithiophosphinsäuren: Experimentelle und theoretische Untersuchungen zur Actinoiden(III)-Abtrennung**
von S. A. H. Nabet (2004), VI, 198 Seiten
ISBN: 389336-351-3

30. **Benchmarking-Methodik für Komponenten in Polymerelektrolyt-Brennstoffzellen**
von Matthias Gebert (2004), 194 Seiten
ISBN: 3-89336-355-6

31. **Katalytische und elektrochemische Eigenschaften von eisen- und kobalthaltigen Perowskiten als Kathoden für die oxidkeramische Brennstoffzelle (SOFC)**
von Andreas Mai (2004), 100 Seiten
ISBN: 3-89336-356-4

32. **Energy Systems Analysis for Political Decision-Making**
edited by J.-Fr. Hake, W. Kuckshinrichs, R. Eich (2004), 180 pages
ISBN: 3-89336-365-3

33. **Entwicklung neuer oxidischer Wärmedämmschichten für Anwendungen in stationären und Flug-Gasturbinen**
von R. Vaßen (2004), 141 Seiten
ISBN: 3-89336-367-X

34. **Neue Verfahren zur Analyse des Verformungs- und Schädigungsverhaltens von MCrAlY-Schichten im Wärmedämmschichtsystem**
von P. Majerus (2004), 157 Seiten
ISBN: 3-89336-372-6

35. **Einfluss der Oberflächenstrukturierung auf die optischen Eigenschaften der Dünnschichtsolarzellen auf der Basis von a-Si:H und μc-Si:H**
von N. Senoussaoui (2004), 120 Seiten
ISBN: 3-89336-378-5

36. **Entwicklung und Untersuchung von Katalysatorelementen für innovative Wasserstoff-Rekombinatoren**
von I.M. Tragsdorf (2005), 119 Seiten
ISBN: 3-89336-384-X

37. **Bruchmechanische Untersuchungen an Werkstoffen für Dampfkraftwerke mit Frischdampftemperaturen von 500 bis 650°C**
von L. Mikulová (2005), 149 Seiten
ISBN: 3-89336-391-2

38. **Untersuchungen der Strukturstabilität von Ni-(Fe)-Basislegierungen für Rotorwellen in Dampfturbinen mit Arbeitstemperaturen über 700 °C**
von T. Seliga (2005), 106 Seiten
ISBN: 3-89336-392-0

39. **IWV-3 Report 2005. Zukunft als Herausforderung**
(2005), 115 Seiten
ISBN: 3-89336-393-9

40. **Integrierter Photodetektor zur Längenmessung**
von E. Bunte (2005), XI, 110 Seiten
ISBN: 3-89336-397-1

41. **Microcrystalline Silicon Films and Solar Cells Investigated by Photoluminescence Spectroscopy**
by T. Merdzhanova (2005), X, 137 Seiten
ISBN: 3-89336-401-3

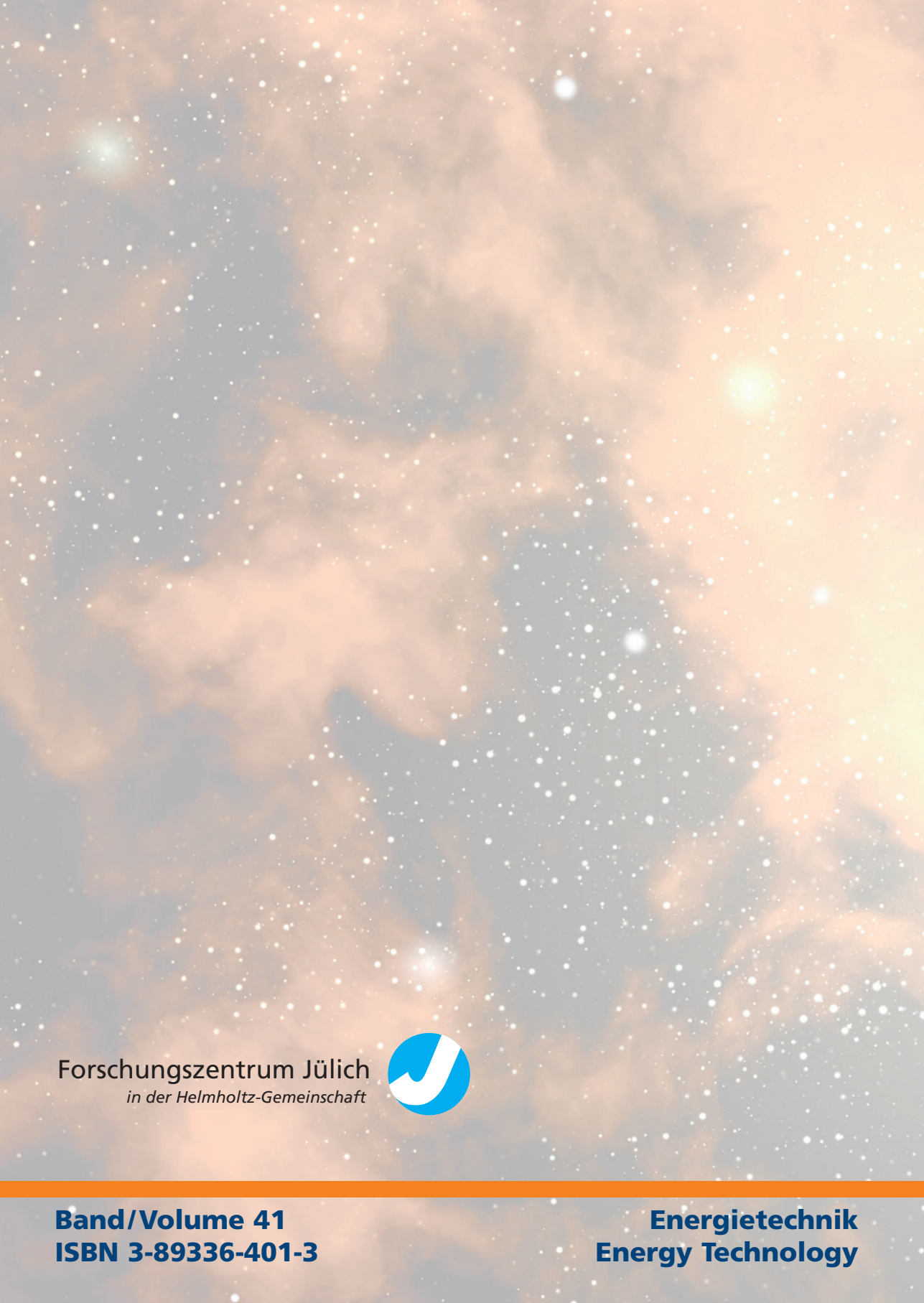

Band/Volume 41
ISBN 3-89336-401-3

Energietechnik
Energy Technology